2017

Computational models for turbulent bubbly flows in bubble columns

Nithin Panicker
Iowa State University

Computational models for turbulent bubbly flows in bubble columns

by

Nithin S. Panicker

A dissertation submitted to the graduate faculty

in partial fulfillment of the requirements for the degree of

DOCTOR OF PHILOSOPHY

Major: Mechanical Engineering

Program of Study Committee:
Alberto Passalacqua, Major Professor
Rodney O. Fox
Mark Wright
Ming-Chen Hsu
Adarsh Krishnamurthy

The student author, whose presentation of the scholarship herein was approved by the program of study committee, is solely responsible for the content of this dissertation. The Graduate College will ensure this dissertation is globally accessible and will not permit alterations after a degree is conferred

Iowa State University

Ames, Iowa

2017

TABLE OF CONTENTS

LIST OF TABLES

LIST OF FIGURES

ACKNOWLEDGEMENTS

I would like to take this opportunity to express my thanks to those who helped me with various aspects of conducting research and the writing of this thesis. First and foremost, Prof. Passalacqua and Prof. Fox for their guidance, patience and support throughout this research and the writing of this thesis. their insights and words of encouragement have often inspired me and renewed my hopes for completing my graduate education. I would also like to thank my committee members for being in my committee: Dr. Ming Chen, Dr. Wright and Dr. Adarsh. I would additionally like to thank Dr. Bo kong and my lab mates for sharing their knowledge throughout the initial stages of my graduate career.

ABSTRACT

Bubble columns are widely used in the chemical and pharmaceutical industries as gas–liquid contactors because of their simple construction and ability to provide high contact area for mass and heat transfer. The design and scale up of bubble columns depends on heat/mass transfer and mixing characteristics provided by it. These two factors highly depend on the bubbly flow hydrodynamics of the column. Although simple in construction, the bubbly flow hydrodynamics inside bubble columns are complex due the presence of turbulence and bubble–bubble interactions (coalescence, breakup), thus, the development of accurate CFD (Computational Fluid Dynamics) models that describe bubbly flows are important and challenging.

Two-fluid models are widely used as CFD models for the prediction of bubbly flows in bubble columns due to its low computational cost.

In this thesis computational models are developed in order to improve the capabilities of two-fluid models in predicting bubbly flows in bubble columns. .

CHAPTER 1. BUBBLY FLOWS IN BUBBLE COLUMNS

1.1 Introduction

Bubble columns are widely used in Chemical and petrochemical industries as gas/liquid contactors. A Chemical plant as shown in Fig 1.1 produce waste gases and these waste gases often contain harmful contents like NH3, CO2 etc. According to EPA regulation these gases are not allowed to be released in to the atmosphere directly, as a remedy these gases are passed through a bubble column which contains a liquid solvent which absorbs these harmful contents prior to the release in to the atmosphere.

The extensive usage of bubble columns as a gas/liquid contactor in the Chemical industry is attributed to:

1. High interfacial area per unit volume for heat and mass transfer.
2. Low maintenance cost due to the absence of moving parts.
3. Less floor space occupied.
4. The capability of performing slow reactons which requires high liquid residence time.

Precise design and construction of bubble columns are important to obtain the desired yield for gas-liquid contacting processes carried out in bubble columns.

The commmon design parameters for bubble columns:

1. Mass transfer coefficient.
2. Heat transfer characterisitcs.
3. Bubble size distribution.

Design parameters significantly depend on the flow inside the column thus, understanding and modeling the physics of bubbly flows is essential to design these systems efficiently. In the most basic design model flow is assumed to behave ideally (e.g. plug flow for gas phase, complete

Figure 1.1 Chemical plant

backmixing for liquid), however in practical applications flow is far from ideal and require CFD models to describe it accurately. The main challenges associated with developing CFD models for bubbly flows:

1. Different hydrodynamic flow regimes based on inlet conditions and dimensions of the column.
2. Complexity of physics involved due to turbulence and size change (coalescence, breakup).

Different hydrodynamic regimes present in bubble columns or bubbly flows in pipes are discussed in the next section.

1.2 Hydrodynamic flow regimes

Bubbly flows can be classified based on the topological distribution of the phases. A particular type of such topology distribution is called as flow regime or flow pattern. Investigation of these flow regimes and transition between these regimes are crucial for both design and safety aspects of Industrial equipments, and mathematical modelling. For instance, if we consider the slug flow which is one of the commonly found multiphase flow regime in many engineering

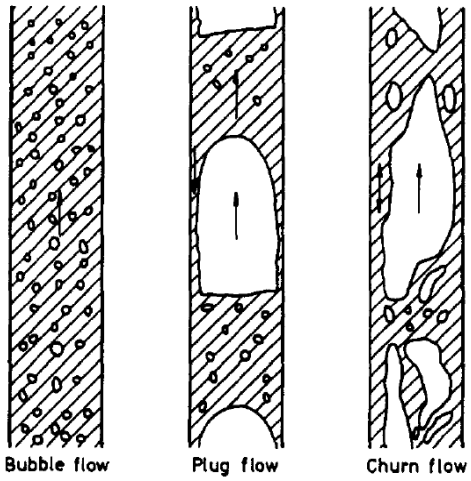

Figure 1.2 picture from McQuillan and Whalley (1985), commonly found flow regimes

applications, particularly in the transport of hydrocarbon fluids in pipelines in the oil and gas industry. The slug flow regime, in which large gas bubbles alternately with liquid slugs at randomly fluctuating frequency, is usually undesirable since the intermittent behaviour of slugs causes severe stress conditions on pipelines. It is therefore important to be able to predict the onset and subsequent development of slug flow. Several such examples can be found in the literature (Fabre and Line, 1992; Wu et al., 2001; Cheng et al., 1999).

There are a plethora of regimes found in the literature (Weisman et al., 1979; Barnea, 1987; Costigan and Whalley, 1997; Woldesemayat and Ghajar, 2007; McGovern et al., 2008) for bubbly flows, we are focusing mainly on bubbly flows in bubble columns and vertical pipes. Three types of flow regimes are commonly observed in these systems, which are the homogeneous (bubbly flow) regime; the heterogeneous (Churn-turbulent) regime and the slug flow regime (Taitel et al., 1980; Kaichiro and Ishii, 1984; Hyndman et al., 1997; McQuillan and Whalley, 1985). There also exists the so-called foaming regime which is not so commonly encountered in bubble columns.

Homogenous flow (Bubble flow):

The homogeneous bubbly flow regime is found at low superficial gas velocity, typically less than 5 cm/s, as can be seen in the flow regime maps found in (Hills, 1976; Fan et al., 1985).

This regime is characterized by a uniform bubble distribution along the cross section of the column with uniform rise velocity. Bubbles are generally mono-dispersed due to the absence of coalescence and breakup. A gentle liquid mixing is observed in the entire cross-sectional area of the column (Hyndman et al., 1997), which depends on the gas velocity rather than the liquid velocity (Ityokumbul et al., 1994). Since there is no coalescence or breakup, the bubble size is entirely dependent on the sparger size and system properties (Thorat and Joshi, 2004). The gas hold up varies linearly with superficial gas velocity in this regime (Ityokumbul et al., 1994).

Slug flow (Plug flow):

Slug flow is observed in bubble columns with high gas flow rates (Hyndman et al., 1997) a nd diameters less than a cutoff diameter, where the cutoff diameter depends on the thermodynamic properties and the Rayleigh taylor instability wavelength of the system (Kolev (2011)), such a relation for cutoff diameter can be found in Taitel et al. (1980). This regime is characterized by large bubbles which almost occupy the entire cross-sectional area of the column. Slugs are generally found in bubble columns up to a diameter of 15 cm (Hills, 1976; Miller, 1980).

Heterogenous flow (Churn flow):

The churn-turbulent flow regime is observed in bubble columns for gas velocity typically greater than 5 cm/s (Deckwer et al., 1980). This regime is characterized by enhanced turbulent motion of gas bubbles with significant bubble coalescence and breakup, which results in wide bubble size distribution (Schumpe and Deckwer, 1980). Cluster formation and wide bubble size distribution were also found by Hyndman et al. (1997). Coalescence and breakup in this regime is controlled by energy dissipation at the bulk (Thorat and Joshi, 2004), Jakobsen et l. (1993), energy dissipation in gas - liquid flows are caused by two mechanisms wall friction and bubble associated dissipation (Merchuk and Berzin, 1995), the area of the bubbles present in the bubble cloumn reactor is usually one order of magnitude larger than the area of the walls, which makes it the main source of energy dissipation in gas - liquid flows. According to Luo and Svendsen (1996), if the energy of the liquid eddy colliding the bubble is greater than the surface energy, bubble breakup occurs. According to there theoretical model for the prediction of bubble size

distribution, the lower bubble sizes exist in the region of low energy dissipation and higher bubble sizes exist in the region of high energy dissipation rate.

Because of coalescence, there is a reduction in effective interphase surface area leading to lower gas-liquid mass transfer rates compared to homogeneous bubbly flows (Schumpe and Deckwer, 1980), but the effective interphase surface area calculation is done by the assumption of two distinct bubble classes (S. and T., ; Schumpe and Deckwer, 1980). The churn-turbulent regime cannot be avoided in industrial bubble columns, as majority of the bubble columns operate with high superficial gas velocities (Hyndman et al., 1997), as a result the churn regime has to be studied carefully. Coalescence and bubble breakup have been studied numerically by (Olmos et al., 2001; Hibiki and Ishii, 2000; Millies and Mewes, 1999; Wu et al., 2001).

Olmos et al. (2001) did a Euler-Euler simulation of gas - liquid flows in a bubble column by coupling the Euler - Euler model with population balance equation. They used the MUSIG (multiple size group) approach in CFX. they also assume that the velocity of all the classes of bubbles is same leading to only one momentum equation and multiple continuity equation for the gas phase. They studied the homogenous and the transition regime by varying the inlet gas velocity. They compared the bubble size distirbution, gas holdup and the axial liquid velocity with there in house experiments. On comparison they found that as long as the homogenous regime persists, hydrodynamic variables are in good agreement with the experiments, but in the transition regime there is an overestimation of gas holdup. The size distributions in the transition regime evolves till an equilibrium, which characterises the bubble properties in the churn-turbulent regime. They also confirm the predictions of Luo and Svendsen (1996), that bubble size distribution depends on the Turbulent kinetic energy dissipation and also on the bubble size.

Millies and Mewes (1999) developed a model for predicting the interphase surface area density in a bubble column reactor. The model is derived from population balance equation, taking in to account the bubble coalescence and breakup. An approximate analytical solution is first obtained, then using that analytical solution population balance equations are reduced to one single partial differential equation. The results obtained from the model is compared with the experimental data and the model gives good prediction of interphase surface area.

Hibiki and Ishii (2000) developed a two group interphase surface area transport equation from the population balance equation, where the bubbles are divided in to two sub classes namely spherical/distorted bubbles and cap/slug bubbles. Each class has its on number density evolution equation and the corresponding interphase surface area transport equation is derived from the number density equation. The bubble coalescence models due to random collision and wake entrainment and the bubble breakage due to turbulence is thoroughly studied. They found that two group interphase surface area transport equation predicts the interphase surface area concentration with in the average relative deviation of 3 percent from the experiments, for bubble to slug flow transition.

1.2.1 Flow regime transition

1.2.1.1 Bubbly to churn regime

Thorat and Joshi (2004) found that the transition gas velocity depends on the sparger design, the column dimensions and the physical properties of the system. There theory to determine the transition criteria is based on linear stability analysis of two-fluid model. The authors concluded that transition hold up increased with decreasing aspect ratio and sparger hole diameter. The transition criteria based on gas hold up can be found in Kolev (2011). According to Kolev (2011) small bubbles with diameter less than 0.89λ, where λ is the Rayleigh Taylor instability wavelength $\lambda = \sqrt{\frac{\tau}{g(\rho_l - \rho_g)}}$, acts like a solid sphere with no coalescence, in which case the transition from bubbly to churn-turbulent flow occurs at a volume fraction 0.54. for large bubbles transiton can occur between $0.24 < \alpha < 0.54$, where the lower limit is not certain.

Krishna et al. (1991) studied the effect of gas density on the regime transition velocity and concluded that regime transition velocity increased with increased gas density.

In order to determine the transition criteria, unfortunately there is no definite range of superficial gas velocities. Different studies performed with different operating conditions, system properties and sparger design gives different regime boundaries. For example, Hyndman et al. (1997) found that below a superficial gas velocity of 4 cm/s, a bubbly flow regime exists,

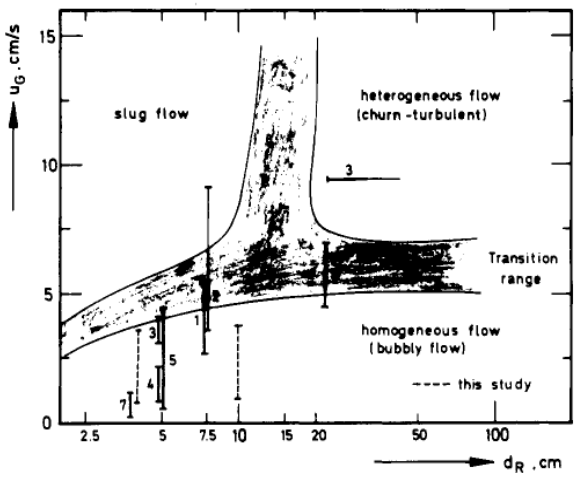

Figure 1.3 picture from Deckwer et al. (1980), flow regime map

pino et al. (1992) agrees with Hyndman et al. (1997), but according to Schumpe and Grund (1986) bubble flow regime can prevail up to 5 cm/s. Bukur and Daly (1987) observed the churn-turbulent regime for gas velocities of 2 - 5 cm/s.

Several flow regime charts are found in the literature (Shah et al., 1982; Fan et al., 1985; Deckwer et al., 1980). Deckwer et al. (1980) reports one of these maps (Fig. 3), which shows the dependence of the flow regime on the column diameter and superficial gas velocities. The shaded region represents the transition between different regimes.

1.2.1.2 Slug to churn regime

Churn flow was considered to be a phenomenon taking place at the entrance region of the column by Taitel et al. (1980). They consider the churn flow as the part of the formation of stable slug flow. hey deduced an entrance length for the pipe as a function of the mixture velocity and the pipe diameter, required to form stable slug flow. The pipe length is below the entrance length, churn flow exists and if not stable slug flow is formed at the end. McQuillan and Whalley (1985), including Nicklin and Davidson (1962), Wallis (1969), Govan et al. (1991) attribute the transition from slug to churn to the flooding of liquid film surrounding the bubble. Several correlations exist to predict the flooding velocity (Wallis (1969), Govier and Aziz (1972),

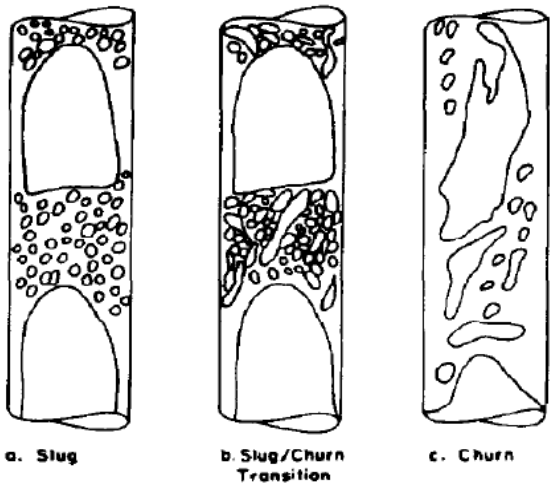

Figure 1.4 picture from Brauner and Barnea (1986), showing slug to churn transition

Bankoff and Lee (1986)) and if the gas velocity is more than the flooding velocity slug to churn transition occurs. Kaichiro and Ishii (1984) attributes the transition of slug to churn to the wake effect of Taylor bubbles (bubble slug with cylindrical tail and hemispherical head). The transition occurs when the average gas hold up in the pipe exceeds the mean void fraction over Taylor bubble region evaluated by them. According to Brauner and Barnea (1986), the transition occurs at a volume fraction of the liquid slug greater than 0.52, because at that point the chances of bubble collision is higher leading to coalescence of bubbles, which ultimately destroys the liquid slug and lead to churn flow.

1.2.1.3 Transition from bubbly flow to slug flow

Radovich and Moissis (1962) suggested the transition of bubble to slug happens due to the coalescence of bubbles, when the bubble volume fraction reaches 0.25 - 0.3. Taitel et al. (1980) confirmed Radovich and Moissis findings, with the exception that the bubble flow regime persists if an equilibrium is maintained bubble coalescence and bubble breakup due to liquid turbulence.

The current hydrodynamic CFD models present in the literature to model these flow regimes are discussed in the further section.

1.3 Hydrodynamic CFD models

In all multiphase models, the main difficulties are attributed to the interphases between the phases and discontinuities associated with them (Ishii and Mishima (1984)). The formulation of the constitutive equations is another difficulty which arises while developing a multiphase model (Drew and Lahey (1979)). Constitutive equations applied still include considerable uncertainties which is discussed in the later sections.

Different multiphase flow models present in the literature for predicting bubbly flows:

1.3.1 Mixture flow model

Mixture flow models are developed mainly for flows with low stokes number $<< 1$, where the influence of the dispersed phase on the continuous phase is almost negligible (for e.g. dusty flows, small gas bubbles in liquid). In those cases flow is modelled in terms of a single momentum equation, and the volume fractions of each phase is determined the individual continuity equations. The mixture flow model is obtained by adding the ensemble averaged momentum and continuity equations (Drew, 1982) for the continuous and the dispersed phase. The following is a mixture model formulated in Ref.

Continuity

$$\frac{\partial \rho_{\mathrm{m}}}{\partial t} + \nabla \cdot (\rho_{\mathrm{m}} \mathbf{u}_{\mathrm{m}}) = 0 \tag{1.1}$$

where $\rho_{\mathrm{m}} = \Sigma_1^n \alpha_{\mathrm{i}} \rho_{\mathrm{i}}$, $\mathbf{u}_{\mathrm{m}} = \frac{1}{\rho_{\mathrm{m}}} \Sigma_1^n \alpha_{\mathrm{i}} \rho_{\mathrm{i}} \mathbf{u}_{\mathrm{i}}$

Momentum

$$\frac{\partial}{\partial t} (\rho_{\mathrm{m}} \mathbf{u}_{\mathrm{m}}) + \nabla \cdot (\rho_{\mathrm{m}} \mathbf{u}_{\mathrm{m}} \mathbf{u}_{\mathrm{m}}) = -\nabla p_{\mathrm{m}} + \nabla \cdot \tau_{\mathrm{m}} + \nabla \cdot \tau_{\mathrm{Dm}} + \rho_{\mathrm{m}} \mathbf{g} + \mathbf{F}_{\mathrm{m}} \tag{1.2}$$

where $\nabla p_{\mathrm{m}} = \Sigma_1^n \alpha_{\mathrm{i}} \nabla p$, $\tau_{\mathrm{m}} = \Sigma_1^n \tau_{\mathrm{i}}$, $\mathbf{F}_{\mathrm{m}} = \Sigma_1^n \mathbf{F}_{\mathrm{i}}$

The term $\nabla \cdot \tau_{\mathrm{Dm}}$ is an unclosed term which arises during the formulation through substituting $\mathbf{u}_{\mathrm{i}} = \mathbf{u}_{\mathrm{m}} + \mathbf{u}_{\mathrm{Mi}}$ in the non linear convection term $\nabla \cdot (\alpha_{\mathrm{i}} \rho_{\mathrm{i}} \mathbf{u}_{\mathrm{i}} \mathbf{u}_{\mathrm{i}})$ (See Ref.) of the Favre averaged equations. The unclosed term $\nabla \cdot \tau_{\mathrm{Dm}}$ appears in the mixture momentum equation as a function of $\mathbf{u}_{\mathrm{Mi}}$, the diffusion velocity or the velocity of phase i relative to the centre of

the mixture mass, which has to closed to solve the mixutre momentum equation to predict the flow. A drift flux model is commonly used in the literature (Zuber and Findlay (1965), Ishii and Hibiki (2010), Fangzhi Chen et al. (2005) , Zhao et al. (2008)) to close the diffusion velocity, it is based on representing the diffusion velocity $\mathbf{u}_{\mathrm{Mi}}$ in terms of mixture velocity and a drift velocity, later the drift velocity the drift velocity is computed from slip velocity as given: $\mathbf{u}_{\mathrm{Di}} = \mathbf{u}_{\mathrm{Cl}} - \Sigma_1^n \alpha_{\mathrm{k}} \mathbf{u}_{\mathrm{Ck}}$, where $\mathbf{u}_{\mathrm{Ck}}$-slip velocity, the slip velocity is formulated in terms of bubble relaxation time and mixture acceleration as given in Ref.. The advantage of the mixture flow model over Euler-Lagrange and Euler-Euler models is that the unclosed terms present in the model are less and can be expressed in a simpler form due to its formulation from the Eulerian averaged model by eliminating the interfacial forces (Johansen et al. (1990)). The mixture model is numerically implemented in the codes PHOENICS, FLUENT, CFX. The application of the mixture model in simulating bubbly flows in bubble columns appears to be scarce (Sanyal et al., 1990), most applications found in the literature are concentrated mainly on flows involving gravity settling and centrifugal forces (Franca and Lahey (1992), Wang and Cheng (1996), Pericleous (1986), Pericleous and Patel (1987), Sakaguchi et al. (1987)). Hence it is not so clear about the applicability of the model with respect to different flow regimes found in bubbly flow in a bubble column. The only limit of appilcability which can be deduced from the literature is that it is applicable for dilute flows with low stokes number.

1.3.2 Euler-Lagrange model

In Euler - Lagrange (EL) approach the dispersed phase (bubble phase) is treated with a lagrangian approach by tracking the bubble with the following governing equations:

$$m_{\mathrm{b}} \frac{d\mathbf{v}_{\mathrm{b}}}{dt} = \mathbf{F}_{\mathrm{net}} \tag{1.3}$$

$$\frac{d\mathbf{x}_{\mathrm{b}}}{dt} = \mathbf{v}_{\mathrm{b}} \tag{1.4}$$

$$\mathbf{F}_{\mathrm{net}} = \mathbf{F}_{\mathrm{D}} + \mathbf{F}_{\mathrm{VM}} + \mathbf{F}_{\mathrm{Lift}} + \mathbf{F}_{\mathrm{B}} \tag{1.5}$$

The models for inter-phase forces $\mathbf{F}_D$, $\mathbf{F}_{VM}$, $\mathbf{F}_{Lift}$ will be discussed elaborately in the next section. The continuous phase is solved on an Eulerian grid using the averaged equations discussed in the next section. The continuous and the dispersed phase in EL approach is coupled to one another with the volume fraction of the continuous phase (α_l) and the inter-phase force $\mathbf{F}_\mathrm{net}$. The α_l in a computational cell is computed from the volume of the bubbles occupying the cell as follows:

$$\alpha_\mathrm{l} = 1 - \frac{\Sigma_\mathrm{i} V_{bi}}{V_\mathrm{cell}} \tag{1.6}$$

The velocity of the continuous phase required to compute the inter-phase force on the particle is obtained on the particle location by interpolating the flow-field data obtained from the continuous phase solver. Then the new inter-phase force obtained from the discrete solver is converted into volume inter-phase forces (Ref.) and fed back to continuous phase solver to compute the new continous flow field. The works (Sokolichin, Lapin, Delnoij) related to simulating bubbly flows in a bubble column using EL approach is rare and explores only the dilute limit (α_g ¡ 10 per) in the homogeneous regime, indicating that the method is not suitable for systems or processes involving large number of bubbles (>100000) or in the high void fraction limit (>10 per) (Heterogenous regime occurs). In the case of large number of bubbles the computational cost and the memory requirement involved to simulate the bubbly flows with EL approach is very high, thus EE approach with less computational cost discussed in the next section is adopted in such concentrated limits. Moreover, Sokolichin and Eigenberger (1990) compared the solutions obtained from the simlulations performed using both EL and EE approach on a rectangular bubble column operating in the dilute limit with global void fraction (<10 per). They concluded that the velocity and void fraction profiles predicted by EE approach with TVD (Total Variation Diminishing) schemes are the same as predicted by the EL approach, which indicates that the bubbly flow simulations performed on a bubble column by EE approach with higher order non-diffusive schemes are comparable to the EL approach also in the dilute limit. Thus, proving EE approach as an effective technique to study bubbly flows in a bubble column for wide range of regimes.

1.3.3 Two-fluid model

The two-fluid model equations which govern the momentum, mass and heat transfer of two-phase flows are solved on a fixed grid for both the phases. This type of approach eliminates the computational memory requirement associated with the tracking of dispersed phase as encountered in EL approach discussed in the previous section. The governing equations in the two-fluid model are obtained by averaging the microscopic equations or the Navier Stokes equation which is valid for both the phases. The averaging of the microscopic equation results in unclosed terms in the two-fluid model equations which needs to be modeled rigorously for accurate prediction of the flow, in other words flow prediction is sensitive to the accuracy of the models. However, the main advantage of such an approach is that the solution for Industrial scale problems can be obtained with relatively lesser computational cost than the microscopic equation, hence it is used in numerous works to simulate bubbly flows (the details of the works will be discussed elaborately in subsec. 1.3.3.1) for wide range of bubbly flow regimes (Homogeneous to Heterogeneous) discussed in subsec. 1.2. and numerous efforts are made in the development of sub-models for the unclosed terms (discussed in 1.3.3.2) present in two-fluid model.

1.3.3.1 Formulation:

Ensemble averaging is applied on the microscopic equations 1.7 and 1.8 to obtain the two-fluid model (Drew, 1983) for two-phase incompressible flows.

Mass:

$$\frac{\partial \rho_{\mathrm{i}}}{\partial t} + \nabla \cdot \rho_{\mathrm{i}} \mathbf{u}_{\mathrm{i}} = 0 \tag{1.7}$$

Momentum:

$$\frac{\partial}{\partial t}\left(\rho_{\mathrm{i}} \mathbf{u}_{\mathrm{i}}\right) + \nabla \cdot \left(\rho_{\mathrm{i}} \mathbf{u}_{\mathrm{i}} \mathbf{u}_{\mathrm{i}}\right) = -\nabla p_{\mathrm{i}} + \nabla \cdot \boldsymbol{\tau}_{\mathrm{i}} + \mathbf{F}_{\mathrm{i}} \tag{1.8}$$

Where i=1, 2 corresponds to liquid and gas phase respectively.

Ensemble averaging of flow variables (velocity, pressure etc.) are performed by repeating measurements of the variables at a fixed time and location for a large number of ensembles (flow configurations) with identical boundary conditions, and finding an average value of the measurements.

Mathematically ensemble average can be represented for any flow variable f as

$$\langle f \rangle (\mathbf{r}, t) = \Sigma_{\omega=1}^{N} f (\mathbf{r}, t; \omega) \tag{1.9}$$

where ω is a running variable over the ensembles and N is the total number of ensembles. Since the ensemble averaging operator $\langle\rangle$ is independent of space and time we can perform the following operation while formulating the two-fluid model

$$\langle \frac{\partial}{\partial t} f \rangle = \frac{\partial}{\partial t} \langle f \rangle \tag{1.10}$$

$$\langle \nabla f \rangle = \nabla \langle f \rangle \tag{1.11}$$

The partial average of f in phase i can be defined as:

$$\langle X_i f \rangle \tag{1.12}$$

Where X_i is the phase indicator function defined as 1 for the gas phase and 0 for the liquid phase.

Phase indicator function evolution equation (Drew, 1983a):

$$\frac{\partial}{\partial t} X_{\mathrm{i}} + \mathbf{u}_{\mathrm{I}} \cdot \nabla X_{\mathrm{i}} = 0 \tag{1.13}$$

It can also be shown that the following conditions are valid (Manninen and Taivassalo (2009)).

$$\langle X_{\mathrm{i}} \nabla f \rangle = \nabla \langle X_{\mathrm{i}} f \rangle - \langle f \nabla X_{\mathrm{i}} \rangle \tag{1.14}$$

$$\langle X_{\mathrm{i}} \nabla \cdot f \rangle = \nabla \cdot \langle X_{\mathrm{i}} f \rangle - \langle f \cdot \nabla X_{\mathrm{i}} \rangle \tag{1.15}$$

$$\langle X_{\mathrm{i}} \frac{\partial}{\partial t} f \rangle = \frac{\partial}{\partial t} \langle X_{\mathrm{i}} f \rangle - \langle f \frac{\partial}{\partial t} X_{\mathrm{i}} \rangle \tag{1.16}$$

By multiplying equations 1.7 and 1.8 with X_i, subtracting 1.13 and ensemble averaging with the conditions (1.10, 1.11, 1.14, 1.15 and 1.16) we get:

Mass:

$$\frac{\partial}{\partial t}\langle X_\mathrm{i}\rho\rangle + \nabla\cdot\langle X_\mathrm{i}\rho\mathbf{u}\rangle = \langle\rho\left(\mathbf{u}-\mathbf{u}_\mathrm{I}\right)\cdot\nabla X_\mathrm{i}\rangle \tag{1.17}$$

Momentum:

$$\frac{\partial}{\partial t}\langle X_\mathrm{i}\rho\mathbf{u}\rangle + \nabla\cdot\langle X_\mathrm{i}\rho\mathbf{u}\mathbf{u}\rangle = \nabla\cdot\langle X_\mathrm{i}\boldsymbol{\tau}\rangle + \langle X_\mathrm{i}\mathbf{F}\rangle + \langle(\rho\mathbf{u}\left(\mathbf{u}-\mathbf{u}_\mathrm{I}\right)-\boldsymbol{\tau})\cdot\nabla X_\mathrm{i}\rangle \tag{1.18}$$

An intrinsic average and Favre average for any variable f can be defined as:

$$\langle f_\mathrm{i}\rangle_\mathrm{p} = \frac{\langle X_\mathrm{i}f\rangle}{\langle X_\mathrm{i}\rangle} = \frac{\langle X_\mathrm{i}f\rangle}{\alpha_\mathrm{i}} \tag{1.19}$$

where $\langle X_\mathrm{i}\rangle = \alpha_\mathrm{i}$

In order to approach a closed set of equation the velocity is decomposed into its Favre averaged value and its fluctuation.

$$\mathbf{u}_\mathrm{i} = \langle\mathbf{u}_\mathrm{i}\rangle_\mathrm{f} + \mathbf{u}_\mathrm{i}^{''} \tag{1.20}$$

By using the above decomposition the convection term becomes

$$\langle X_\mathrm{i}\rho\mathbf{u}\mathbf{u}\rangle = \alpha_\mathrm{i}\rho_\mathrm{i}\langle\mathbf{u}_\mathrm{i}^{''}\rangle_\mathrm{f}\langle\mathbf{u}_\mathrm{i}^{''}\rangle_\mathrm{f} + \alpha_\mathrm{i}\langle\rho_\mathrm{i}\mathbf{u}_\mathrm{i}^{''}\mathbf{u}_\mathrm{i}^{''}\rangle \tag{1.21}$$

The term $\langle\rho_\mathrm{i}\mathbf{u}_\mathrm{i}^{''}\mathbf{u}_\mathrm{i}^{''}\rangle$ is called as the turbulent stress because it involves fluctuations. However, according to Fox (2012), it is incorrect to name the term as turbulent stress tensor, because the velocity fluctuations can arise from sources other than turbulence such as bubble movement.

We can get the final set of mass and momentum equation for each phase as

Mass:

$$\frac{\partial}{\partial t}\alpha_\mathrm{i}\langle\rho_\mathrm{i}\rangle_\mathrm{p} + \nabla\cdot\alpha_\mathrm{i}\langle\rho_\mathrm{i}\rangle_\mathrm{p}\langle\mathbf{u}_\mathrm{i}\rangle_\mathrm{f} = \Gamma_\mathrm{i} \tag{1.22}$$

Momentum:

$$\frac{\partial}{\partial t}\left(\alpha_\mathrm{i}\langle\rho\rangle_\mathrm{p}\langle\mathbf{u}\rangle_\mathrm{f}\right) + \nabla\cdot\left(\alpha_\mathrm{i}\langle\rho\rangle_\mathrm{p}\langle\mathbf{u}\rangle_\mathrm{f}\langle\mathbf{u}\rangle_\mathrm{f}\right) = \nabla\cdot\left(\alpha_\mathrm{i}\langle\boldsymbol{\tau}\rangle_\mathrm{f} + \langle X_\mathrm{i}\rho\mathbf{u}_\mathrm{i}^{''}\mathbf{u}_\mathrm{i}^{''}\rangle\right) + \alpha_\mathrm{i}\langle\mathbf{F}\rangle_\mathrm{f} + M_\mathrm{i} \tag{1.23}$$

Where,

$$\Gamma_{\mathrm{i}} = \langle \rho \left(\mathbf{u} - \mathbf{u}_{\mathrm{I}} \right) \cdot \nabla X_{\mathrm{i}} \rangle$$

$$M_{\mathrm{i}} = \langle (\rho \mathbf{u} \left(\mathbf{u} - \mathbf{u}_{\mathrm{I}} \right) - \boldsymbol{\tau}) \cdot \nabla X_{\mathrm{i}} \rangle$$

The inter-phase force term M_{i} has to be modeled to get a closed set of equation 1.23, which can be solved to obtain the two-phase flow field. On inspection of the term M_{i}, it can be inferred that this term is generated due to the stress distribution and mass transfer at the interface the bubbles. It is modelled by decomposing it into different components namely Drag, lift and virtual mass force under the assumption of no phase change or mass transfer at the interface. Some of the models available for these forces will be discussed in the next section.

1.3.3.2 Inter-phase force models

The accuracy of two-phase flow prediction using two-fluid model largely depends on the inter-phase force modeling. Inter-phase interaction term (M_{i}) with no mass transfer is decomposed into the drag, virtual mass, lift, wall lubrication and force due to hydrodynamic interaction between bubbles.

$$M_1 = M_{\mathrm{D}} + M_{\mathrm{VM}} + M_{\mathrm{LF}} + M_{\mathrm{WL}} + M_{\mathrm{HF}} \tag{1.24}$$

and also it assumed that

$$M_1 = -M_2 \tag{1.25}$$

It is also well known that the inviscid two-fluid model equations are ill-posed (discussed in Chapter 2), hence the well-posed ness of the equations also depends on the modeling and choice of inter-phase force models.

The following are the common set of force models used in the literature for accurate prediction and to achieve well posedness of the two-fluid model for bubbly flows (it should be noted that all the sub-models discussed in the section accounts for the unresolved stress distribution at the interface of the bubbles).

Drag force (M_{D}):

The models for the drag force present in the literature falls mainly under two categories: low gas fraction limit and high gas fraction limit. In the low gas fraction limit the interaction between bubbles is negligible, both due to bubble-bubble collisions and the interaction through the fluid flow modification due to the neighbouring bubbles. In this case, the bubbles can be treated as single bubble moving in the fluid and drag correlations for single bubbles can be used. The drag force on a single bubble can be expressed as:

$$\mathbf{F_D} = 0.5\rho_g C_D A_p |\mathbf{u_g} - \mathbf{u_l}| (\mathbf{u}_g - \mathbf{u}_l) \tag{1.26}$$

where A_p is the projected area of the sphere on a plane normal to the flow andC_D is the drag coefficient. For an Euler-Euler approach the equation 1.24 can be reformulated in terms of gas volume fraction as given by Drew (1983a) as:

$$\mathbf{F_D} = \frac{3}{4}\frac{\alpha_g}{d_s}\left(\frac{d_s}{d_D}\right)\rho_g C_D A_p |\mathbf{u_g} - \mathbf{u_l}| (\mathbf{u}_g - \mathbf{u}_l) \tag{1.27}$$

where d_s is the sauter mean bubble diameter.

The Drag coefficent C_D is obtained mainly as a function of bubble Reynolds number (Re) and Eotvos number (Eo). The drag coefficient reported in Levich et al. (1962) is only a function of Reynolds number.

$$C_{\mathrm{D}} = \frac{48}{Re} \tag{1.28}$$

The expression is derived analytically by considering the flow field around a single bubble with the assumption of spherical bubbles, hence it is valid for small bubbles of diameter $\sim$ 1 mm which does not loose its sphericity. For bubbles with shapes different from sphere (typically bubble sizes $>$ 1 mm) form drag becomes significant and the drag coefficient is expressed in terms of Eo as given in Johansen and Boysan (1988).

$$C_{\mathrm{D}} = \frac{0.622}{\frac{1}{Eo} + 0.235} \tag{1.29}$$

where $Eo = \frac{g\Delta\rho d_p^2}{\sigma}$ and σ is the surface tension. Tomiyama et al. (2002a) performed experiments on single bubble rise and deduced a drag coefficient C_{D} which switches between Re dependence

and Eo dependence based on bubble size as shown:

$$C_{\mathrm{D}} = max\left(\frac{48}{Re}, \frac{8Eo}{3\left(Eo+4\right)}\right) \tag{1.30}$$

When the gas fraction of the gas increases, bubble coalescence and breakup increases, resulting in the modification of the flow field in the vicinity of the bubble which affects the neighboring bubble caught in the flow field. In such cases drag formulation based on single bubble independent of other bubbles, may not be an appropriate choice, one has to account for the influence of the neighbouring bubbles. Ishii and Zuber (1979) developed a correlation for drag coefficient in the churn turbulent regime as a function of gas holdup, however, according to Jakobsen (1993) who implemented Ishii and Zuber's correlation, the physical effect of the correlation was to decrease the relative velocity with decreasing gas fraction, which is against the experimental evidence by (Yao et al., 1991; Grienberger and Hofmann, 1992) that the bubble velocity increases while moving in a group of bubbles. Garnier et al. (2002) developed a drag correlation for bubble swarms, which seems to behave qualitatively well with the experimental findings, however the correlation holds good only for bubble diameter less than 5.5 mm. The effects of the presence of other dispersed phase is implemented in Behzadi et al. (2001) as

$$C_{\mathrm{d}} = C_{\mathrm{do}} f\left(\alpha_2\right) \tag{1.31}$$

where the function $f\left(\alpha_2\right)$ that takes into account the effects arising from other dispersed phase elements is defined as:

$$f\left(\alpha_2\right) = exp(K_1\alpha_2) + \alpha_2^{K_2} \tag{1.32}$$

Such functions are obtained from experiments through curve fitting (see for e.g. Rusche and Issa (2000)).

Despite the above works on drag coefficient for high gas fraction regime, most works associated with bubbly flow simulation using two-fluid model discussed in section 1.3.3.3 employs drag coefficients based on single bubbles. This may be due to the lack of rigorous testing and validation of drag coefficient models for high gas fraction limit.

Virtual mass force (M_{VM}):

Drag force accounts for the interaction of bubble and liquid in a non-accelerating flow. However, if the bubble is accelerated part of the surrounding liquid also gets accelerated leading

to an additional force called added mass or virtual mass force. In bubble columns as the bubble rises from the inlet it undergoes acceleration, hence the virtual mass force is inevitable in the simulation of bubbly flows in bubble columns. Moreover, to improve the well-posedness of the two-fluid model discussed in chapter 2, virtual mass force is often employed in multi-phase flow calculations.

Many formulations for virtual mass force can be found in the literature (Drew, 1987), the most commonly used formulation in multi-phase flow calculations, even in commercial packages (FLUENT, OpenFOAM) is given by

$$\mathbf{F}_{\mathrm{vm}} = \alpha_{\mathrm{g}}\rho_{\mathrm{l}}C_{\mathrm{vm}}\left(\frac{\partial \mathbf{u}_{\mathrm{l}}}{\partial t} + \mathbf{u}_{\mathrm{l}}\cdot\nabla\mathbf{u}_{\mathrm{l}} - \frac{\partial \mathbf{u}_{\mathrm{g}}}{\partial t} - \mathbf{u}_{\mathrm{g}}\cdot\nabla\mathbf{u}_{\mathrm{g}}\right) \tag{1.33}$$

where, C_{vm} is the virtual mass coefficient

The virtual mass coefficient is obtained as 0.5 from the potential flow solution around a rigid spherical particle (Drew et al., 1979). Cook and Harlow (1986) used a value of 0.25 for bubbles in water, while Homsy et al. (1980) deduce a coefficient which is a function of gas fraction as given in Eqn. 1.34 using cell model.

$$C_{\mathrm{vm}} = \frac{3 - 2\alpha_2}{2\alpha_2} \tag{1.34}$$

The usage of complex functionality for virtual mass coefficient is not widely found, most works adopt a constant virtual mass coefficient of 0.5. This again may be due to the lack of rigorous testing and validation of such functions for bubbly flow simulations.

Lift force (M_{LF}):

When a bubble rises in a shear field (lateral velocity gradient) of the liquid it experiences a lateral force called lift force. This lateral force decides whether the bubble gas fraction peaks close to the wall or close to the centre of the column.

Svendsen et al. (1992) have done a good review of the lift force as below:

The lateral movement of bubbles in a bubble column is a combined effect of many forces. Factors that influence the radial movement are Bubble rotation around its own axes in a flow field (Magnus lift force), relative gas-liquid velocity and a liquid velocity gradient, viscous shear, radial pressure gradients, bubble shape changes, turbulent dispersion and phsicochemical prop-

erties like coalescence tendency. The magnus force was first described for the moderate to high Reynolds number (Re) region as discussed by Swanson (1961) as an asymmetric pressure distribution around a body created by the interaction between the flow field and the body rotation. Thomas et al. (1983) has used the theory for Re numbers around 1000, which is a region relevant for bubble columns, concluding that the force acts towards the high speed side if the bubble moves against the flow or moves with the flow but more slowly than the flow. It is toward the low speed side if the bubble moves with the flow and faster than the flow. This is confirmed for upward bubble flow by Beyerlein et al. (1985) for low gas fractions (<5 percent). However, negative lift forces have also been observed. An experimental investigation by Taneda (1957) on the Magnus force showed that in certain ranges of Re and rotational speed, rotating spheres in a uniform flow field suffer lifts having a direction opposite to those of the ordinary Magnus force. This has been confirmed by Hoglund (1962) and Swanson (1961). It was concluded that this effect can be explained by a transition of the boundary layer from laminar to turbulent flow. Both the direction and magnitude of the force depend on the local flow conditions such that using mean values of force coefficients is in reality misleading. Unfortunately, the previous research work is concentrated in two ranges of Re. Workers concerned with suspension rheology and allied topics have concentrated on motion at very low Re (for e.g. Saffman, 1965, 1968; Rubinow and Keller, 1961) while very high Re-number motion have concerned aerodynamicists and allied physicist (e.g. Hoglund, 1962 and Swanson, 1961). The gap between these two ranges is wide and experimentally uncharted. the general problem is clearly very involved, so rather ideal situations are the only ones which have been examined in any detail.

The model reported for lift force by Thomas et al. (1983) which is dependent on mean lateral velocity gradient, slip velocity and a lift coefficient C_{L}:

$$F_L = C_{\mathrm{L}} \alpha_g \alpha_l \rho_l \left(u_g - u_l\right) \frac{\partial u_l}{\partial r} \tag{1.35}$$

The value of K was calculated to be 0.5 for potential flow. The vlaue of the force also depends on the bubble size, shape and turbulence. An expression which accounts for all the

factors is modelled by Jakobsen et al. (1993)

$$F_L = K\alpha_g\rho_l\left(u_g - u_l\right)\frac{\partial u_l}{\partial r}\left(C_{\mathrm{L}} - \frac{3\mu_t C_D C_T}{4\mu_L Re_p\left(1+\frac{\tau_L}{t_p}\right)}\right) \tag{1.36}$$

where C_L was selected to be 0.5

Drag coefficient

$C_D = \frac{5.645}{Eo^{-1}+2.385}$, $d_b > 2mm$

$C_D = \frac{8}{3}\left(1-\alpha_g\right)^2$, $d_b < 2mm$

where μ_L and μ_t are molecular and eddy viscosities respectively. In the literature, equation with out the correction is used and C_{L} is tuned to match the observed hold up profile. The classical model 1.35 for the lift force predicts the force to be radially outwards in a heterogenous regime, on the contrary the force is radially inwards, hence they (Torvik and Svendsen, 1990; Svendsen et al., 1992; Grienberger and Hofmann, 1992; Hillmer et al., 1994) have to use negative lift coefficient to simulate there flow. Which questions the universality of the expression 1.35. The study of the effect of the presence of other bubbles on lift coefficient is rare. A study performed by Beyerlein et al. (1985) shows that lift coefficient has to be modelled by accounting for the presence of other dispersed phases to obtain a good prediction of holdup profile. They modelled it as:

$$C_{\mathrm{L}} = 1.65X10^{-1}\alpha_{2\mathrm{inlet}}^{-0.78} \tag{1.37}$$

where $\alpha_{2\mathrm{i}}$ is the mean inlet volume fraction of the gas. The correlation suggested by Beyerlein et al. (1985) donot depend on the local volume fraction hence, a new correlation is developed by Behzadi et al. (2001) based on the local volume fraction of the gas and is given as:

$$C_{\mathrm{L}} = 6.51X10^{-4}\alpha_2^{-1.2} \tag{1.38}$$

Wall lubrication force (M_{WL}):

When a bubble comes in close proximity to a wall a liquid film is trapped between the bubble and the wall, which results in pressure build up close to the wall. This high pressure drives the bubble away from the wall resulting in almost zero void fraction close to the wall. According to Antal et al. (1991b) there is no analytical three dimensional solution of the flow between a

bubble and a wall to describe this phenomena, hence they propose the following model from the two dimensional solution for flow between a cylinder and a wall.

$$\mathbf{F}_{\mathrm{WL}} = -C_{\mathrm{WL}}\alpha_2\rho_1|\mathbf{u}_{\mathrm{r}}^*|^2\mathbf{n} \tag{1.39}$$

where C_{WL} is a function of distance from the wall y_{w} as given in Eqn. 1.41. The force rapidly decreases as the distance from the wall increases. The vector $\mathbf{n}$ is the outward-facing unit normal at the nearest point on the wall. $\mathbf{u}_{\mathrm{r}}^*$ is the relative velocity parallel to the wall, that is

$$\mathbf{u}_{\mathrm{r}}^* = \mathbf{u}_{\mathrm{r}} - (\mathbf{u}_{\mathrm{r}} \cdot \mathbf{n})\,\mathbf{n} \tag{1.40}$$

C_{WL} is expressed as:

$$C_{\mathrm{WL}}\,(y_{\mathrm{w}}) = max\{\frac{C_{\mathrm{W1}}}{d} + \frac{C_{\mathrm{W2}}}{y_{\mathrm{w}}}, 0\} \tag{1.41}$$

The coefficients C_{W1} and C_{W2} are chosen so that C_{W1} is negative and the force vanishes for $y_{\mathrm{w}}/d > -C_{\mathrm{W2}}/C_{\mathrm{W1}}$ which is usually a few bubble diameters away from the wall.

Hydrodynamic interaction force (M_{HF}):

Hydrodynamic interaction force accounts for the hydrodynamic interaction between bubbles or the drag induced by one bubble over the other through the liquid. Our preliminary simulations (without the addition of this force) showed unphysical probability distribution of volume fraction (dotted line) of gas at high gas fraction limit (discussed in chapter 2). The addition of this force corrected the unphysical probability distribution of α_{g} by controlling the degree of segregation of gas.

$$\mathbf{F}_{\mathrm{HF}} = -C_{\mathrm{d}}\frac{\delta_{\mathrm{dis}}}{\alpha_{\mathrm{g}}\alpha_{\mathrm{l}}}\nabla\alpha_{\mathrm{g}} \tag{1.42}$$

coefficients

$$\delta_{\mathrm{dis}} = C_{\mathrm{dis}}d_{\mathrm{p}}|\mathbf{u}_{\mathrm{g}} - \mathbf{u}_{\mathrm{l}}|\sqrt{\alpha_{\mathrm{g}}\alpha_{\mathrm{l}}} \tag{1.43}$$

$$C_{\mathrm{dis}} \sim 1 \tag{1.44}$$

$$C_{\mathrm{d}} = \frac{3C_{\mathrm{s}}\rho_{\mathrm{l}}\alpha_{\mathrm{g}}|\mathbf{u}_{\mathrm{g}} - \mathbf{u}_{\mathrm{l}}|}{4d_{\mathrm{p}}} \tag{1.45}$$

Also this force is known to stabilize (Lucas et al., 2005) the bubbly flow by smoothing out the non-uniformity in the gas fraction profile. Bubble columns are known to stay stable qualitatively up to a global void fraction of 0.25 - 0.3 (Harteveld, 2005b), hence the addition of this force also contributes towards achieving that goal.

1.3.3.3 Application of two-fluid model for bubbly flow simulation

Lai and Salcudean (1987) performed simulation of bubbles rising in a stagnant liquid using two-fluid model. They simplified the two-fluid model by assuming that the gas phase momentum and viscous forces are negligible. They use the standard (std) single phase extension of the k - ϵ model to capture the effects of turbulence in the liquid phase. The calculated liquid velocity profile showed good agreement with the experimental data. However, they have not compared the gas fraction profile with the experiment in their study.

Schwarz and Turner (1988) used the two-fluid model coupled with the std k - ϵ model to simulate a gas stirred bath. They found that a k - ϵ model with the standard constants for single phase flows works well, if a sufficiently accurate two-fluid model (like for e.g. separate momentum equation has to be solved for each phase and no assumptions should be made about the hold up) is used. The compared Liquid velocities and turbulent kinetic energy with the experimental data showed good agreement, but there is no comparison of void fraction reported in the work. In comparison to Lai and Salcudean (1987) and Schwarz and Turner (1988) works where drag was the only inter-phase force considered, Torvik and Svendsen (1990), Jakobsen et al. (1993) and Grevscott et al. (1996) have used two-fluid model with inter-phase forces lift and virtual mass force along with drag to simulate the bubble column operating in homogenous and transition regime. The turbulence in the flow was captured by the extended k - ϵ model similar to the works (Lai and Salcudean, 1987; Schwarz and Turner, 1988). Also, Jakobsen et al., (1993) and Grevscott et al., (1996) used a correlation for predicting the bubble size distribution and coupled it with the drag force appearing in the Euler-Euler model, based on the assumption that bubble size is proportional to the turbulent eddy size.

$$d_p = C_{sm}\left(\frac{k^{3/2}}{\epsilon}\right) \tag{1.46}$$

where C_{sm} is an empirical parameter obtained from the experiments. They observed a good prediction of liquid velocity, volume fraction and turbulence with the experiments.

Celik and Wang (1994) used two-fluid model to study the circulation in a bubble column with only drag force as the interphase force. There main objective was to study the impact of prescribed and predicted gas fraction on the flow. They concluded that the predicted gas fraction profile gives much better results than the prescribed gas fraction profile.

Ranade (1997) developed a computational model for predicting flows in bubble columns within two-fluid model framework by adding two source terms in the momentum equation along with drag and lift. The first source term accounts for the correlation generated due to drag on time averaging and the other source term accounts for the contribution of liquid wakes on the slip velocity. The source term added was a function of radial volume fraction gradien, radial velocity gradient and the turbulent diffusivity.

$$S = K\rho_l\nu_t\frac{\partial\alpha_g}{\partial r}\frac{\partial V_{gz}}{\partial r} \tag{1.47}$$

They used a std single phase k - ϵ model without any additional source terms accounting for the production of turbulent kinetic energy due to bubbles, under the assumption, that the turbulent kinetic energy produced due to the bubbles is balanced by the dissipation at the bubble surface (Kataoka and Serizawa, 1989). Their model showed good agreement in the prediction of velocity and holdup with experiments for both homogenous and heterogenous regime.

Sokolichin and Eigenberger (1994a) modelled gas-liquid flow in bubble columns with two-fluid model. They found out that no steady state solution for uniformly aerated bubble columns can be obtained above a certain gas velocity for very fine grid. If one attempts to refine the grid above 20x20 grid points the numerical code diverges since the steady state equations are not able to describe the dynamic local phenomena. This seems to be the reason why in all (Torvik and Svendsen, 1990; Grienberger and Hofmann, 1992; Svendsen et al., 1992; Jakobsen

et al., 1993; Hillmer et al., 1994) works the space grid did not exceed more than 20 x 20 grid points.

From the literature, it is evident that Euler-Euler approach predicts the averaged liquid velocity profile in the bubble column reasonably well. However, the holdup was not accurately predicted according to the experiment. Though the models proposed by (Ranade, 1997; Torvik and Svendsen, 1990; Jakobsen et al., 1993) improved the holdup prediction, it is tested only for low gas fraction and low inlet gas velocity. The improvement in these models were achieved due to the improved modelling of turbulence and the inclusion of the algebraic model for the bubble size dependence. At high gas fraction and inlet gas velocity, the turbulence and the variation of bubble size is predominant. Hence it is important to provide improved models (not just the std k-ϵ model for single phase flow) accounting for turbulence and bubble size change to accurately model the complex multi-phase flow for better prediction of parameters like gas holdup.

1.4 Turbulence in bubbly flows and modeling

Bubbly flows encountered in industrial systems often operate in turbulent conditions due to the high gas fractions involved. Turbulence in these flows control the phase distribution in these systems (Chahed et al., 2003b) thereby influencing the heat and mass transfer properties. Hence, an accurate prediction of turbulence is important to properly quantify the heat and mass transfer in these systems.

Multi-fluid models such as Euler-Lagrange (Delnoij et al., 1997a) and Euler-Euler (Drew, 1983a) discussed in the previous sections can be used to predict turbulent flows in these systems, however these models are restricted to small scale systems (e.g. laboratory bubble column). The computational effort involved in predicting such flows in the large scale systems (e.g. industrial bubble column) using these models is very high due to the presence of wide range of turbulent scales. To reduce the computational load one has to capture the large scale turbulent motion through multi-fluid models and add the effects of small scales through sub-grid scale models.

The sub-grid scale turbulence modeling associated with bubbly flows is a challenging task due to the additional mode of turbulence production due to the bubbles, which introduces additional scales along with the existing scales of turbulence due to the shear induced turbulence (SIT). This bubble induced turbulence (BIT) or turbulence due to the bubbles is generated due to the interphase forces at the mesoscale ($l \sim d_{\mathrm{p}}$) and the turbulence in the wakes, formed due to the boundary layer separation on the bubbles at the microscale ($l << d_{\mathrm{p}}$). The production of turbulence at the microscale due to the wake formation is of the order of $Re_{\mathrm{p}}^{-1/2}$ (Biesheuvel and Wijngaarden, 1984), where Re_{p} is the bubble Reynolds number $\frac{d_{\mathrm{p}} v_{\mathrm{r}} \rho}{\mu}$. The microscale turbulence could be neglected for bubbly flows with moderate bubble Reynolds number ($200 < Re_{\mathrm{p}} < 500$) encountered in engineering applications. However, the turbulence induced due to the bubbles at the mesoscale level due to the interphase coupling could be significant and has to be modelled appropriately.

The significance of BIT is pointed out by several authors (Lance and Bataille, 1991; Liu and Bankoff, 1993a; Shawkat and Ching, 2011) in modifying the liquid turbulence characteristics by altering the mechanisms of production, redistribution and dissipation of turbulence. Furthermore, the recent review of Balachandar and Eaton (2010) on turbulent disperse flow indicate the modification of phase distribution due to the turbulence instabilities caused due to the presence of bubbles.

Hence, while developing turbulence models for bubbly flows, the incorporation of effects due to SIT, BIT and its interactions is essential for accurate prediction of turbulent bubbly flows. A literature review is performed in the next section on the current state of turbulence models available in the literature to predict SIT and BIT in bubbly flows, by keeping in mind the importance of interactions between BIT and SIT.

Many investigators who have studied the turbulent bubbly flows in the literature have neglected BIT (Torvik and Svendsen, 1990; Grienberger and Hofmann, 1992; Ranade, 1992; Hillmer et al., 1994) and modelled only the SIT using single phase turbulence models. The investigators (Svendsen et al., 1992; Thakre et al., 1999) who have added the BIT on an extended framework of single phase turbulence model and derived a multiphase turbulence model (Kataoka and Serizawa, 1989; Ranade, 1997; Lahey, 1990a; Chahed et al., 2003a) by Reynolds

averaging (Pope, 2000) the instantaneous multiphase flow equations have not rigorously accounted for the BIT production due to each interphase force (Drew, 1983a). A good account of these models present in the literature for predicting turbulence in bubbly flows are given in chapter 4.

1.5 Thesis layout

Chapter 2 provides a brief introduction of the ill-posed nature of the two-fluid model and the methods involved in the literature to resolve the ill-posedness. Discusses a new inter-phase force model which accounts for the hydrodynamic effects of the bubbly flows and also corrects the ill-posedness of the two-fluid model. Discusses hyperbolicity analysis on the two-fluid model with the inter-phase sub-model. Additionally, the chapter contains the CFD study on 1D falling liquid mixture and 2D bubble column with the well-posed two-fluid model to asses the effect of the model in real physical systems.

Chapter 3 provides a brief introduction of the isotropic turbulence models (k-ϵ, k-ω). Furthermore, the chapter discusses the formulation of an ad-hoc k-ω model. Additionally, the chapter discusses the performance of the formulated k-ω model with other isotropic multiphase turbulence models for predicting the flow inside the bubble columns and vertical pipes.

Chapter 4 discusses different techniques to obtian multi-phase turbulence data through simulations and experiments and its weaknesses. provides steps followed to obtain a new multi-phase RST (Reynolds Stress Transport) model from the multi-phase flow equations or two-fluid model. The chapter discusses the the unclosed terms generated after the formulation of the RST model and the models available in the literature to close the terms and the terms for which models are not available. The chapter contains the details of the mesoscale DNS and the budget obtain through the simulation for the momentum and the turbulence energy. Furthermore, the chapter discusses the significance of each terms appearing in the derived momentum and RST equations.

Chapter 5 discusses the current multi-phase turbulence models and its weaknesses. Furthermore, the chapter discuss about the Reynolds stress model developed from the mesoscale DNS data in chapter 3.

CHAPTER 2. HYPERBOLICITY OF TWO-FLUID MODEL

This chapter is modified from a paper submitted
to *Applied Mathematical Modeling Journal*
N. Panicker, A. Passalacqua, R.O. Fox

2.1 Abstract

The hyperbolicity condition of the system of partial differential equations (PDEs) of the incompressible two-fluid model, applied to gas–liquid flows, is investigated. It is shown that the addition of a dispersion term, which depends on the drag coefficient and the gradient of the gas volume fraction, is required to ensure the hyperbolicity of the PDEs, and to prevent the nonphysical onset of instabilities in the predicted multiphase flows upon grid refinement. A constraint to be satisfied by the coefficient of the dispersion term to ensure hyperbolicity is obtained. The effect of the dispersion term on the numerical solution and on its grid convergence is then illustrated with numerical experiments in a one-dimensional shock tube, in a column with a falling fluid, and in a two-dimensional bubble column.

2.2 Introduction

The two-fluid model (Drew, 1971, 1983b,a; Jackson, 1997) probably represents the most widely adopted approach to describe the spatial and temporal evolution of gas–liquid flows in systems of practical relevance, due to its moderate computational cost. For this reason, the correct formulation of the model has been subject of several studies, which aimed, on one hand, to ensure the desired mathematical property of hyperbolicity of the model equations, and, on the other hand, to appropriately incorporate the description of physical phenomena experimentally observed in bubbly flows. In particular, the numerical stability of the solution

obtained from the two-fluid model depends on the characteristics of the underlying equations, which, as shown in Stuhmiller (1977); Lyczkowski et al. (1978); Stewart (1979), may be complex. In such a case, the discretized equations do not allow a grid-converged solution to be achieved, and unstable modes in the solution appear, severely affecting the model prediction and its sensitivity to grid refinement. Several approaches were suggested in the literature to address this problem. Stuhmiller (1977) observed that the addition of a certain amount of dissipation mitigates the problem for a specific grid resolution. Ramshaw and Trapp (1978) proposed to address the problem of complex characteristics with the introduction of surface tension effects. Stewart (1979) provided a criterion for the grid resolution that ensures the well-posedness of two-fluid problem, relating the minimum grid size to a multiple of the bubble radius. Sursock (1982) demonstrated that real characteristics of the two-fluid equations are a necessary condition in order not to violate the causality requirement. In particular, his work shows that, when the two-fluid equations have complex characteristics, it is necessary to know all the values at the solution at future times $t > t_i$, in order to determine an accurate solution at an arbitrary time t_i. Such a result clearly violates the physical constraint of causality, and highlights the importance of ensuring that the mathematical model is hyperbolic. Based on these observations, several researchers proposed modified version of the two-fluid model that guarantee hyperbolicity under certain conditions. Fitt (1989); Tiselj and Petelin (1997); Dinh et al. (2003) performed numerical regularization of the ill-posed equation, which, however, comes at the expense of accuracy, since it relies on the addition of numerical dissipation.

Several investigators (Stuhmiller, 1977; Bestion, 1990; Ramshaw and Trapp, 1978; Banerjee and Chan, 1980; Ransom and Hicks, 1984; Saurel and Abgrall, 1999; Lee et al., 1998; Chung et al., 2001) ensured the hyperbolicity of the two-fluid model by introducing an pressure term in the phase momentum equation. Stuhmiller (1977) assumed the same mean bulk pressure P_k in both the phases and added an interface pressure term $(p_{\mathrm{ki}} - P_{\mathrm{k}})\,\nabla\alpha$, where p_{ki} is the interface pressure for phase k, in order to make the two-fluid model hyperbolic. He considered the interface pressures p_{ki} for both the phases to be equal, and modeled them based on the analytical solution of pressure distribution around an isolated sphere (Lamb, 1932). Bestion (1990) used an interface pressure term $p_{\mathrm{i}}\nabla\alpha$, where, differently from Stuhmiller (1977), p_i is

a coefficient determined to ensure the hyperbolicity of the set of equations, without physical justification. Tiselj and Petelin (1997) pointed out that the addition of this term is controversial, as shown by Sha and Soo (1979).

Ramshaw and Trapp (1978) ensured that the two-fluid model has real characteristics by assuming the mean bulk pressures in both the phases to be different. These pressures were related through the Laplace constraint, in which, the surface tension coefficient is found mathematically through linear stability analysis. In the works of Banerjee and Chan (1980); Ransom and Hicks (1984); Saurel and Abgrall (1999); Lee et al. (1998); Chung et al. (2001) the two-fluid model is made hyperbolic using a two-pressure formulation for compressible two-phase flows, where pressures in each phases are computed using an equation of state. However, these authors follow different approaches to model the interface pressure term $(p_{\mathrm{ki}} - P_{\mathrm{k}})\,\nabla\alpha$. Banerjee and Chan (1980); Ransom and Hicks (1984) assumed the interface pressures p_{ki} to be equal. Their model is valid only for stratified flows, and it requires an additional transport equation for the volume fraction in terms of the interface velocity to close the set of equations. Saurel and Abgrall (1999) considered equal interface pressures, and calculated them as a function of the mixture pressure. The works of Chung et al. (2001); Lee et al. (1998) modeled the interface pressure coefficient $(p_{\mathrm{ki}} - P_{\mathrm{k}})$ in both the phases in terms of the surface tension and bulk modulus.

Hancox et al. (1980); Cheng et al. (1985) performed an analysis of wave propagation in bubbly flows, and found a significant effect of the virtual mass term on the dispersion of waves in these flows. Thorley and Wiggert (1985); Chung et al. (2001) confirmed that the two-fluid model with virtual mass term admits complex characteristics. In order to ensure the hyperbolicity of the model equations, they proposed the introduction of an interfacial pressure jump term, directly proportional to the surface tension between the phases. The resulting model with virtual mass and interfacial pressure jump resulted to be hyperbolic, but the wave dispersion may become excessive, depending on the value of the coefficient used in the virtual mass model. A detailed study of the pressure forces in disperse two-phase flows can be found in Prosperetti and Jones (1984). Jones and Prosperetti (1985) studied the stability of a two-fluid model containing only first-order differential terms and algebraic closures, showing that the

stability properties of the model do not depend on the wavelength of the perturbation, which is unphysical. Their study was extended in Prosperetti and Jones (1984) to incorporate the effect of terms with derivatives of arbitrary order. However, the authors of this study concluded that the introduction of these terms is ineffective at improving the long-wavelength stability of the hyperbolic two-fluid model containing only first-order differential terms.

Biesheuvel and Gorissen (1990) analyzed the stability of a uniform suspension of bubbles, identifying a critical value of volume fraction below which the suspension is stable. This result is confirmed experimentally by the work of Harteveld (2005a), who performed experiments in of air injection in bubble columns. The standard two-fluid model, however, predicts flow instabilities also in these conditions.

Davidson (1990) modeled the interfacial momentum transfer term in the two-fluid model including a dispersion term proportional to the drag coefficient and to the gradient of the gas volume fraction, and an interfacial pressure jump based on the work of Pauchon and Banerjee (1986); Stuhmiller (1977). Davidson defined the dispersion coefficient as a function of the turbulent eddy viscosity. Tiselj and Petelin (1997) enforced the hyperbolicity of the two-fluid equations by modifying the virtual mass coefficient as a function of the volume fraction and of the density ratio of the phases, obtained assuming the multiphase mixture is incompressible. Song and Ishii (2001) studied the hyperbolicity, and the consequent stability of the two-fluid model in terms of the momentum flux parameters they introduced in the model to incorporate the effect of void fraction and phase velocities. The hyperbolicity condition was then determined to identify when the model equation are *stable*, in a mathematical sense, for specific flow conditions.

Syamlal (2011) investigated the hyperbolicity of the two-fluid model for gas–particle systems, and proposed a modification of the form of the buoyant term to incorporate the effect of the relative motions of the phases. His development is based on the observation made by Bouillard et al. (1989), who attributed the origin of the complex characteristics of the two-fluid equations to the buoyancy term. However, for gas–particle systems the compressible particle phase has a separate pressure related to the granular temperature, which is often sufficient to ensure that the resulting two-fluid model is hyperbolic.

More recently Picardi et al. (2016) tried to define a criterion for the grid resolution to avoid the numerical difficulties. Their study, however, did not account for the required momentum exchange terms to properly describe bubbly flows, and did not study the hyperbolicity of the model equations. It is worth observing at this point that approaches that define a minimum grid resolution to ensure that a solution of the model can be obtained do not address the actual challenge of formulating a model that allows a grid-converged solution to be achieved. The constraint on the grid resolution, on one hand, relates a purely numerical aspect of solution procedure to a physical parameter, typically the bubble radius, which has been removed from the equations by means of the averaging procedure. On the other hand, it introduces an arbitrary limit to the spatial scales that can be resolved. As a consequence, a formulation of the two-fluid model that allows a solution to be achieved on an arbitrarily fine grid should be preferred.

In the present work, we investigate the hyperbolicity of the two-fluid equations examining the role of momentum transfer terms in ensuring this condition. We focus our attention on a dispersion term analogous to the one proposed by Davidson (1990). Differently from Davidson, however, we argue that such a dispersion term should be present also when laminar bubbly flows are considered, since it describes the effect on the drag acting on one bubble due to the disturbances in the flow caused by the presence of other bubbles. We propose a closure based on the considerations of Batchelor (1988); Biesheuvel and Gorissen (1990), with a dispersion coefficient determined to ensure the hyperbolic nature of the two-fluid equations. We demonstrate that the introduction of this dispersion term allows the hyperbolicity of the two-fluid model, and its grid convergence, to be ensured without introducing a second pressure term, whose physical justification is not always clear, in particular in the case of incompressible phases.

The remainder of this article is organized as follows: in Sec. 2.3 the equations of the two-fluid model and the constitutive equations used as closure are summarized. In Sec. 2.4 the hyperbolicity of the one-dimensional form of the model is investigated, and a constraint on the dispersion coefficient to ensure the hyperbolic nature of the equations is determined. Sec. 2.6 illustrates an application to a one-dimensional shock tube problem, where the role of the dispersion term in preventing unphysical behavior with grid refinement is demonstrated.

The effectiveness of the proposed modification is further tested with numerical experiments performed in a column with falling liquid, with progressively finer grid resolutions, as shown in Sec. 2.7. Finally, an example application to a two-dimensional bubble column is illustrated in Sec. 2.8, showing how the addition of the dispersion term removes nonphysical oscillations in the flow, without compromising the experimentally observed fluctuations of the gas plume.

2.3 Equations of the two-fluid model for bubbly flows

The equations of the two-fluid model typically used to describe the evolution of gas–liquid systems (Drew, 1971, 1983a,b) are summarized in this section, since they are the base of the study discussed in this work, and they are used to perform the numerical experiments here described.

The continuity equation for the generic phase φ is

$$\frac{\partial}{\partial t}\left(\alpha_\varphi \rho_\varphi\right) + \nabla \cdot \left(\alpha_\varphi \rho_\varphi \mathbf{U}_\varphi\right) = 0, \tag{2.1}$$

where α_φ is the phase fraction, ρ_φ is the thermodynamic density of the phase, and $\mathbf{U}_\varphi$ is the phase velocity.

The phase momentum equation for the liquid phase is

$$\frac{\partial}{\partial t}\left(\alpha_\mathrm{l} \rho_\mathrm{l} \mathbf{U}_\mathrm{l}\right) + \nabla \cdot \left(\alpha_\mathrm{l} \rho_\mathrm{l} \mathbf{U}_\mathrm{l} \otimes \mathbf{U}_\mathrm{l}\right) = \nabla \cdot \boldsymbol{\tau}_\mathrm{l} - \alpha_\mathrm{l} \nabla p + \alpha_\mathrm{l} \rho_\mathrm{l} \mathbf{g} + \mathbf{M}_\mathrm{gl}, \tag{2.2}$$

while for the gas phase

$$\frac{\partial}{\partial t}\left(\alpha_\mathrm{g} \rho_\mathrm{g} \mathbf{U}_\mathrm{g}\right) + \nabla \cdot \left(\alpha_\mathrm{g} \rho_\mathrm{g} \mathbf{U}_\mathrm{g} \otimes \mathbf{U}_\mathrm{g}\right) = \nabla \cdot \boldsymbol{\tau}_\mathrm{g} - \alpha_\mathrm{g} \nabla p + \alpha_\mathrm{g} \rho_\mathrm{g} \mathbf{g} + \mathbf{M}_\mathrm{lg}, \tag{2.3}$$

where $\boldsymbol{\tau}_\varphi$ is the phase stress tensor, p is the shared pressure, $\mathbf{g}$ the gravitational acceleration vector, $\mathbf{M}_\mathrm{gl} = -\mathbf{M}_\mathrm{lg}$ is the momentum exchange term, except for buoyancy which is included in the shared pressure. This last term is computed as the sum of the drag $\mathbf{M}_\mathrm{D}$, lift $\mathbf{M}_\mathrm{L}$, virtual mass $\mathbf{M}_\mathrm{VM}$, wall-lubrication $\mathbf{M}_\mathrm{WL}$, and dispersion forces $\mathbf{M}_\mathrm{dis}$. For the purpose of this work, we focus our attention on the drag, virtual mass and dispersion terms because they will be subject of the hyperbolicity study in Sec. 2.4. We should note that the closure for the phase stress tensor introduces second-order spatial derivatives, which do not affect the hyperbolicity

of the system. Thus, in Sec. 2.4 the $\boldsymbol{\tau}_\varphi$ are set to zero. Stress tensors are, however, preserved in the numerical implementation, and a Newtonian behavior is assumed for each of the phases.

The drag term is defined as $\mathbf{M}_\mathrm{D} = K\mathbf{U}_\mathrm{r}$, where $K = \alpha_\mathrm{g}\rho_\mathrm{l}\beta$, $\mathbf{U}_\mathrm{r}$ is the slip velocity, and

$$\beta = \frac{3}{4}\frac{|\mathbf{U}_\mathrm{r}|}{d_\mathrm{p}}C_\mathrm{s}, \tag{2.4}$$

with C_s the drag coefficient. The virtual mass term is defined, following Drew and Lahey (1987), as

$$\mathbf{M}_\mathrm{VM} = C_\mathrm{VM}\alpha_\mathrm{g}\rho_\mathrm{l}\left(\frac{\mathrm{D}\mathbf{U}_\mathrm{l}}{\mathrm{D}t} - \frac{\mathrm{D}\mathbf{U}_\mathrm{g}}{\mathrm{D}t}\right), \tag{2.5}$$

where

$$\frac{\mathrm{D}\mathbf{U}_\varphi}{\mathrm{D}t} = \frac{\partial\mathbf{U}_\varphi}{\partial t} + \mathbf{U}_\varphi\cdot\nabla\mathbf{U}_\varphi \tag{2.6}$$

is the material derivative of the velocity of phase φ. Finally, the bubble dispersion term $\mathbf{M}_\mathrm{dis}$, which modifies the slip velocity in the drag term, is defined as

$$\mathbf{M}_\mathrm{dis} = \frac{\rho_\mathrm{l}\beta\delta_\mathrm{dis}}{\alpha_\mathrm{l}}\nabla\alpha_\mathrm{g}, \tag{2.7}$$

with dispersion coefficient (Batchelor, 1988; Biesheuvel and Gorissen, 1990)

$$\delta_\mathrm{dis} = C_\mathrm{dis}d_\mathrm{p}|\mathbf{U}_\mathrm{r}|\sqrt{\alpha_\mathrm{g}\alpha_\mathrm{l}}. \tag{2.8}$$

Here, C_dis is a parameter whose value will be investigated in the next section, and is linked to the hyperbolicity of the two-fluid equations. The dispersion term in Eq. (2.7) in unrelated to the pressure difference between phases but, instead, arises due to the presence of bubble-bubble interaction through the fluid phase.

It was observed in the introduction that some authors (Davidson, 1990) used a term formally similar to the one of Eq. (2.7), but related it to the dispersion of the gas phase caused by turbulent fluctuations. However, it is known (Faxén, 1922) that, also in the case of purely laminar flows, the drag force acting on each bubble is affected by the disturbances induced in the liquid-phase velocity field by the other bubbles. This effect is typically neglected in the two-fluid model, where the momentum transfer term due to drag only accounts for the mean drag, often modeled with closures describing the force acting on an isolated sphere in an undisturbed flow field. The introduction of the dispersion term in Eq. (2.7) allows the effect

of the disturbances in the flow field due to the presence of other bubbles to be taken into account, which results in a modified slip velocity in the drag term. In the next section we will illustrate the role of this dispersion term in ensuring the hyperbolicity of the equations of the two-fluid model, and we will relate the dispersion coefficient to the drag coefficient through the hyperbolicity condition.

2.4 Study of the hyperbolicity of the one-dimensional two-fluid model

We study in this section the hyperbolicity of the set of PDEs describing the evolution of the gas and liquid phase in a gas–liquid system. To this purpose, we consider the one-dimensional two-fluid model, writing its equations in non-conservative form.

The phase continuity equation for the gas phase then reads

$$\frac{\partial \alpha_{\mathrm{g}}}{\partial t} + U_{\mathrm{g}} \frac{\partial \alpha_{\mathrm{g}}}{\partial x} + \alpha_{\mathrm{g}} \frac{\partial U_{\mathrm{g}}}{\partial x} = 0, \tag{2.9}$$

while, for the liquid phase, it is

$$\frac{\partial \alpha_{\mathrm{l}}}{\partial t} + U_{\mathrm{l}} \frac{\partial \alpha_{\mathrm{l}}}{\partial x} + \alpha_{\mathrm{l}} \frac{\partial U_{\mathrm{l}}}{\partial x} = 0. \tag{2.10}$$

Similarly, we consider the phase momentum equations in non-conservative form, including the momentum coupling terms due to drag, virtual-mass and dispersion forces. We then have, for the gas phase,

$$\begin{aligned} \alpha_{\mathrm{g}} \left(\rho_{\mathrm{g}} + C_{\mathrm{VM}} \rho_{\mathrm{l}}\right) \frac{\partial U_{\mathrm{g}}}{\partial t} - \alpha_{\mathrm{g}} C_{\mathrm{VM}} \rho_{\mathrm{l}} \frac{\partial U_{\mathrm{l}}}{\partial t} \\ + \frac{\rho_{\mathrm{l}} \beta \delta_{\mathrm{dis}}}{\alpha_{\mathrm{l}}} \frac{\partial \alpha_{\mathrm{g}}}{\partial x} + \alpha_{\mathrm{g}} \frac{\partial p}{\partial x} + \alpha_{\mathrm{g}} U_{\mathrm{g}} \left(\rho_{\mathrm{g}} + C_{\mathrm{VM}} \rho_{\mathrm{l}}\right) \frac{\partial U_{\mathrm{g}}}{\partial x} \\ - \rho_{\mathrm{l}} \alpha_{\mathrm{g}} U_{\mathrm{l}} C_{\mathrm{VM}} \frac{\partial U_{\mathrm{l}}}{\partial x} = -\alpha_{\mathrm{g}} \rho_{\mathrm{l}} \beta \left(U_{\mathrm{g}} - U_{\mathrm{l}}\right) + \alpha_{\mathrm{g}} \rho_{\mathrm{g}} g, \end{aligned} \tag{2.11}$$

and for the liquid phase

$$\begin{aligned} \rho_{\mathrm{l}} \left(1 - \alpha_{\mathrm{g}} + C_{\mathrm{VM}} \alpha_{\mathrm{g}}\right) \frac{\partial U_{\mathrm{l}}}{\partial t} - \alpha_{\mathrm{g}} C_{\mathrm{VM}} \rho_{\mathrm{l}} \frac{\partial U_{\mathrm{g}}}{\partial t} \\ - \frac{\rho_{\mathrm{l}} \beta \delta_{\mathrm{dis}}}{\alpha_{\mathrm{l}}} \frac{\partial \alpha_{\mathrm{g}}}{\partial x} + \left(1 - \alpha_{\mathrm{g}}\right) \frac{\partial p}{\partial x} - \alpha_{\mathrm{g}} U_{\mathrm{g}} C_{\mathrm{VM}} \rho_{\mathrm{l}} \frac{\partial U_{\mathrm{g}}}{\partial x} \\ + \left[\rho_{\mathrm{l}} \left(1 - \alpha_{\mathrm{g}}\right) U_{\mathrm{l}} + \alpha_{\mathrm{g}} U_{\mathrm{l}} C_{\mathrm{VM}} \rho_{\mathrm{l}}\right] \frac{\partial U_{\mathrm{l}}}{\partial x} \\ = \alpha_{\mathrm{g}} \rho_{\mathrm{l}} \beta \left(U_{\mathrm{g}} - U_{\mathrm{l}}\right) + \left(1 - \alpha_{\mathrm{g}}\right) \rho_{\mathrm{l}} g. \end{aligned} \tag{2.12}$$

For the purpose of the hyperbolicity study, we rewrite the model equations in matrix form

$$\mathbf{A}\frac{\partial \mathbf{X}}{\partial t} + \mathbf{B}\frac{\partial \mathbf{X}}{\partial x} = \mathbf{C}, \tag{2.13}$$

where the vector $\mathbf{X}$ is defined as

$$\mathbf{X} = \left[\alpha_{\mathrm{g}}, p, U_{\mathrm{g}}, U_{\mathrm{l}}\right]^{\mathrm{T}}, \tag{2.14}$$

and the matrices $\mathbf{A}$, $\mathbf{B}$ and $\mathbf{C}$ are

$$\mathbf{A} = \begin{bmatrix} 1 & 0 & 0 & 0 \\ -1 & 0 & 0 & 0 \\ 0 & 0 & \alpha_{\mathrm{g}}\left(\rho_{\mathrm{g}} + C_{\mathrm{VM}}\rho_{\mathrm{l}}\right) & -\alpha_{\mathrm{g}} C_{\mathrm{VM}}\rho_{\mathrm{l}} \\ 0 & 0 & -\alpha_{\mathrm{g}} C_{\mathrm{VM}}\rho_{\mathrm{l}} & \rho_{\mathrm{l}}\left(1 - \alpha_{\mathrm{g}} + \alpha_{\mathrm{g}} C_{\mathrm{VM}}\right) \end{bmatrix}, \tag{2.15}$$

$$\mathbf{B} = \begin{bmatrix} U_{\mathrm{g}} & 0 & \alpha_{\mathrm{g}} & 0 \\ -U_{\mathrm{l}} & 0 & 0 & 1 - \alpha_{\mathrm{g}} \\ \frac{\rho_{\mathrm{l}}\beta\delta_{\mathrm{dis}}}{\alpha_{\mathrm{l}}} & \alpha_{\mathrm{g}} & \alpha_{\mathrm{g}} U_{\mathrm{g}}\left(\rho_{\mathrm{g}} + C_{\mathrm{VM}}\rho_{\mathrm{l}}\right) & -\rho_{\mathrm{l}}\alpha_{\mathrm{g}} u_{\mathrm{l}} C_{\mathrm{VM}} \\ -\frac{\rho_{\mathrm{l}}\beta\delta_{\mathrm{dis}}}{\alpha_{\mathrm{l}}} & 1 - \alpha_{\mathrm{g}} & -\alpha_{\mathrm{g}} U_{\mathrm{g}} C_{\mathrm{VM}}\rho_{\mathrm{l}} & \rho_{\mathrm{l}}\left(1 - \alpha_{\mathrm{g}}\right) U_{\mathrm{l}} + \alpha_{\mathrm{g}}\rho_{\mathrm{l}} U_{\mathrm{l}} C_{\mathrm{VM}} \end{bmatrix}, \tag{2.16}$$

and

$$\mathbf{C} = \begin{bmatrix} 0 \\ 0 \\ \alpha_{\mathrm{g}}\rho_{\mathrm{g}} g - \alpha_{\mathrm{g}}\rho_{\mathrm{l}}\beta\left(U_{\mathrm{g}} - U_{\mathrm{l}}\right) \\ \left(1 - \alpha_{\mathrm{g}}\right)\rho_{\mathrm{l}} g + \alpha_{\mathrm{g}}\rho_{\mathrm{l}}\beta\left(U_{\mathrm{g}} - U_{\mathrm{l}}\right) \end{bmatrix}. \tag{2.17}$$

In order to study the effect of momentum exchange terms on the hyperbolic nature of Eq. (2.13), we find the characteristic polynomial associated to Eq. (2.13), defined by

$$|\mathbf{A}\lambda - \mathbf{B}| = 0. \tag{2.18}$$

The roots of Eq. (2.18) are real if

$$b^2 - 4ac \geq 0, \tag{2.19}$$

with

$$a = \alpha_{\mathrm{g}}\left[2\alpha_{\mathrm{g}}\rho_{\mathrm{g}} + \alpha_{\mathrm{g}}^2\rho_{\mathrm{l}} - \left(\rho_{\mathrm{g}} + \rho_{\mathrm{g}}\alpha_{\mathrm{g}}^2 + \rho_{\mathrm{l}}\alpha_{\mathrm{g}} + \rho_{\mathrm{l}} C_{\mathrm{VM}}\right)\right], \tag{2.20}$$

$$b = 2\alpha_{\mathrm{g}}\rho_{\mathrm{g}}U_{\mathrm{g}}\left(1-2\alpha_{\mathrm{g}}\right) + 2\alpha_{\mathrm{g}}^{2}\rho_{\mathrm{l}}U_{\mathrm{l}}\left(1+C_{\mathrm{VM}}\right) + 2\alpha_{\mathrm{g}}^{3}\left(\rho_{\mathrm{g}}U_{\mathrm{g}}-\rho_{\mathrm{l}}U_{\mathrm{l}}\right) + 2C_{\mathrm{VM}}\rho_{\mathrm{l}}\alpha_{\mathrm{g}}U_{\mathrm{g}}\left(1-\alpha_{\mathrm{g}}\right), \quad (2.21)$$

and

$$c = \beta\delta_{\mathrm{dis}}\rho_{\mathrm{l}}\alpha_{\mathrm{g}} + \rho_{\mathrm{g}}U_{\mathrm{g}}^{2}\alpha_{\mathrm{g}}\left(2\alpha_{\mathrm{g}}-1\right) + \alpha_{\mathrm{g}}^{2}\rho_{\mathrm{l}}U_{\mathrm{l}}^{2}\left(\alpha_{\mathrm{g}}-1\right) + C_{\mathrm{VM}}\alpha_{\mathrm{g}}^{2}\rho_{\mathrm{l}}\left(U_{\mathrm{g}}^{2}-U_{\mathrm{l}}^{2}\right) - \alpha_{\mathrm{g}}^{3}\rho_{\mathrm{g}}U_{\mathrm{g}}^{2} - C_{\mathrm{VM}}\alpha_{\mathrm{g}}\rho_{\mathrm{l}}U_{\mathrm{g}}^{2}. \quad (2.22)$$

The hyperbolicity condition $b^2 - 4ac \geq 0$ leads to the following inequality:

$$\frac{3}{4}C_{\mathrm{s}}C_{\mathrm{dis}} \geq \frac{\sqrt{\alpha_{\mathrm{g}}\left(1-\alpha_{\mathrm{g}}\right)}\left[\rho_{\mathrm{g}}\left(1-\alpha_{\mathrm{g}}\right)+\rho_{\mathrm{l}}C_{\mathrm{VM}}\right]\left(1-\alpha_{\mathrm{g}}+C_{\mathrm{VM}}\right)}{\rho_{\mathrm{l}}\alpha_{\mathrm{g}}\left(1-\alpha_{\mathrm{g}}\right)+\rho_{\mathrm{g}}\left(1-\alpha_{\mathrm{g}}\right)^{2}+\rho_{\mathrm{l}}C_{\mathrm{VM}}}, \quad (2.23)$$

where equality identifies the curve of the minimum value of the dispersion coefficient C_{dis} that ensures the system of PDEs in Eq. (2.13) is hyperbolic.

An example of the hyperbolicity curve for a case with large density ratio ($\rho_{\mathrm{l}} \gg \rho_{\mathrm{g}}$) is shown in Fig. 2.1, where the virtual mass coefficient is set to $C_{\mathrm{VM}} = 0.5$ (Drew and Lahey, 1987), and the drag coefficient is set to the constant value $C_{\mathrm{s}} = 0.44$, obtained for a spherical bubble when the Reynolds number based on the slip velocity between the phases is $\mathrm{Re} > 1000$.

The behavior of the curve allows to conclude that, depending on the local value of the gas volume fraction, assuming $\mathrm{Re} > 1000$, the coefficient of the dispersion term in Eq. (2.8) must be $C_{\mathrm{dis}} \in [0.2, 1.2]$ to ensure that the PDEs that define the two-fluid model are hyperbolic. In particular, in no case the dispersion term can be removed from the phase momentum equations for any value of the gas-phase fractions, because this would cause Eq. (2.13) not to be hyperbolic, leading to nonphysical predictions. This is demonstrated in the numerical experiments discussed in the following sections. To conclude the mathematical analysis, we examine a few special cases that occur when some of the momentum exchange effects are not taken into account:

- If $C_{\mathrm{VM}} = 0$ and $C_{\mathrm{dis}} = 0$, Eq. (2.18) admits real roots if, and only if, the slip velocity between the phases $U_{\mathrm{g}} - U_{\mathrm{l}}$ is null. This allows us to conclude that the equations of the two-fluid model in Eq. (2.13) are never hyperbolic if the momentum coupling term only accounts for the drag force without dispersion.

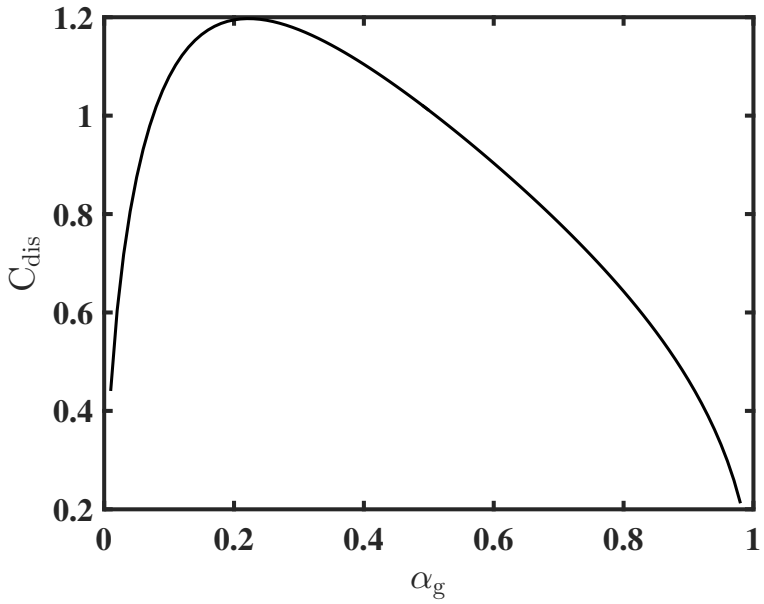

Figure 2.1 Minimum C_{dis} for large density ratios as a function of gas fraction and $C_{\text{s}} = 0.44$, $C_{\text{VM}} = 0.5$.

- If $C_{\text{VM}} > 0$ and $C_{\text{dis}} = 0$, Eq. (2.18) does not admit real roots for any positive value of the virtual mass coefficient C_{VM}. This results implies that Eq. (2.13) never defines an hyperbolic set of PDEs if the momentum exchange term only incorporates the effect of drag (without dispersion) and virtual mass forces.

- The case $C_{\text{VM}} = 0, C_{\text{dis}} > 0$, in which the effect of the virtual mass force is neglected, but the dispersion term is added to the drag force, leads to real roots for Eq. (2.18) under the condition

$$\frac{3}{4} C_{\text{s}} C_{\text{dis}} \geq \frac{\rho_{\text{g}} (1 - \alpha_{\text{g}}) \sqrt{\alpha_{\text{g}} (1 - \alpha_{\text{g}})}}{\rho_{\text{g}} (1 - \alpha_{\text{g}}) + \rho_{\text{l}} \alpha_{\text{g}}}, \tag{2.24}$$

  which is a special case of (2.23), with $C_{\text{VM}} = 0$.

2.5 Numerical approach

The two-fluid model was solved using the *reactingTwoPhaseEulerFoam* solver available in the open-source code OpenFOAM (2016). The solver implements a pressure-based solution algorithm designed for a co-located grid arrangement (Ferziger and Peric, 2002). The checker-

board effect is avoided by means of an improved formulation of the Rhie–Chow interpolation (Rhie and Chow, 1983; Zhang and Zhao, 2004). The buoyancy term is incorporated in the pressure, and other contributions to the momentum exchange term are treated as fluxes, at cell faces (Zhang and Zhao, 2004). The drag contribution to the momentum exchange term is treated with the partial elimination procedure (Spalding, 1980, 1983; Karema and Lo, 1999). The boundedness of the phase volume fraction is ensured by a flux-corrected scheme (Weller, 2006). A second-order scheme with the Sweby (1984) limiter is used to reconstruct the face value of the flow variables from the corresponding variable at cell centers. A first-order Euler implicit scheme is used for time integration. The time step is adapted to ensure the Courant-Friedrichs-Lewy condition is satisfied. Coupling between pressure and velocity is achieved by means of the PIMPLE algorithm (OpenFOAM, 2016), which is a combination of the SIMPLE (Patankar, 1980; Ferziger and Peric, 2002) and the PISO procedures (Issa, 1986; Oliveira and Issa, 2001; Ferziger and Peric, 2002).

2.6 One-dimensional two-phase shock tube problem

We consider a one-dimensional shock tube with two incompressible phases to investigate the effect of the dispersion term of Eq. (2.7) on the numerical solution. We compare the solution of the two-fluid model with and without $\mathbf{M}_{\text{disp}}$ to illustrate that the addition of this term, with a coefficient satisfying the condition of Eq. (2.23), ensures that the solution of the two-fluid equations consistently converges with grid refinement, without showing nonphysical behavior across the discontinuity. The geometry of the shock tube and its configuration are shown in Fig. 2.2, while the condition considered in the numerical experiments are reported in Tab. 2.1. The drag coefficient of Tomiyama et al. (1998) was used in all the simulations. It is apparent from Fig. 2.3 that the volume fraction profile along the shock tube predicted by the model without the dispersion term shows a significant undershoot at the location of the discontinuity in the flow properties. Similarly, Fig. 2.4 shows that, in the absence of the dispersion term, the numerical predictions show overshoots in the liquid velocity. This is clearly incorrect, since the analytical solution is a sharp change in the gas-phase fraction, without overshoot and undershoot. We also note that the problem becomes more serious when the

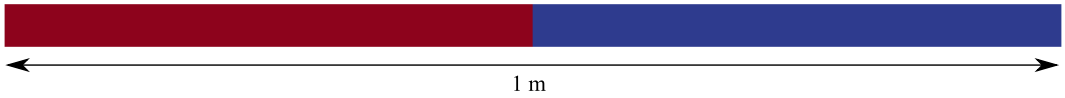

Figure 2.2 Shock tube geometry and boundary conditions.

Table 2.1 Initial conditions for the shock tube problem.

Quantity	**Left**	**Right**
α_{g}	0.25	0.1
U_{g} (m/s)	0.5	0.5
U_{l} (m/s)	0	0
C_{dis}	1.3	1.3

resolution of the computational grid is increased. The solution obtained after the addition of the dispersion term of Eq. (2.7), on the other hand, does not present the nonphysical behavior of overshoot and undershoot observed when this term is absent. Additionally, in the case with the dispersion term, the numerical solution converges with grid refinement, allowing to numerically demonstrate the independence of the solution from the grid resolution.

As shown in Fig. 2.3, we consider three progressively finer grid resolutions with 4000, 8000 and 16000 grid cells, respectively.

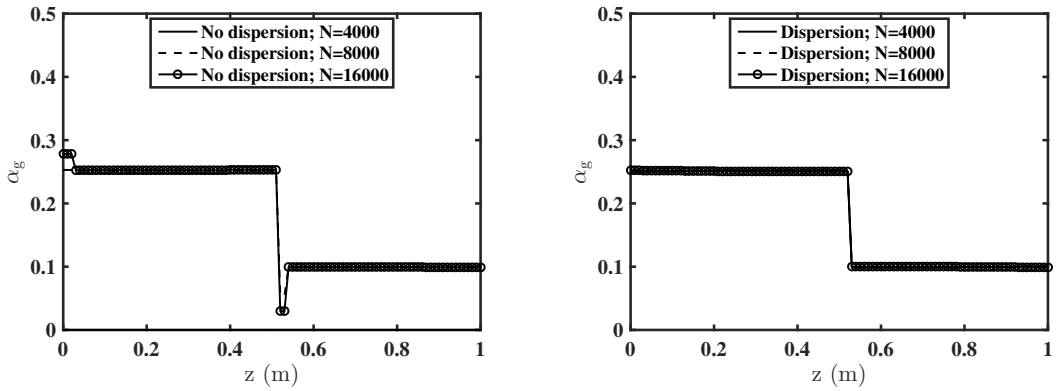

(a) No dispersion. (b) With dispersion.

Figure 2.3 Volume fraction profiles of the gas phase in the shock tube problem at $t = 0.13$ s.

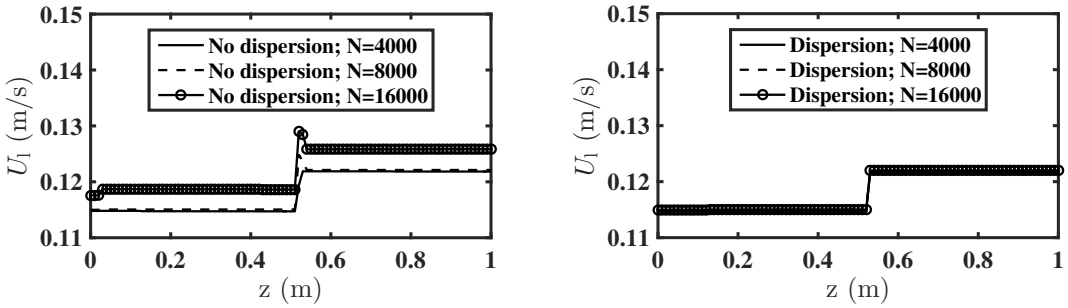

(a) No dispersion.

(b) With dispersion.

Figure 2.4 Liquid velocity profiles of the gas phase in the shock tube problem at $t = 0.13$ s.

2.7 One-dimensional falling fluid problem

We repeat the numerical experiment of grid refinement described in Sec. 2.6 in a system constituted by a one-dimensional two-phase system with the liquid phase at the top, and falling under the effect of gravity. The geometric configuration of the problem is reported in Fig. 2.5, and the initial conditions used in the numerical simulations are summarized in Tab. 2.2. The same closure models used in Sec. 2.6 are used for all the simulations discussed in this section.

The profiles of volume fraction at $t = 1$ s, with 8,000, 16,000 and 32,000 grid cells, are reported in Fig. 2.6. The profiles obtained without the dispersion term show nonphysical behavior across the discontinuity in the profile, which manifest with undershoot and overshoot in the values of the volume fraction. The introduction of the dispersion term addresses the problem, leading to the expected results, and to a convergent solution with grid refinement. It is also worth observing that the solution for the grid with 32,000 cells without the dispersion term is not reported because the numerical procedure was unable to provide a solution and terminated with error in such case (i.e., nonphysical values for α_g). This numerical difficulty disappeared with the introduction of the dispersion term.

Table 2.2 Initial conditions for the falling fluid problem.

Quantity	**Top**	**Bottom**
α_g	0.1	0.25
U_g (m/s)	0	0
U_l (m/s)	0	0

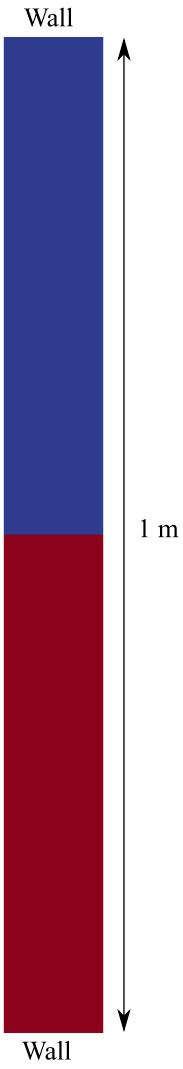

Figure 2.5 Falling liquid geometry and boundary conditions.

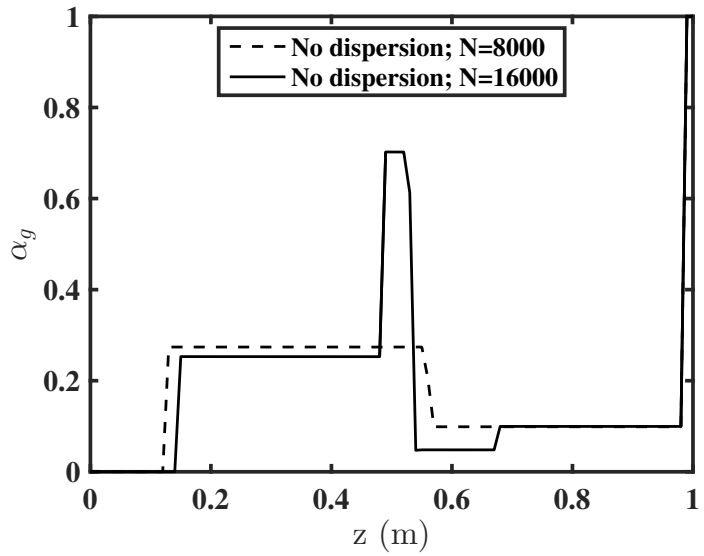

(a) No dispersion.

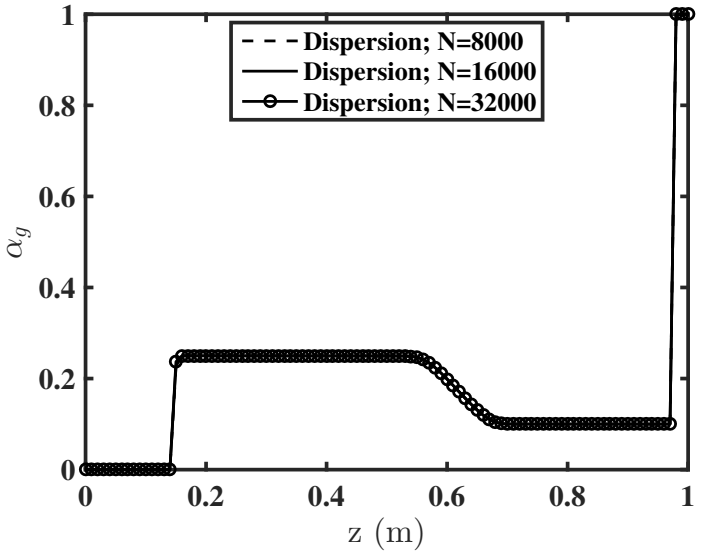

(b) With dispersion.

Figure 2.6 Volume fraction profiles of the gas phase in the falling fluid problem at $t = 1$ s.

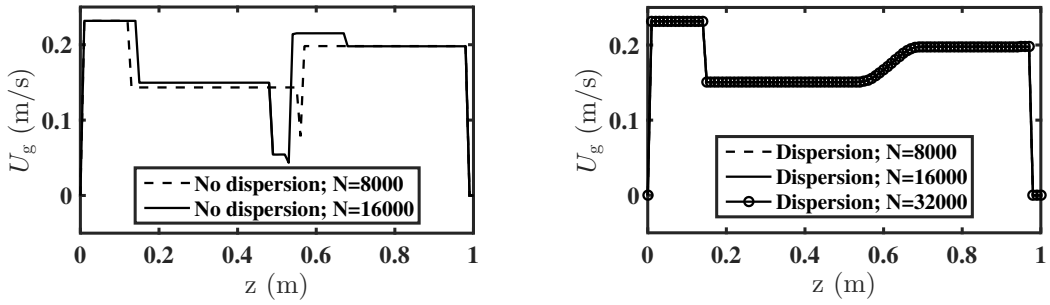

(a) No dispersion. (b) With dispersion.

Figure 2.7 Gas-phase velocity profiles in the falling fluid problem at $t = 1$ s.

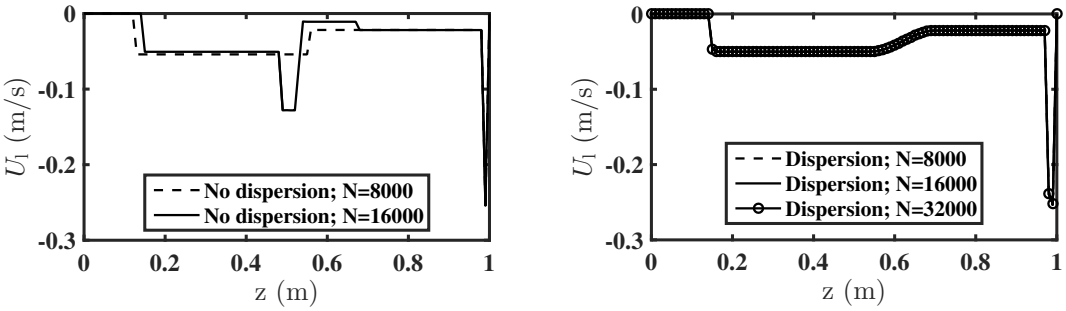

(a) No dispersion. (b) With dispersion.

Figure 2.8 Liquid-phase velocity profiles in the falling fluid problem at $t = 1$ s.

2.8 Application to an example bubble column

A two-dimensional bubble column, 45 cm tall and 10 cm wide, was considered to study the effect of the dispersion term proposed in this work on the prediction of a typical gas–liquid flow encountered in applications. In particular, the solution of the two-fluid model is reported for different grid resolutions (44×200, 88×400, 166×800, 322×1600) to illustrate how the addition of the dispersion term, on one hand, allows a grid-convergent solution to be reached, and, on the other hand, that the absence of the term leads to the predictions of nonphysical structures with high concentration of gas not observed in experiments.

The drag coefficient in these simulations is modeled following Tomiyama et al. (1998), the lift force coefficient was calculated using the expression of Legendre and Magnaudet (1998), and the wall-lubrication force with the model of Antal et al. (1991c). The virtual mass coefficient was set to $C_{\mathrm{VM}} = 0.5$ (Drew and Lahey, 1987).

The bubble column is initially filled with water ($\rho_{\mathrm{l}} = 1000$ kg m^{-3}, $\mu_{\mathrm{l}} = 8.90 \times 10^{-4}$ Pa s) up to the height of 38 cm. Air is injected through an orifice located at the bottom-right of the column, with a velocity whose only non-zero component is vertical, with a magnitude of 5 cm s^{-1}. The orifice is 5 cm wide, and its rightmost side is at a distance of 5 mm from the right wall of the column. The no-slip condition is applied to walls for both the phases, while the pressure is set to the atmospheric at the outlet, located at the top of the column, where a Neumann condition is used for all other variables.

Figs. 2.9, 2.10 and 2.11 show the color maps of the gas volume fraction in the bubble column in an instantaneous snapshot taken at $t = 1$ s of actual flow time. It is apparent that, in absence of the dispersion term, the numerical solution shows nonphysical structures in the flow, whose size depends on the grid resolution, and in which the value of the gas-phase volume fraction increases with grid refinement. From a numerical perspective, this sensitivity of the model to the grid resolution does not allow a grid-converged solution to be achieved, while, from the perspective of correctly describing the physical flow behavior, it leads to the prediction of features that are not observed in experiments, such as an excess of bubble clustering and a premature onset of flow instability in homogeneous suspension of bubbles. Similar structures

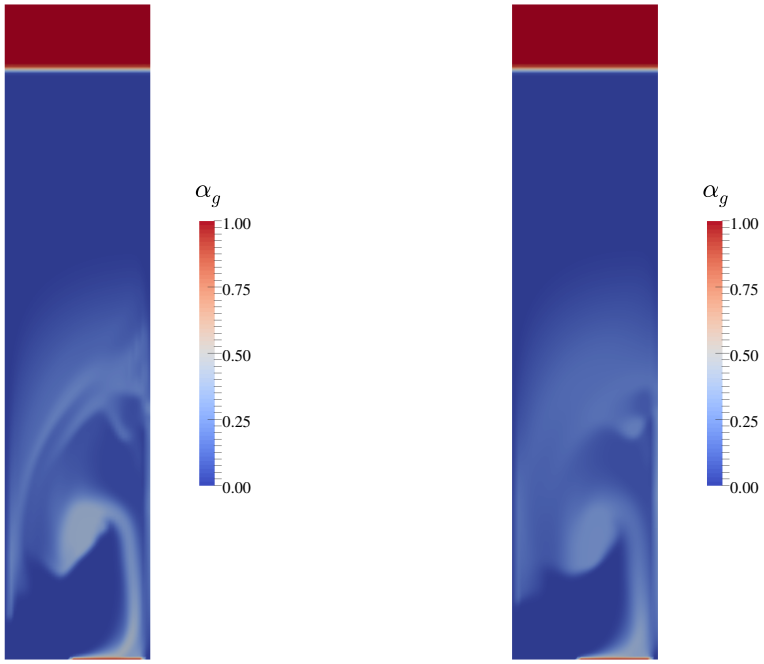

(a) No dispersion (b) With dispersion

Figure 2.9 Color map of volume fraction in bubble column at $t = 1$ s, with grid resolution of 44×200.

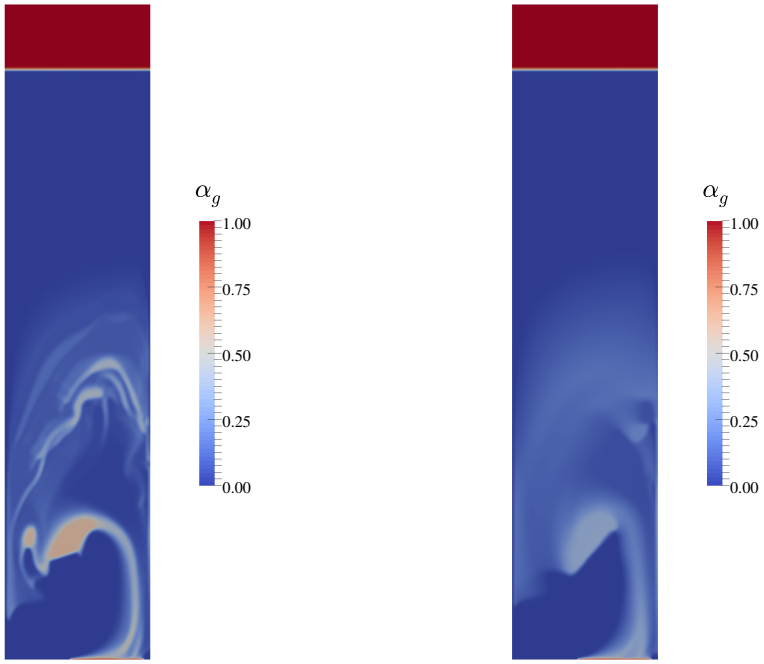

(a) No dispersion (b) With dispersion

Figure 2.10 Color map of volume fraction in bubble column at $t = 1$ s, with grid resolution of 88×400.

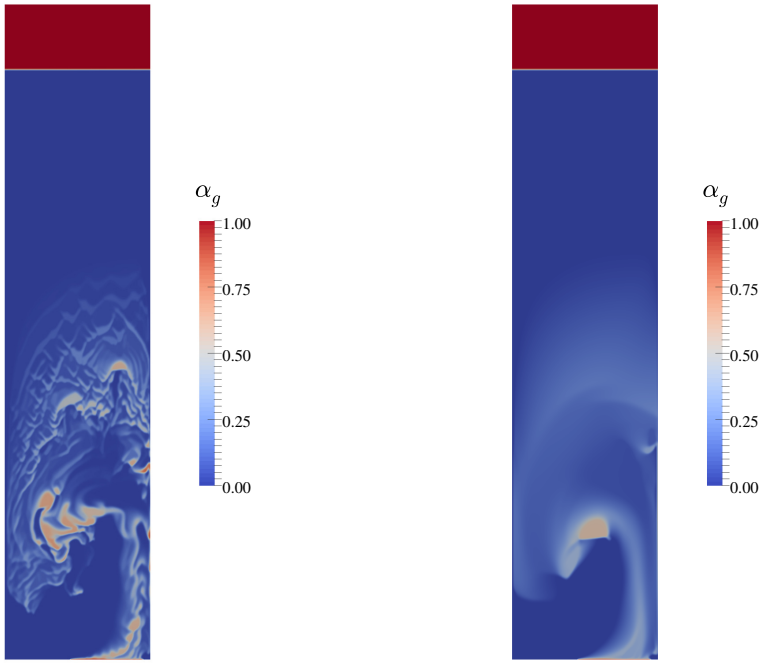

(a) No dispersion (b) With dispersion

Figure 2.11 Color map of volume fraction in bubble column at $t = 1$ s, with grid resolution of 166×800.

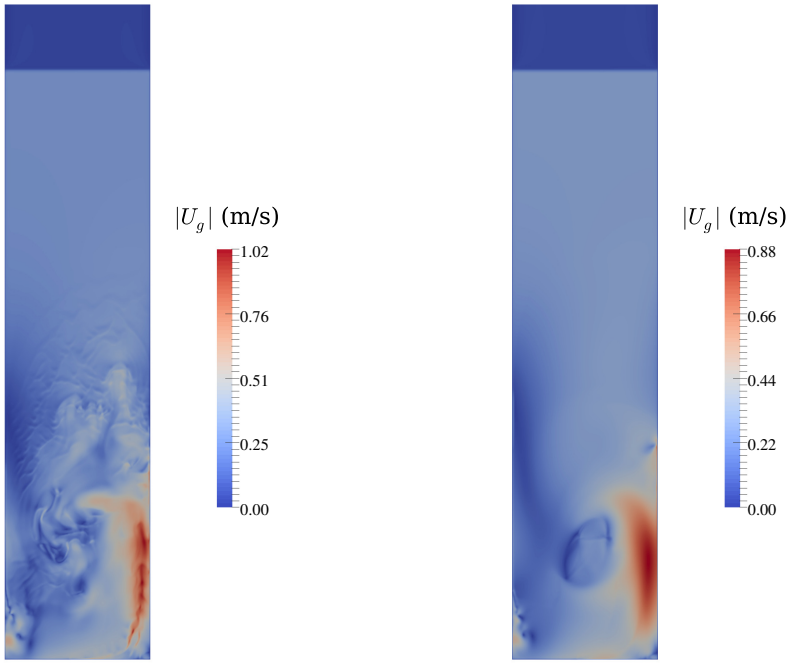

(a) No dispersion

(b) With dispersion

Figure 2.12 Color map of gas velocity in bubble column at $t = 1$ s, with grid resolution of 166×800.

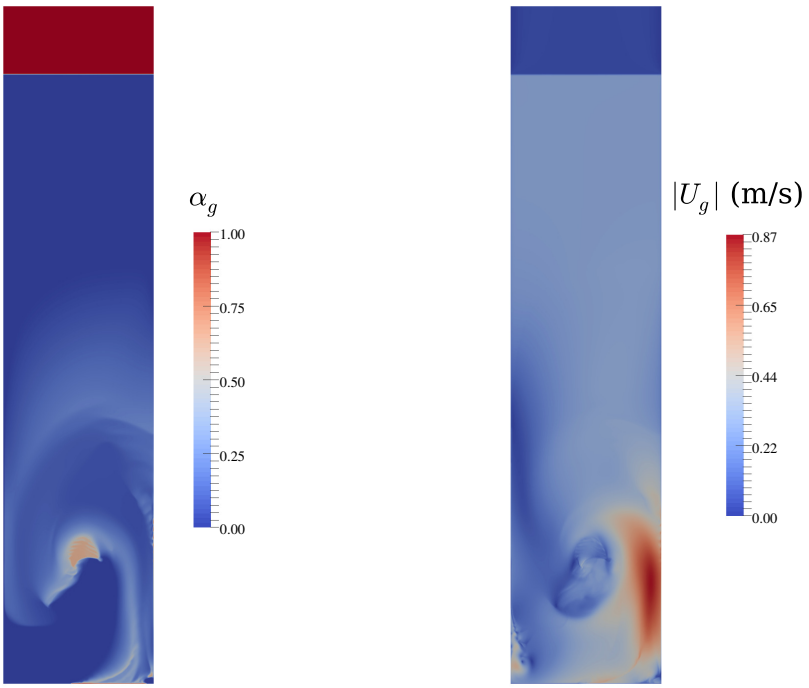

(a) α_g (b) $|U_g|$

Figure 2.13 Color map of gas volume fraction and of gas velocity in bubble column at $t = 1$ s, with grid resolution of 322×1600 and dispersion term.

are observed in the gas-phase velocity field, as shown in Fig. 2.12(a), and, consequently, in the liquid velocity field (not reported here). The introduction of the dispersion term described in Sec. 2.3 addresses the prediction of these nonphysical features by ensuring the hyperbolicity of the model equations, without qualitatively altering the large-scale unsteady behavior of the gas plume.

Observing the sequence of Figs. 2.9(b), 2.10(b), 2.11(b), 2.12(b), 2.13(a), we conclude that the addition of the dispersion term also allows a grid-converged solution to be achieved for the fields of gas volume fraction and velocity. The velocity field shows some small structures on the bottom-left of Fig. 2.12(b) that may be interpreted as oscillations, questioning the stabilizing effect of the dispersion term. However, further grid refinement (Fig. 2.13) shows that these structures do not become finer with the increased grid resolution, and do not originate oscillations that amplify with grid refinement. This indicates that the finer grid resolution is resolving structures of the flow that were not captured by the coarser grids. Furthermore, these results stress the importance of including the dispersion term in order to achieve the desired level of spatial accuracy. Indeed, when the dispersion term is removed, nonphysical structures will be predicted by the two-fluid model since it is not guaranteed to be hyperbolic.

2.9 Conclusions

The effect of the momentum transfer term on the hyperbolicity of the equations of the two-fluid model with shared pressure was investigated. It was shown that the introduction of a dispersion term, whose role is to effectively modify the slip velocity in the drag term appearing in the two-fluid equations, leads to a conditionally hyperbolic set of equations depending on the value assigned to the dispersion coefficient. An expression for the minimum value of the dispersion coefficient that ensures the hyperbolic nature of the equations of the two-fluid model was obtained.

The proposed dispersion term was applied to the simulation of two one-dimensional problems, involving a shock tube and a falling liquid. In both cases it was shown that the absence of the dispersion term leads to nonphysical profiles in the flow variables where sharp discontinuities are present. The solution of the model without the dispersion term (non-hyperbolic

model) also prevented a grid-converged solution to be achieved. The results obtained with the dispersion term (hyperbolic model) provided the expected results across sharp discontinuities, and led to a numerical solution convergent with grid refinement.

An example of a two-dimensional bubble column was considered to illustrate the importance of ensuring the hyperbolicity of the equations of the two-fluid model in applications of practical interest. It was observed that, in the absence of the dispersion term, the numerical solution remained sensitive to the grid resolution even at the finest grid refinement used in this work, and showed the presence of nonphysical regions with high concentration of disperse phase, which are not observed experimentally. These artifacts were not observed in the same simulations repeated with the hyperbolic two-fluid model.

Finally, it is worth observing that the coefficient obtained here for the dispersion term is based on mathematical considerations. The purpose of the study is to show that such a term needs to be present when simulating bubbly flows, independently from their laminar or turbulent nature. The physically correct formulation of the coefficient, as well as the impact on the agreement of the model predictions with experimental measurements need further investigation. Physically consistent models for the coefficient could be obtained, for example, by performing direct numerical simulations on ensembles of buoyant particles with gradients in the volume fraction.

CHAPTER 3. PERFORMANCE OF CURRENT ISOTROPIC TURBULENCE MODELS: k-ω, k-ϵ

3.1 Introduction

Dispersed gas-liquid flows are encountered in several applications of industrial interests e.g. nuclear reactors, chemical reactors, oil and gas flow through pipelines etc., modeling of these flows accurately is important, as it influences the design parameters of these equipments. Several modeling approaches such as DNS, Euler-Lagrange and Euler-Euler have been proposed by different authors in the past, a good account of these approaches can be found in the reviews of (Jakobsen et al., 1997; Joshi, 2001). Since the first two approaches (DNS and Euler-Lagrange) requires high computational cost, majority of the work on dispersed gas-liquid flows related to industrial application use Euler-Euler approach and its extensions, to predict the flow. In Euler-Euler approach both phases are treated as interpenetrating continua and the flow equations for both the phases are derived by ensemble averaging the microscopic equations with the interface jump conditions (Drew, 1983a). The performance of this approach is analyzed by several authors (Lai and Salcudean, 1987; Schwarz and Turner, 1988; Torvik and Svendsen, 1990; Jakobsen et al., 1993; Celik and Wang, 1994; Sokolichin and Eigenberger, 1994a; Grevskott et al., 1996; Ranade, 1997).

Lai and Salcudean (1987) performed a simulation of bubbles rising in a stagnant liquid using a steady state Euler-Euler approach. They simplified their model by assuming the gas phase inertia and viscous forces to be negligible. The liquid velocity profile obtained from the simulation showed good agreement with the experimental data. However, they do not report the void fraction profile.

Schwarz and Turner (1988) used the Euler-Euler approach coupled with the standard(std) $k-\epsilon$

model to simulate a gas stirred bath. They found that a $k-\epsilon$ model with the standard constants for single phase flows works well, if a sufficiently accurate Euler-Euler model (like for e.g. separate momentum equations has to be solved for each phase and no assumptions should be made about the hold up) is employed. They compared the Liquid velocities and turbulent kinetic energy with the experimental data and found a good agreement, but there is no comparison of void fraction reported in their work.

Grienberger and Hofmann (1992) performed a simulation on a 2D bubble column using the Euler-Euler approach by accounting for turbulence with the aid of standard $k-\epsilon$ model. They studied the flow in both homogeneous and heterogeneous regime. They could obtain a good prediction of Liquid velocity for both the regimes, however the hold predictions were not accurate especially in the near wall region.

Celik and Wang (1994) used a steady state Euler-Euler approach to study the circulation in a bubble column with only drag force as the inter-phase force. Their main objective was to study the impact of prescribed and calculated gas fraction on the flow prediction. They concluded that the gas fraction profile computed from the simulation gives much better prediction of velocity than the prescribed gas fraction profile.

(Torvik and Svendsen, 1990; Jakobsen et al., 1993; Grevskott et al., 1996) have used a steady state Euler-Euler model with expressions for lift, drag and virtual mass force coupled with $k-\epsilon$ model accounting for the effect of bubble induced turbulence, to simulate the bubble column operating in homogeneous and transition regime. They observed a good prediction of liquid velocity, volume fraction and turbulence with the experiments.

Ranade (1997) developed a computational model for predicting flows in bubble columns within Eulerian-Eulerian framework by adding two source terms in the momentum equation along with drag and lift. The first source term accounts for the correlation generated due to drag on time averaging and the other source term accounts for the contribution of liquid wakes on the slip velocity. They used a std single phase $k-\epsilon$ model without any additional source terms accounting for the production of turbulent kinetic energy due to bubbles, under the assumption, that the turbulent kinetic energy produced due to the bubbles is balanced by the dissipation at the bubble surface (Katoaka, 198). Their model showed good agreement in

the prediction of velocity and holdup with experiments for both homogenous and heterogenous regime.

From the literature, it can be concluded that Euler-Euler approach predicts the averaged liquid velocity profile in the bubble column reasonably well. However, the holdup prediction was not reported in many works (Lai and Salcudean, 1987; Schwarz and Turner, 1988) or not predicted accurately (Grienberger and Hofmann, 1992). Though the models proposed by (Ranade, 1997; Torvik and Svendsen, 1990; Jakobsen et al., 1993) improved the holdup prediction, it is tested only for low inlet gas velocities.

At high gas fractions and inlet gas velocities, the turbulence is predominant and becomes one of the key phenomena which influences the prediction of the flow in multiphase flow systems, Hence it is very important to accurately account for these phenomena.

Turbulence is one of the principle unresolved problems in single phase flows, and for the multiphase flows the problem becomes more complex due to the presence of the secondary phase (for e.g. bubbles, particles etc.). In this type of flow field, fluctuations are not only induced by the shear-induced turbulence, but also due to the continuous bubble movement of the gas phase, the wake motion behind the bubbles and the motion of the bubble's interface. Mudde et al. (1997) measured the eddy viscosity in a bubble column applying PIV technique. They found that the shear-induced turbulence contribution to the eddy viscosity is one order of magnitude higher than the bubble-induced contribution, however they performed their experiments with very low superficial gas velocities and gas fractions. Bubble induced turbulence might be equally important for high superficial inlet gas velocities and gas fractions.

Single phase two equation $k - \epsilon$ models are used to predict the turbulence in the flow in several publications (Becker et al., 1994; Pfleger and Becker, 2001; Sokolichin and Eigenberger, 1999; Buwa and Ranade, 2002).

Becker et al. (1994) performed a 2D simulation with the standard $k - \epsilon$ model to study the dynamic behaviour of the flow in a bubble column. They found that the standard $k - \epsilon$ model results in a much higher increase in the viscosity causing the damping of the plume leading to unsatisfactory results. Pfleger and Becker (2001) and Sokolichin and Eigenberger (1999) performed a 3D simulation with the same column used by Becker et al. (1994) and found out

that the overprediction of turbulent viscosity is corrected by the damping effect of the wall in the third direction, which results in the accurate capture of the dynamic behaviour of the flow in the column. A similar line of conclusion is made by Buwa and Ranade (2002) and Oey et al. (2003) from their simulations. One of the main shortcoming of the $k-\epsilon$ models used by these authors are that, it doesnot account for the production of turbulent kinetic energy by the bubbles, restricting the model to be used only for systems with weak turbulent interactions of gas and liquid. Several experiments have shown the significance of interphase interactions on the structure of turbulence in the liquid in bubbly flows (Wang et al., 1987b; Moursali et al., 1995; Liu and Bankoff, 1993b). These experiments show that the interfaces, by modifying the characteristic scales of the turbulence, alter the different mechanisms (e.g. production, redistribution and dissipation). There are many works (Elghobashi and Aboua Arab, 1983; Kataoka and Serizawa, 1989; Troshko and Hassan, 2001a; Behzadi et al., 2004) in the literature which account for these interactions by introducing source terms in the transport equations of k and ϵ.

Elghobashi and Abouarab (1983) and Kataoka and Serizawa (1989) derived a transport equation for turbulent kinetic energy by performing statistical averaging on the flow equations. The correlations generated due to the averaging of the interphase terms which quantifies the interphase turbulent kinetic energy transfer is modelled by assuming it to be proportional to the product of interface forces and slip velocity. Troshko and Hassan (2001) performed a simulation on dispersed gas-liquid flows in a turbulent vertical pipe using the model proposed by Kataoka and Serizawa (1989), they could obtain a good agreement in gas fraction and liquid velocity profiles with the experiments. Pfleger and Becker (2001) performed a 3D simulation of a cylindrical bubble column by using a standard $k-\epsilon$ model accounting for bubble induced turbulence. They concluded that the incorporation of bubble induced turbulence improved the prediction of the radial profiles of liquid velocities, however, the model deteriorates the prediction of gas fraction. They also concluded that the detailed understanding of the influences of bubble induced turbulence requires the employment of fine numerical grids and further test cases. Behzadi et al. (2004) derived a model for the transport of mixture turbulent kinetic energy in the high phase fraction limit by assuming that both phases tend to fluctuate as one

entity at high phase fractions. The effect of turbulence generated due to bubbles is accounted through a source term which is a function of turbulence response coefficient ($C_{\mathrm{t}} = \frac{u_1^{'}}{u_2^{'}}$). They tested the performance of their model by applying it to predict the bubbly flow in a sudden expansion of a circular pipe. They could get reasonable predictions of phase fraction and velocity, however, they concluded that a more accurate model is required to account for bubble induced turbulence.

The above literature survey suggests that the literature is flooded with $k-\epsilon$ models both with and without source terms to predict the multiphase flow turbulence, however, the works related to $k-\omega$ models appears to be scarce, to our knowledge only Bech (2005) has used a $k-\omega$ model to simulate dispersed gas-liquid flow in a bubble column. He concluded that, with low Reynolds number corrections in his $k-\omega$ model, he could predict the plume oscillation more accurately than the $k-\epsilon$ model, although he used $k-\omega$ model in his simulations, he didn't account for the production of turbulent kinetic energy by the bubbles. $k-\omega$ model has been proven to be better than $k-\epsilon$ model for single phase flow applications with adverse pressure gradients and also it can be integrated through the viscous sublayer without the aid of any damping functions (Pope, 2000). However, what advantages it could provide for multiphase flows is unclear from the literature, firm conclusions cannot be derived about the performance of $k-\omega$ models for multiphase flow applications unless tested rigorously for multiphase flow scenarios. Hence, we derive a multiphase $k-\omega$ model, both High and low Reynolds number form, by accounting for the interphase exchange of turbulent kinetic energy and implement it in the open source code OpenFOAM. The performance of the implemented model is compared with the two equation $k-\epsilon$ model of Jr. (2005) and validated with the experiments related to bubble columns and pipe flows (Monrs-Andreu et al., 2013; Troshko and Hassan, 2001; Harteveld, 2001).

3.2 Governing equations

3.2.1 Euler-Euler approach

The flow equations in an Euler-Euler framework are represented as (Drew, 1983):

Mass:

$$\frac{\partial}{\partial t}\left(\rho_{\mathrm{i}}\alpha_{\mathrm{i}}\right)+\nabla\cdot\left(\alpha_{\mathrm{i}}\rho_{\mathrm{i}}\mathbf{u}_{\mathrm{i}}\right)=0 \tag{3.1}$$

Momentum:

$$\frac{\partial}{\partial t}\left(\rho_{\mathrm{i}}\alpha_{\mathrm{i}}\mathbf{u}_{\mathrm{i}}\right)+\nabla\cdot\left(\alpha_{\mathrm{i}}\rho_{\mathrm{i}}\mathbf{u}_{\mathrm{i}}\mathbf{u}_{\mathrm{i}}\right)=-\nabla\cdot\left(\alpha_{\mathrm{i}}\boldsymbol{\tau}_{\mathrm{i}}\right)-\alpha\nabla p+\alpha_{\mathrm{i}}\rho_{\mathrm{i}}g+\mathbf{M}_{\mathrm{F,i}} \tag{3.2}$$

The stress term in each phase i is computed as:

$$\boldsymbol{\tau_{\mathrm{i}}}=-\mu_{\mathrm{eff}}\left(\nabla\mathbf{u}_{\mathrm{i}}+\left(\nabla\mathbf{u}_{\mathrm{i}}\right)^{T}-\frac{2}{3}\mathbf{I}\left(\nabla\cdot\mathbf{u}_{\mathrm{i}}\right)\right) \tag{3.3}$$

where μ_{eff} is the effective viscosity which captures the effect of both molecular and turbulent transport. In multiphase flows, the turbulent transport can be subdivided in to the shear induced turbulence and the turbulence caused due to the movement of bubbles referred to as pseudo turbulence. Hence, μ_{eff} becomes,

$$\mu_{\mathrm{eff}}=\mu_{1}+\mu_{1\mathrm{T}}+\mu_{BI,1} \tag{3.4}$$

$\mu_{BI,1}$ can be accounted from the model proposed by Sato and Sekoguchi (1975a),

$$\mu_{BI,1}=\rho_{1}C_{\mathrm{BI}}\alpha_{2}d_{\mathrm{p}}|\mathbf{u}_{1}-\mathbf{u}_{2}| \tag{3.5}$$

turbulent viscosity $\mu_{1\mathrm{T}}$ is computed as in single phase flows (Wilcox, 2000),

$$\mu_{1\mathrm{T}}=C_{\mu}\frac{k^{2}}{\epsilon} \tag{3.6}$$

where the turbulent kinetic energy (k) and the dissipation (ϵ) are obtained by solving the derived transport equation for k and ϵ discussed in the subsequent sections.

3.2.2 Interphase forces

The interphase force term $\mathbf{M}_{\mathrm{F,i}}$ in equation (2.2) represents the momentum transfer between the phases. It is modeled as the superposition of drag, lift, virtual mass, turbulent dispersion and wall lubrication forces.

$$\mathbf{M}_{\mathrm{F,i}} = \mathbf{M}_{\mathrm{D,i}} + \mathbf{M}_{\mathrm{L,i}} + \mathbf{M}_{\mathrm{VM,i}} + \mathbf{M}_{\mathrm{W,i}} + \mathbf{M}_{\mathrm{td,i}} \tag{3.7}$$

Drag force

Drag force ($\mathbf{M}_{\mathrm{D,i}}$) resists the motion of the bubbles. For a spherical bubble of uniform size it is related to the slip velocity $\mathbf{u}_{\mathrm{r}}$ by the expression given by Ishii and Mishima (1984)

$$\mathbf{M}_{\mathrm{D,i}} = -\frac{3}{4}\alpha_2 \frac{C_{\mathrm{D}}\rho_1}{d_{\mathrm{p}}}|\mathbf{u}_{\mathrm{r}}|\mathbf{u}_{\mathrm{r}} \tag{3.8}$$

Several correlations for drag coefficient (C_{D}) are available in the literature for both single bubble (Schwarz and Turner, 1988; Johansen and Boysan, 1988; Tomiyama et al., 2002) and bubble swarms (Ishii and Zuber, 1979; Behzadi et al., 2001; Garnier et al., 2002), we adopt the correlation proposed by Tomiyama (1998), which relates the drag coefficient to the Eotvos number (Eo) and Reynolds number (Re) as

$$C_{\mathrm{D}} = \max\left\{\min\left[\frac{24}{Re}\left(1 + 0.15Re^{0.687}\right), \frac{48}{Re}\right], \frac{8}{3}\frac{Eo}{Eo+4}\right\} \tag{3.9}$$

Virtual mass force

When the bubble accelerates, the liquid surrounding the bubble gets accelerated leading to an additional force called added mass or virtual mass force ($\mathbf{M}_{\mathrm{VM,i}}$), it can be calculated by (Milne - Thomson, 1968)

$$\mathbf{M}_{\mathrm{VM,i}} = -\alpha_2\rho_1 C_{VM}\left(\frac{d\mathbf{u}_1}{dt} - \frac{d\mathbf{u}_2}{dt}\right) \tag{3.10}$$

where C_{VM} is the virtual mass coefficient which is 0.5 according to Auton et al. (1988).

Lift force

In a shear flow a spherical particle experience forces which move the particle in the direction normal to the flow, it can be expressed with the expression given by Auton (1981)

$$\mathbf{M}_{\mathrm{L,i}} = -\alpha_2\rho_1 C_{\mathrm{L}}\mathbf{u}_{\mathrm{r}} \times \nabla \times \mathbf{u}_1 \tag{3.11}$$

We use the lift coefficient (C_{L}) proposed by Tomiyama (1998)

Wall lubrication

Wall lubrication force ($\mathbf{M}_{\mathrm{W,i}}$) prevents the bubbles from touching the wall. The main effect of this force is to assure zero void condition found experimentally near vertical walls, while not significantly effecting the void fraction distribution away from the wall (Antal et al., 1991a).

$$\mathbf{M}_{\mathrm{W,i}} = -\alpha_2 \rho_1 C_{\mathrm{W}} |\mathbf{u}_{\mathrm{r}} - (\mathbf{u}_{\mathrm{r}} \cdot n_{\mathrm{w}})|^2 n_{\mathrm{w}} \tag{3.12}$$

where C_{WL} is expressed as:

$$C_{\mathrm{WL}}(y_{\mathrm{w}}) = max\left[\frac{C_{\mathrm{W1}}}{d_{\mathrm{p}}} + \frac{C_{\mathrm{W2}}}{y_{\mathrm{w}}}, 0\right] \tag{3.13}$$

where $C_{\mathrm{W1}} = -0.104 - 0.06\mathbf{u}_{\mathrm{r}}$ and $C_{\mathrm{W2}} = 0.147$

Turbulent dispersion

Turbulent dispersion force ($\mathbf{M}_{\mathrm{td,i}}$) accounts for the turbulent fluctuations due to liquid phase on the gas phase and can be expressed as **?**)

$$\mathbf{M}_{\mathrm{td,i}} = -\rho_2 C_{\mathrm{td}} k_1 \nabla \alpha_2 \tag{3.14}$$

where $C_{\mathrm{td}} = 0.1$

3.2.3 Two Equation $k - \epsilon$

The two equation $k - \epsilon$ model is taken from Jr. (2005), it is an extended single phase $k - \epsilon$ model which solves for turbulent kinteic energy and dissipation for the liquid phase.

Turbulent kinetic energy:

$$\frac{\partial}{\partial t}(\rho_1 \alpha_1 k_1) + \nabla \cdot (\rho_1 \alpha_1 k_1 \mathbf{u}_1) = \nabla \cdot (\Gamma_1 \nabla k_1) + \rho_1 \alpha_1 \Pi_1 - \rho_1 \alpha_1 \epsilon_1 + \alpha_1 \rho_1 \Pi_{12} \tag{3.15}$$

Dissipation:

$$\frac{\partial}{\partial t}\left(\rho_1\alpha_1\epsilon_1\right) + \nabla\cdot\left(\rho_1\alpha_1\epsilon_1\mathbf{u}_1\right) = \nabla\cdot\left(\Gamma_1\nabla\epsilon_1\right) + \frac{\epsilon_1}{k_1}\left(C_1\rho_1\alpha_1\Pi_1 - C_2\rho_1\alpha_1\epsilon_1\right) + C_3\frac{\epsilon_1}{k_1}\alpha_1\rho_1\Pi_{12} \tag{3.16}$$

where the source term Π_{12} accounts for the turbulence production at the bubble surface

$$\Pi_{12} = C_\mathrm{p}\left(1 + C_\mathrm{D}^{4/3}\right)\alpha_2\frac{|\mathbf{u}_\mathrm{r}|^3}{d_\mathrm{p}} \tag{3.17}$$

where $C_\mathrm{p} = 0.25$ for potential flow around a sphere and C_D is the drag coefficient. A similar transport equation can be written for the gas phase, but they compute the gas phase turbulent stress as given by Drew and Passman (1998),

$$\boldsymbol{\tau}_2^\mathrm{T} = \boldsymbol{\tau}_1^\mathrm{T}\Omega\left(\frac{\overline{\rho}_2}{\rho_1} + \frac{3}{20}\right) - \frac{2}{5}\rho_1 k_1\Omega\boldsymbol{I} \tag{3.18}$$

Where the effective density ($\overline{\rho}_2$) and the turbulence parameter (Ω) are

$$\overline{\rho}_2 = \rho_1 + C_\mathrm{vm}\rho_1 \tag{3.19}$$

$$\Omega = \frac{\left[1 - \exp\left(\frac{\theta_1}{\theta_2}\right)\right]^2}{1 - \exp\left(\frac{2\theta_1}{\theta_2}\right)} \tag{3.20}$$

$$\theta_1 = \frac{k_1}{\epsilon_1} \tag{3.21}$$

$$\theta_2 = \frac{1}{18\mu_1}\overline{\rho}_2 d_\mathrm{p}^2 \tag{3.22}$$

3.2.4 Two Equation k-ω

HRN (High Reynolds number)

The turbulent viscosity becomes

$$\mu_\mathrm{T} = \frac{k_1}{\omega_1} \tag{3.23}$$

Turbulent kinetic energy:

$$\frac{\partial}{\partial t}\left(\rho_1\alpha_1 k_1\right) + \nabla\cdot\left(\rho_1\alpha_1 k_1\mathbf{u}_1\right) = \nabla\cdot\left(\Gamma_\mathrm{i}\nabla k_1\right) + \rho_1\alpha_1\Pi_1 - \rho_1\alpha_1\epsilon_1 + \alpha_1\rho_1\Pi_{12} \tag{3.24}$$

Omega:

$$\frac{1}{k_1}\left[C_\omega \alpha_1 \rho_1 \omega_1 \frac{\partial k}{\partial t} + C_\omega \alpha_1 \rho_1 \omega_1 \left(\mathbf{u}_1 \cdot \nabla k_1\right)\right] + \left[\frac{\partial}{\partial t}\left(\alpha_1 \rho_1 \omega_1\right) + \nabla \cdot \left(\alpha_1 \rho_1 \omega_1 \mathbf{u}_1\right)\right] = \nabla \cdot \left(\Gamma_1 \nabla \omega_1\right) + \left[\frac{2\Gamma_1}{k_1}\left(\nabla \omega_1 \cdot \nabla k_1\right) + \frac{\omega_1}{k_1}\nabla \cdot \left(\Gamma_1 \nabla k_1\right)\right] + \frac{\omega_1}{k_1}\left(C_1 \rho_1 \alpha_1 \Pi_1 - C_2 \rho_1 \alpha_1 C_\omega k_1 \omega_1\right) + \frac{S_{\omega 1}}{k_1} \quad (3.25)$$

Where,

$$\Gamma_1 = \mu_1 + \frac{\mu_{\mathrm{T}1}}{\sigma_\epsilon} + \mu_{\mathrm{BI}} \quad (3.26)$$

$$\mu_{\mathrm{BI}} = 0.6 d_{\mathrm{p}} \alpha_2 |\mathbf{u}_{\mathrm{r}}| \quad (3.27)$$

$$\Pi_{12} = C_{\mathrm{p}}\left(1 + C_{\mathrm{D}}^{4/3}\right)\alpha_2 \frac{|\mathbf{u}_{\mathrm{r}}|^3}{d_{\mathrm{p}}} \quad (3.28)$$

$$\Pi_1 = 2\nu_{\mathrm{T}} \mathbf{S}_1 : \mathbf{S}_1 - \frac{2}{3} k_1 \nabla \cdot \mathbf{u}_1 \quad (3.29)$$

$$C_\eta = 0.09; C_1 = 1.44; C_2 = 1.92; C_3 = 0.8; C_\omega = 1; C_{\mathrm{p}} = 0.25 \quad (3.30)$$

The turbulent kinetic energy production at the bubble surface is accounted by the source terms of Lahey (2005) as given in section 2.2 by modifying it for $k - \omega$ model.

LRN (Low Reynolds number)

Low Reynolds number corrections as proposed by **?**) is used for the derivation of low Reynolds number form.

$$\mu_{\mathrm{T}} = \alpha^* \frac{k_1}{\omega_1} \quad (3.31)$$

$$\alpha^* = \frac{\alpha_0^* + Re_{\mathrm{t}}/R_{\mathrm{k}}}{1 + Re_{\mathrm{t}}/R_{\mathrm{k}}} \quad (3.32)$$

Turbulent kinetic energy:

$$\frac{\partial}{\partial t}\left(\rho_1 \alpha_1 k_1\right) + \nabla \cdot \left(\rho_1 \alpha_1 k_1 \mathbf{u}_1\right) = \nabla \cdot \left(\Gamma_{\mathrm{i}} \nabla k_1\right) + \rho_1 \alpha_1 \Pi_1 - \beta^* \rho_1 \alpha_1 k_1 \omega_1 + \alpha_1 \rho_1 \Pi_{12} \quad (3.33)$$

$$\beta^* = \frac{9}{100}\frac{5/18 + \left(Re_{\mathrm{t}}/Re_\beta\right)^4}{1 + \left(Re_{\mathrm{t}}/Re_\beta\right)^4} \quad (3.34)$$

Omega:

$$\frac{\partial}{\partial t}\left(\alpha_1\rho_1\omega_1\right) + \nabla\cdot\left(\alpha_1\rho_1\omega_1\mathbf{u}_1\right) = \nabla\cdot\left(\Gamma_1\nabla\omega_1\right) + \frac{2\Gamma_1}{k_1}\left(\nabla\omega_1\cdot\nabla k_1\right) + \frac{\omega_1}{k_1}\left(\alpha C_1\rho_1\alpha_1\Pi_1 - C_2\rho_1\alpha_1 C_\omega k_1\omega_1\right) + \frac{S_{\omega 1}}{k_1} \quad (3.35)$$

$$\alpha = \frac{1}{\alpha^*}\frac{5}{9}\frac{\alpha_0 + Re_\mathrm{t}/R_\omega}{1 + Re_\mathrm{t}/R_\omega} \quad (3.36)$$

where the turbulent Reynolds number

$$Re_\mathrm{t} = \frac{k}{\nu\omega} \quad (3.37)$$

$$\alpha_0 = 1/10; \alpha_0^* = \beta/3; \beta = 3/40; \sigma^* = 1/2; \sigma = 1/2 \quad (3.38)$$

$$R_\beta = 8; R_\mathrm{k} = 27/10; R_\omega = 6 \quad (3.39)$$

3.3 Turbulent boundary condition

LRN

Walls:

For low Reynolds number model we integrate the $k-\omega$ equations through the boundary layer by specifying $k = 0$ at the wall and ω is calculated using the correlation (Wilcox et al., 1998)

$$\omega = \frac{6\nu}{\beta y_\mathrm{w}^2} \quad (3.40)$$

A wall function (y^+) in the range of 1 - 4 is used to specify the first grid point from the boundary.

Inlet: Inlet values are computed for k and ω as given in Pope (2000).

$$k = \frac{3}{2}\left(u_L I\right)^2 \quad (3.41)$$

where I,

$$I = 0.16\left(Re\right)^{-1/8} \quad (3.42)$$

$$\omega = \frac{k^{1/2}}{C_\mu^{1/4} l} \tag{3.43}$$

where, $l = 0.07L$

Outlet:

Fully developed flow where gradients of turbulent kinetic energy and specific dissipation rate tend to 0.

HRN

Walls

A wall function approach (Launder and Spalding, 1974) as in single phase flows are used to specify the boundary condition at the wall for HRN model. In this approach the velocity profile in the inertial sub-layer close to the wall is assumed to obey a log - law given by $\frac{u_1}{u_\tau} = \frac{1}{\kappa} ln\,(Ey^+)$ where the wall friction velocity $u_\tau = C_\mu^{1/4} k_1^{1/2}$, $\tau_\mathrm{w} = u_\tau^2$, $E = 7.77$ and $\kappa = 0.41$.
The following procedure is used to compute the variables close to the wall:

1. Solve the momentum equation with a modified wall turbulent viscosity as

$$\mu_{\mathrm{t}1} = \mu_1 \left(\frac{y^+ k_1}{ln\,(Ey^+)} - 1 \right) \tag{3.44}$$

where, $y^+ = \frac{y_\mathrm{w} C_\mu^{1/4} k_1^{1/2}}{\mu_1}$

2. Since the first grid point is placed at the intertial sub-layer the laminar shear stress is negligible and by assuming that shear stress is constant

$$\tau_\mathrm{t} = \tau_\mathrm{w} \tag{3.45}$$

With the above assumption turbulence production at the node point close to the wall can be set as:

$\Pi_1 = \tau_\mathrm{w} \frac{\mathbf{u}_1}{y_\mathrm{w}}$

where, $\tau_{\mathrm{w}} = \frac{u_\tau \mathbf{u}_1 k_1}{ln(Ey^+)}$

3. By assuming the production equal to the dissipation, ω can be set as

$$\omega_1 = \frac{k_1}{C_\mu^{1/4} \kappa y_{\mathrm{w}}} \tag{3.46}$$

A wall y^+ of 30 - 50 is used to specify the first grid point so that it lies in the inertial sub-range for the assumptions to be valid.

3.4 Numerical method

The flow equations are implemented in the open source code OpenFOAM. Second order accurate schemes present in OpenFOAM are used to discretize the spatial derivatives and a first order accurate scheme for time derivatives. explicit MULES solver is used to integrate the alpha equation. A PIMPLE algorithm which is a combination of PISO and SIMPLE is used to couple the pressure and velocity.

Algorithm

1. Solve the void fraction equation.
2. Calculate the interfacial forces.
3. Solve the momentum equation.
4. Solve the pressure equation.
5. Correct the velocity and flux.
6. Solve the k and ω equation with the corrected velocity.
7. Go to step 1 and repeat the same procedure for next time step.

3.5 Results and discussion

3.5.1 Simulation cases

The models are validated for bubble column flows (Harteveld, 2005) and turbulent vertical pipe flow experiments (Wang, 1987; Monros-Andreu et al., 2013) for wide range of flow conditions. Also, the performance of the models are analyzed by comparing it with the already

established $k-\epsilon$ model (Lahey, 2005). The simulation conditions and experimental setup used for the study, followed by the comparison and validation of the simulation results are discussed in the subsequent sections.

3.5.1.1 case 1 (Harteveld, 2005)

The experiments performed by Harteveld (2005), on a bubble column are used to validate the models in the low void fraction (0 - 10 percent), low Reynolds number (3000 - 4000) regime. In their experiment, they study a 2D bubble column with the aid of particle image velocimetry (PIV) and particle tracking velocimetry (PTV). The bubble column used for the study was 0.243 m wide, 0.041 m deep and 0.99 m high. The top portion of the column was open to the atmosphere and air was injected with a velocity of 0.02 m/s through the bottom portion of the column. The injected air move through the stagnant water inducing turbulent fluctuations and gets ejected at the top to the atmosphere. The needle injectors were used to keep a narrow bubble size distribution ranging from 3.5 to 4.5 mm, due to the narrow bubble size distribution the flow could be assumed close to a monodispersed flow with bubble diameter 4 mm. Seven aeration patterns were used by varying the width of the inlet to investigate the flow structure inside the column. The aeration pattern 5 as shown in 3.5.1.1 is chosen for the validation of the solver. A 3D simulation is performed with inlet and boundary conditions as given in Tables 3.1 and 3.2 respectively. The results obtained from the simulation are extracted from the location z = 0.05 m is compared with the experiment.

Fig. 3.2 shows the comparison of volume fraction and velocity profiles for different turbulence models and high resolution (mesoscale DNS) with experiments. The results indicate that the volume fraction is better predicted by the k-ω model compared to k-ϵ model. It is expected that the two-fluid model with high resolution or mesoscale DNS gives the best prediction compared to any turbulence models. The velocity prediction is comparable for both turbulence models at the center of the column, however k-*epsilon* model predicts better close to the boundary. The mesoscale DNS predicts the even the velocity profile better compared to both turbulence models both at the center and close to the boundary.

Table 3.1 Inlet conditions

Runs	InletGasVelocity(m/s)	InletLiquid (m/s)	Inlet VF	Inlet Re = $\frac{D_{in} u_1}{\nu_1}$
1	0.02	0	1	4860

Table 3.2 Boundary conditions

Boundary	Bubble vel	Liquid vel	Pressure
Bottom	fixed value	fixed value	zeroGradient
Top	outlet	outlet	fixed
Side	wall	wall	zeroGradient

3.5.2 case 2 (Monros-Andreu et al., 2013)

The performance of the models for low void fraction (0 - 10 percent), high Reynolds number (27000 - 40000) regime are validated with the turbulent vertical pipe flow experiments performed by Monros-Andreu et al. (2013). They performed the experiments on a pipe of diameter 0.052 m and height 5.5 m. The working fluids in operation were air and water. The air was injected at the bottom of the pipe by a sparger, which kept the bubble diameters ranging from 1 to 3 mm in the pipe. They investigate the flow structure inside the pipe for wide range of inlet superficial liquid velocities (0.5 - 3 m/s) and void fractions (0 - 30 percent) The void fraction and the liquid velocities are measured with the four sensor conductivity probe and Laser Doppler Anemometry (LDA) respectively. Measurements are taken at three different axial locations (L/D = 22.4, 61, 98.7).

Pipe simulated in the current work has a diameter of 0.052 m and is a section of the original pipe (Monros-Andreu et al., 2013) taken between the axial locations z/D = 61 and z/D = 98.7, which results in a pipe length of 1.95 m. The experimental readings of the volume fraction, gas velocity and liquid velocity at z/D = 61 are averaged over the cross section and given as the inlet conditions. A case with inlet void fractions 0.066 is chosen from the experiments for the validation of the solver as given in Table 3.3. A 2D axi-symmetric simulation is performed with inlet and boundary conditions as given in Table 3.4 respectively. Steady and fully developed profiles of volume fraction and liquid velocity at z = 1.95 m are extracted from the simulation and compared with the experimental readings.

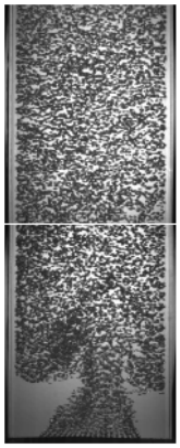

Figure 3.1 Aeration patterns (Harteveld, 2005)

Fig. 3.3 shows the comparison of volume fraction and velocity profiles for the k-ω model with different turbulent source terms. The results indicate that the volume fraction prediction close to the wall is not affected by the turbulent source terms, however, at the centre the volume fraction is under predicted by the k-ω model for all the source terms. The velocity prediction is comparable for all the source terms.

Table 3.3 Simulation runs

Runs	InletGasVelocity(m/s)	InletLiquid (m/s)	Inlet VF	Re
1	0.5354	0.7575	0.066	27840

Table 3.4 Boundary conditions

Boundary	Bubble vel	Liquid vel	Pressure
Bottom	fixed value	fixed value	zeroGradient
Top	Outlet	Outlet	fixed
Side	Slip	wall	zeroGradient

3.5.3 case 3 (Wang, 1987)

The models are validated for high void fraction (α >20 percent), high Reynolds number regime with the experiments performed by Wang (1987). They performed the experiments on a pipe of diameter 0.057 m and about 2 m tall. The working fluids in operation were air and

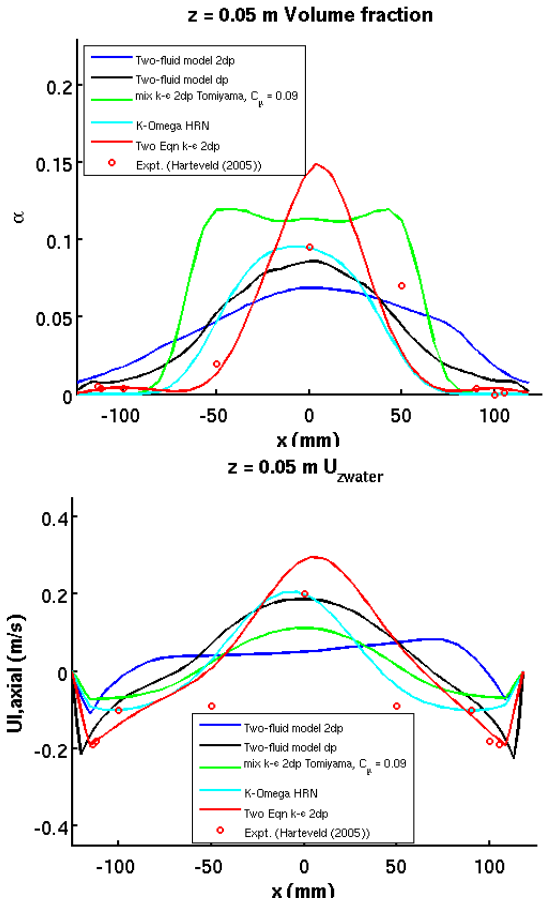

Figure 3.2 Volume fraction and velocity profiles

water. The fully developed void fraction profile and liquid velocity profiles at the outlet are measured by a single sensor cylindrical hot-film probe. They study the flow structure inside the pipe for a constant superficial liquid velocity 0.43 m/s by varying the void fractions from 0 to 40 percent at the inlet. We choose a case with high inlet void fraction as given in Table 3.5. A 2D axi-symmetric simulation is performed with same set of boundary conditions as used for Case 2. Steady and fully developed profiles of volume fraction and liquid velocity at the outlet are extracted from the simulation and compared with the experiments.

Table 3.5 Simulation run

Runs	InletGasVelocity(m/s)	InletLiquid (m/s)	Inlet VF	Inlet Re
1	1.044	0.6969	0.38	59508

Fig. 3.4 shows the comparison of volume fraction and velocity profiles for the k-ω HRN

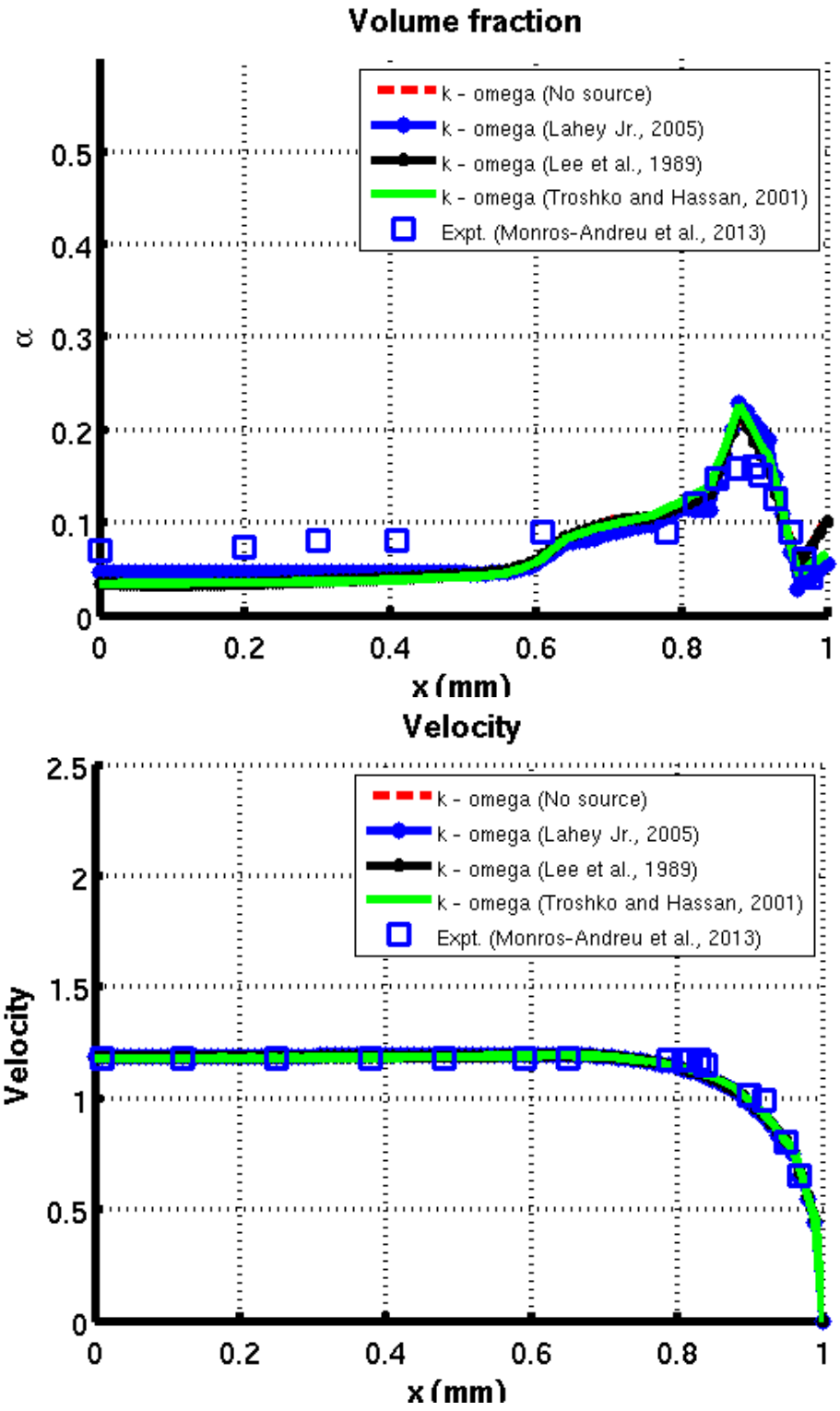

Figure 3.3 Volume fraction and velocity profiles

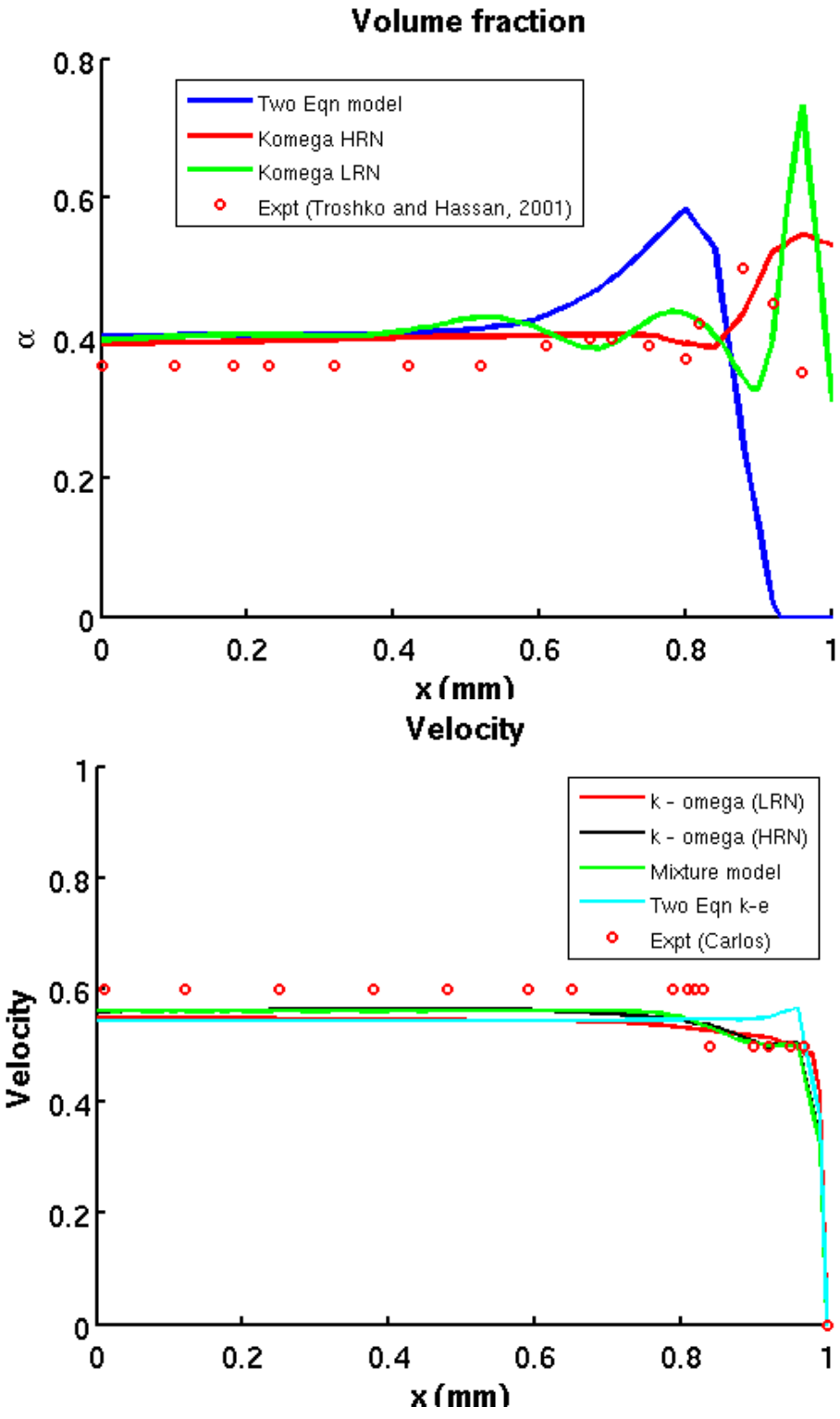

Figure 3.4 Volume fraction and velocity profiles

3.6 Conclusion

In the current study an ad-hoc multiphase $k-\omega$ model is derived, both high and low Reynolds number form, by accounting for the interphase exchange of turbulent kinetic energy. The derived model implement it in the open source code OpenFOAM. The performance of the implemented model is compared with the two equation $k-\epsilon$ model of Jr. (2005) and validated with the experiments related to bubble columns and pipe flow.

Harteveld's experiments comparison

The comparisons with Harteveld's experiments indicate that the volume fraction is better predicted by the k-ω model compared to k-ϵ model. It is expected that the two-fluid model with high resolution or mesoscale DNS gives the best prediction compared to any turbulence models. The velocity prediction is comparable for both turbulence models at the center of the column, however k-ϵ model predicts better close to the boundary. The meso-scale DNS predicts the even the velocity profile better compared to both turbulence models both at the center and close to the boundary.

Monros's experiments comparison

The results indicate that the volume fraction prediction close to the wall is not affected by the turbulent source terms, however, at the center the volume fraction is under predicted by the k-ω model for all the source terms. The velocity prediction is comparable for all the source terms.

Wang's experiment comparison

The results indicate that the volume fraction prediction by the k-ϵ, k-ω LRN close to the wall is not good. However, k-ω HRN model seems to reasonably well close to the wall. The velocity profile close to the boundary is better predicted by the k-ω models (HRN, LRN) than the k-ϵ model.

The study shows the ad-hoc isotropic turbulence models may not be sufficient for accurate

prediction of turbulence in gas-liquid flows, hence a turbulence model has to be derived from the conservation equations (two-fluid model) and the unclosed terms appearing in the model has to be closed using mesoscale DNS study.

CHAPTER 4. MESOSCALE DNS

This chapter is modified from a paper in preparation for

Physics of Fluids Journal

N. Panicker, A. Passalacqua, R.O. Fox

4.1 Abstract

Swarm driven turbulent bubbly flows are typically encountered in the bubble columns operating in the dense heterogeneous regime. The columns operating in this regime are vulnerable to buoyancy induced instabilities resulting in the formation of mesoscale bubble swarms which while rising agitates the fluid and causes turbulence. The efficient design of these systems with the aid of CFD simulations requires accurate prediction of turbulence due to these swarms through turbulence models. The development of turbulence models requires turbulence data in this regime which is challenging to obtain with the experimental techniques like PIV, LDA for dense bubbly flows due to high scattering of light (Mudde, 2005; Roghair et al., 2011a) due to the bubbles. The multi-phase simulation techniques to acquire turbulence data like particle resolved (**?**) and point particle DNS methods (Subramaniam, 2013) require high computational cost due to the large domain size and number of bubbles involved in achieving the turbulence in dense heterogeneous flow regime.

In the present study we derive a general Reynolds stress equations for turbulent bubbly flows by phase averaging (PA) the two-fluid model with the procedures discussed in (Fox, 2014). The unclosed terms generated due to PA, which accounts for turbulence exchange between the phases are quantified by performing mesoscale two-fluid flow simulations on statistically homogeneous flows in the dense heterogeneous regime. The computational domain for mesoscale simulations considered in the study is a 3-dimensional domain with square cross-section. Peri-

odic boundary conditions are applied to all sides of the domain to create a statistically homogeneous turbulent flow in order to isolate and study the mean-gradient-independent unclosed terms that account for the exchange of turbulence quantities between the phases. The turbulence statistics, length and time scales, mean momentum budget and the turbulence energy budget computed from the simulations for different gas fractions are reported and analyzed.

4.2 Introduction

Bubble columns are widely used in the chemical and pharmaceutical industries as gas–liquid contactors because of their simple construction and ability to provide high contact area for mass and heat transfer. The design and scale up of bubble columns depend on two key factors: heat/mass transfer and mixing characteristics. These two factors highly depend on the bubbly flow hydrodynamics of the column. Although simple in construction, the bubbly flow hydrodynamics inside bubble columns are complex due the presence of turbulence and bubble–bubble interactions (coalescence, breakup), thus, the development of computational models that accurately describe bubbly flows are challenging.

Bubbly flows typically fall in either the homogeneous or heterogeneous regime (Joshi et al., 1998; Ruzicka et al., 2001), depending on low and high inlet gas flow rate, respectively.

The homogeneous regime is characterized by a uniform rise of bubbles with the absence of any large scale turbulent instabilities due to buoyancy. In this regime, the main sources of turbulence are the flow disturbances generated due the movement of the bubbles in the vicinity of the bubble and the wake formation behind the bubble. In the limit of high bubble Reynolds number (200 - 700) as in the current study, the bubble induced liquid fluctuations are governed by wake formation (**?**). In many works (Ma et al., 2015; Zhang et al., 2006; Dhotre et al., 2008; Deen et al., 2001) the effect of bubble induced turbulence is added as an effective liquid viscosity (Sato and Sekoguchi, 1975a) in the stress term of the liquid momentum conservation equation, however, to our knowledge the model developed in Sato and Sekoguchi (1975a) considers only the effect of liquid disturbances not the wake turbulence. The bubble induced turbulence (BIT) due to the wake formation is modelled for bubbly flows in the recent works (Riboux et al., 2013; Ma et al., 2017), however the applicability of the model is restricted to very dilute bubbly flows

with non-interacting wakes. The experimental investigation of mixing due to bubble induced turbulence performed by Alméras et al. (2015) for moderately dense bubbly flows ($\alpha_g \sim 13\%$) shows that the bubble induced turbulence production in the moderately dense limit reaches a saturation due to the increase in dissipation caused due to the wake interactions. Thus, the BIT models (Sato and Sekoguchi, 1975a; Riboux et al., 2013; Ma et al., 2017) developed in the dilute limit as a linear function of α_g without considering the dissipation of wake interactions may overpredict the BIT in the dense limit ($\alpha_g \sim 30\% - 50\%$).

The heterogeneous regime consists of highly buoyant bubble swarms generating large-scale turbulent structures that significantly influence the hydrodynamics. In most applications, the gas flow rates are high and the columns operate in the heterogeneous regime. Hence, understanding the swarm-induced turbulence in the heterogeneous regime is crucial for the development of accurate turbulence models.

The current turbulence models for the heterogeneous regime (Torvik and Svendsen, 1990; Grienberger and Hofmann, 1992; Ranade, 1992; Hillmer et al., 1994; Hjertager and Morud, 1995; Svendsen et al., 1992; Lahey, 1990a) are inadequate mostly because they are ad-hoc without a proper description of how the interphase forces are modified by the bubble swarms. Moreover, most turbulence models were developed based on the assumption of isotropic turbulence, which is not appropriate for predicting the highly anisotropic flows (Mudde et al., 1997) found in the heterogeneous regime. Moving forward, the validation of turbulence models will require accurate data for bubbly flows coming either from experiments or simulations. In order to understand the correlation between the instantaneous fluid velocity and local bubble volume fraction due to bubble swarms, simultaneous measurements of both quantities are required.

Experimental investigations have been performed by many investigators (Yang et al., 1993; Degaleesan et al., 2001; Cui and Fan, 2004; Mudde et al., 1997) to understand the characteristics of the large-scale turbulent structures in the bubbly flows. Yang et al. (1993) performed experiments using CARPT (computer-automated radioactive-particle tracking) and studied turbulence for different superficial gas velocities and column diameters. Their study showed that the axial Reynolds stress component is large compared to the radial Reynolds stress, and

they commented that the eddy-viscosity model based on the assumption may not be suitable for predicting turbulence in bubble flows. They also computed the auto-correlation function, which indicates a strongly correlated flow in the axial direction compared to the radial direction. Furthermore, they suggested gradient based modeling of mixing or turbulent stresses is inadequate and more sophisticated models have to be developed.

Degaleesan et al. (2001) used the CARPT technique to investigate the turbulence in bubble columns. They analyzed the time-averaged liquid velocity profiles and Reynolds stresses for various inlet gas flow rates and column sizes. They found that the time-averaged liquid axial velocity and Reynolds stress profiles undergo a steep change as the superficial gas velocity is increased from 2.4 to 12 cm/s, which indicates a transition from the homogeneous to the heterogeneous regime. Their findings also show that the axial normal Reynolds stress contribution is highest compared to the other components, indicating a high degree of anisotropy in the turbulence.

Cui and Fan (2004) used particle image velocimetry (PIV) to investigate the influence of turbulence due to the bubbles on the liquid-phase in a bubble column for a wide range of superficial gas velocities encompassing the homogeneous and heterogeneous regimes. They found that the turbulence production due the bubbles in the liquid phase is much higher compared to the shear-induced turbulence production, thereby dominating the total turbulence kinetic energy balance in the flow. They demonstrated that the increase in superficial gas-velocity, which led to the transition to the heterogeneous regime, resulted in increased frequency of the largest vortex spanning the entire column, thereby changing the length scales of turbulence.

Experimental optical techniques (PIV, LDA) are limited to moderate gas fractions (10–20%) flows (Mudde, 2005; Roghair et al., 2011a), because of large scattering of light by the bubbles, making it almost impossible to visualize the liquid flow field. Due to the limitation of experiments in exploring these high-gas-fraction, industrially relevant regime, one has to resort to simulation techniques.

Many investigators (Druzhinin and Elghobashi, 1998; Murai et al., 2000; Liu et al., 2011; Roghair et al., 2011b; Uchiyama and Kusamichi, 2013; Yang et al., 2002; Lakkaraju et al., 2011; Pang et al., 2013; Nierhaus et al., 2007; Fujiwara et al., 2004; Rensen et al., 2005)

have performed DNS simulations using various multi-phase simulation methods Euler-lagrange, front-tracking and Euler-Euler methods to study bubbly flow turbulence. Most studies revolve around turbulent channel or pipe flows with shear induced turbulence, which may show a different turbulent behaviour compared to purely buoyancy driven turbulent flows found in the bubble columns. Furthermore, almost all the works perform simulations in the low gas fraction (0.1%) limit to study the small-scale turbulence of the order of bubble diameter $\sim d_{\mathrm{p}}$, where the large-scale instabilities found in the heterogeneous regime are not formed.

Climent and Magnaudet (1999) performed a fundamental investigation on the effect of bubbles in generating the large-scale instabilities using Euler-Lagrange approach based on different Rayleigh numbers. They found that below a critical Rayleigh number 2×10^5, bubbles rise almost in straight lines with no particular large scale structures and the amplitude of the fluctuations in the liquid velocity field is small in this regime. On the contrary, for Rayleigh numbers $> 2 \times 10^5$, bubble trajectories significantly differs from straight lines and large scale structures starts to emerge. The authors have tried to explain the mechanism behind onset of such instabilities by comparing it to the Rayleigh–Taylor instabilities based on density gradients. Furthermore, they have stressed on the need of 3D simulations over 2-D simulations as performed in their work to fully understand the phenomena.

In the current study, we use the Reynolds-stress equation for bubbly flow in order to analyze the anisotropic turbulence found in the heterogeneous regime. The derivation is performed by applying the phase-averaging (PA) techniques discussed in (Fox, 2014a) to the two-fluid model for bubbly flows. Application of the PA procedure results in unclosed terms in both mean two-fluid equations and Reynolds-stress transport equations. To quantify and study the variation of those unclosed terms as a function of gas fraction, we perform 3-D simulations of bubbly flows on a periodic box by varying the gas fractions between 15–50%. Moreover, we study the turbulence characteristics at high gas fractions in order to understand (i) the one-point statistics and anisotropy of bubbly flows, (i) the distribution of turbulent energy among different length scales, and (iii) the length and time scales of the fluid vorticity and bubble swarms.

4.3 Two-Fluid Model for Bubbly Flow

Two-fluid equations can be obtained by ensemble averaging the instantaneous conservation equations (Drew, 1983a). As a result of averaging, unclosed terms appear in the equations, which have to be closed with appropriate closure models. The predictive capability of two-fluid equations depend largely on these closure models. Hence, it is essential to seek accurate interphase closure models from the literature.

A single pressure formulation as given in Eq. (4.2), is adopted by most works (Svendsen et al., 1992; Sokolichin and Eigenberger, 1994b; Lapin and Lübbert, 1994; Sommerfeld et al., 2003; Yeoh and Tu, 2006) to simulate bubbly flows. The assumption of a single pressure is valid if the surface tension force at the gas–liquid interface is negligible (Drew, 1983a). However, a bubble-dispersion term must be included in order for the two-fluid equations to be hyperbolic. The two-fluid model used in this work is as follows.

Continuity:

$$\frac{\partial \alpha_\phi}{\partial t} + \nabla \cdot \alpha_\phi \mathbf{u}_\phi = 0 \tag{4.1}$$

Momentum:

$$\frac{\partial \alpha_\phi \mathbf{u}_\phi}{\partial t} + \nabla \cdot \alpha_\phi \mathbf{u}_\phi \mathbf{u}_\phi = -\frac{\alpha_\phi}{\rho_\phi} \nabla p_\mathrm{l} + \frac{1}{\rho_\phi} \nabla \cdot \boldsymbol{\sigma}_\phi + \alpha_\phi \mathbf{g} + \mathbb{I}_\phi \frac{1}{\rho_\phi} \left(\mathbf{F}_\mathrm{D} + \mathbf{F}_\mathrm{VM} + \mathbf{F}_\mathrm{LF} + \mathbf{F}_\mathrm{BD} \right) \tag{4.2}$$

where the viscous stress tensor is modeled by

$$\boldsymbol{\sigma}_\phi = \alpha_\phi \mu_\phi \left[\nabla \mathbf{u}_\phi + (\nabla \mathbf{u}_\phi)^\mathrm{T} - \frac{2}{3} (\nabla \cdot \mathbf{u}_\phi) \mathbf{I} \right]$$

and the index $\phi = \mathrm{g}, \mathrm{l}$ corresponds to gas and liquid, respectively. The function $\mathbb{I}_\phi$ is 1 for $\phi = \mathrm{l}$ and -1 for $\phi = \mathrm{g}$. The microscale liquid fluctuatons induced due to the bubble wakes is added as an effective liquid visosity:

$$\mu_\mathrm{leff} = \mu_\mathrm{l} + \mu_\mathrm{BIT}$$

The modeling of μ_BIT and its effects on mesoscale turbulence is discussed in subsec. 4.6.4.

The swarm-induced turbulence investigated in this work will be nearly unchanged for inviscid flow (i.e. $\mu_\phi = 0$) in the simulations.

4.3.1 Interphase force models

4.3.1.1 Drag force $\mathbf{F}_\mathrm{D}$

Drag force accounts for the resistance experienced by the bubble while moving in the liquid phase, it is a result of the shear and form drag of the fluid flow. Drag force is considered to be very significant in bubbly flows as it controls the rise velocity determining the gas residence time and contributes towards the generation of liquid vortices. The models proposed for drag force can be subdivided into two main categories: stokes drag (Happel and Brenner, 2012) and inertial drag Schiller and Naumann (1935); Beetstra et al. (2007). Stokes drag model is used in the limit of bubble Reynolds number (Re_p) ~ 1. The simulations in the current work involve Re_p of the order of 600 - 700, hence an inertial drag law as given in Eq. (4.3) is adopted, where the drag coefficient C_D is generally modeled as a function of Re_p (Schiller and Naumann, 1935; Levich et al., 1962).

$$\mathbf{F}_\mathrm{D} = \alpha_\mathrm{g}\rho_\mathrm{l}C_\mathrm{D}|\mathbf{u}_\mathrm{g} - \mathbf{u}_\mathrm{l}|\left(\mathbf{u}_\mathrm{g} - \mathbf{u}_\mathrm{l}\right) \tag{4.3}$$

$$C_\mathrm{D} = \max\left\{\min\left[\frac{24}{Re}\left(1 + 0.15Re^{0.687}\right), \frac{48}{Re}\right], \frac{8}{3}\frac{Eo}{Eo+4}\right\} \tag{4.4}$$

$$Eo = \frac{g\left(\rho_\mathrm{l} - \rho_\mathrm{g}\right)d_\mathrm{p}^2}{\sigma}$$

In bubbly flows, bubbles have a tendency to deform as the size increases, which influence the form drag component of the drag force, hence correlations for drag coefficient has to be developed to accomodate the effect of shape change. Tomiyama (1998) have developed a correlation as given in Eq. (4.4), which accomodates the effect of shape change on the drag force, through Eotvos number (Eo), it can be noted from the expression given in Eq. (4.4) that the drag coefficient purely depends on Eotvos numer rather than Reynolds number after a critical bubble diameter $\sim$ 4 mm indicating the importance of shape change on the drag force after a critical bubble diameter.

4.3.1.2 Virtual mass force $\mathbf{F}_{\mathrm{VM}}$

Virtual mass force is the force resulting from the acceleration of displaced fluid in the neighbourhood of the bubble (Milne-Thomson, 1968). It is modeled as given in Eq. (4.5),

$$\mathbf{F}_{\mathrm{VM}} = \alpha_{\mathrm{g}} C_{\mathrm{VM}} \rho_{\mathrm{l}} \left[\frac{D\mathbf{u}_{\mathrm{g}}}{Dt} - \frac{D\mathbf{u}_{\mathrm{l}}}{Dt} \right] \tag{4.5}$$

$$C_{\mathrm{VM}} = 0.5$$

The significance of virtual mass force depends on the density ratio of continuous and dispersed phase, higher density ratio corresponds to higher virtual mass force (Prosperetti and Tryggvason, 2009), typically in gas-particle flows virtual mass force is neglected due to the low density ratio, however in bubbly flows it is significant. In the region near to the sparger bubble accelerates significantly, addition of this force controls the acceleration and facilitates the bubble to achieve a realistic terminal velocity. Moreover, it is reported by many (Drew, 1983a; No and Kazimi, 1985; Watanabe et al., 1990) the addition of virtual mass force improves the numerical stability by modifying the eigen values associated with the two-fluid model system of equations, hence it is used in some low density ratio flows as well, eventhough it is not significant in that limit. A value of $C_{\mathrm{VM}} = 0.5$ is deduced theoretically for spherical rigid particles in potential flow by Maxey and Riley (1983) and is used in many works (Buwa and Ranade, 2002; Lahey, 1990a; Ekambara et al., 2008) to successfully predict bubbly flows. In the current work a value of 0.5 is retained for the virtual mass coefficient.

4.3.1.3 Lift force $\mathbf{F}_{\mathrm{LF}}$

Lift force is significant in bubbly flows with high strain rate such as vertical pipe flows. Flow inside the bubble column exhibit low velocity gradients due to the stagnant nature of the liquid. However, lift force is known to contribute towards the stability of the bubble column (Lucas et al., 2005; Krepper et al., 2007; Mazzitelli and Lohse, 2009). A local increase of the gas fraction causes a local acceleration of the liquid in the upward direction leading to the gradient in the vertical velocity component, such velocity gradient pushes the bubbles from the region of increased gas fraction to regions with low void fraction, thus stabilizing the flow. We adopt a lift force formulation Eq. (4.6) given in Zun (1980), which is used in many works (Torvik

and Svendsen, 1990; Delnoij et al., 1997b; Joshi, 2001; Lahey, 1990a) to predict bubbly flow behaviour.

$$\mathbf{F}_{\mathrm{LF}} = \alpha_{\mathrm{g}}\rho_{\mathrm{l}}C_{\mathrm{L}}\left(\mathbf{u}_{\mathrm{g}} - \mathbf{u}_{\mathrm{l}}\right) \times \nabla \times \mathbf{u}_{\mathrm{l}} \tag{4.6}$$

$$C_{\mathrm{L}} = \begin{cases} \min[0.288\tanh\left(0.121Re\right), f\left(Eo\right)] & Eo \leq 4 \\ f\left(Eo\right), & 4 \leq Eo \leq 10.7 \end{cases}$$

where,

$$f\left(Eo\right) = 0.00105Eo^3 - 0.00159Eo^2 - 0.0204Eo + 0.474$$

The lift coefficient (C_{L}) in these works were assumed to be constant 0.5. However, in the experimental investigation of Tomiyama et al. (2002b), it was found that the lift coefficient is a strong function of size, lift coefficient decreases with the increase in the bubble size and eventually turns negative after a critical bubble size of approximately 5 mm. Depending on the sign of this coefficient, lift force may have a stabilizing or destabilizing effect on the flow. Hence, it is essential to add an appropriate lift coefficient model which incorporates the dependency on bubble size, to accurately predict the instabilities in the flow.

4.3.1.4 Bubble dispersion $\mathbf{F}_{\mathrm{BD}}$

Bubble dispersion accounts for the hydrodynamic interaction between bubbles or the drag induced by one bubble over the other through the liquid. The addition of bubble dispersion ensures that the two-fluid model is hyperbolic, thereby removing unphysical fluctuations in α_{g}.

$$\mathbf{F}_{\mathrm{BD}} = -\alpha_{\mathrm{g}}\rho_{\mathrm{l}}C_{\mathrm{D}}|\mathbf{u}_{\mathrm{g}} - \mathbf{u}_{\mathrm{l}}|\frac{\delta_{\mathrm{dis}}}{\alpha_{\mathrm{g}}\alpha_{\mathrm{l}}}\nabla\alpha_{\mathrm{g}} \tag{4.7}$$

where $\delta_{\mathrm{dis}} = C_{\mathrm{dis}}d_{\mathrm{p}}|\mathbf{u}_{\mathrm{g}} - \mathbf{u}_{\mathrm{l}}|\sqrt{\alpha_{\mathrm{g}}\alpha_{\mathrm{l}}}$ and $C_{\mathrm{dis}} = 1.3$. In addition to ensuring a hyperbolic system, bubble dispersion is known to stabilize (Lucas et al., 2005) the bubbly flow by smoothing out the non-uniformity in the gas fraction profile. Bubble columns are known to stay stable qualitatively up to a global void fraction of 0.25–0.3 (Harteveld, 2005b), hence the addition of this force also contributes towards achieving that result.

4.4 Reynolds-Averaged Equations

Bubble columns are commonly operated in very large scales, in the order of tens of meters. At such scales it is computationally impossible to resolve the turbulent flow structures. Hence we derive the Reynolds-averaged equations by phase averaging the two-fluid model, by assuming that the two-fluid equations with high grid resolution will accurately predict the large-scale features like turbulence generated due to bubble swarms. Detailed description of the steps involved in the derivation of the Reynolds-averaged equations can be found in Fox (2014a). In the current work we extend the model given in Fox (2014a), for bubbly flows by adding the appropriate interphase submodels into the two-fluid equations (Eq. (4.1) and (4.2)) specifically adopted for bubbly flows and phase averaging them.

By performing phase averaging on the two-fluid equations (Eqs. (4.1) and (4.2)), we get the Reynolds-averaged equations in the following form:

Continuity:

$$\frac{\partial \langle \alpha_\phi \rangle}{\partial t} + \nabla \cdot \langle \alpha_\phi \rangle \langle \mathbf{u}_\phi \rangle_\phi = 0 \tag{4.8}$$

Momentum:

$$\begin{aligned}\frac{\partial \langle \alpha_\phi \rangle \langle \mathbf{u}_\phi \rangle_\phi}{\partial t} + \nabla \cdot \left(\langle \alpha_\phi \rangle \langle \mathbf{u}_\phi \rangle_\phi \langle \mathbf{u}_\phi \rangle_\phi + \langle \alpha_\phi \rangle \langle \mathbf{u}_\phi'' \mathbf{u}_\phi'' \rangle_\phi - \frac{1}{\rho_\phi} \langle \boldsymbol{\sigma}_\phi \rangle \right) \\ = (-1)^\phi \langle C_\mathrm{D} \rangle \langle \alpha_\phi \rangle \left(\langle \mathbf{u}_\mathrm{g} \rangle_\mathrm{g} - \langle \mathbf{u}_\mathrm{l} \rangle_\mathrm{l} - \frac{\langle \alpha_\mathrm{g}' \mathbf{u}_\mathrm{l}'' \rangle}{\langle \alpha_\mathrm{l} \rangle \langle \alpha_\mathrm{g} \rangle} + \mathbf{F}'_\mathrm{nonlin} \right) - \frac{\langle \alpha_\phi \rangle}{\rho_\phi} \nabla \langle p_\mathrm{l} \rangle \\ - \frac{1}{\rho_\phi} \langle \alpha_\mathrm{g}' \nabla p_\mathrm{l}' \rangle + \langle \alpha_\phi \rangle \mathbf{g} + (-1)^\phi \frac{\langle \alpha_\mathrm{g} \rangle}{\rho_\phi} \left(\langle \mathbf{F}_\mathrm{VM} \rangle_\mathrm{g} + \langle \mathbf{F}_\mathrm{LF} \rangle_\mathrm{g} + \langle \mathbf{F}_\mathrm{BD} \rangle_\mathrm{g} \right)\end{aligned} \tag{4.9}$$

where $\langle \cdot \rangle_\mathrm{g}$ is the phase average with respect to the gas phase, and $\langle \cdot \rangle_\mathrm{l}$ is the phase average with respect to the liquid phase.

The continuity equation does not have any unclosed term appearing in the equation. However, if you notice the momentum equation Eq. (4.9), it has several unclosed terms due to the phase averaging of the non-linear convection and interphase force terms. The influence of these unclosed terms on driving the flow patterns are quantified in the study through mesoscale simulations.

The unclosed term due the convection term which is Reynolds stress is generally modeled

(Svendsen et al., 1992; Hjertager and Morud, 1995; Grienberger and Hofmann, 1992; Lahey, 1990b) using Boussinesq approximation (Pope, 2000), where it is assumed to be proportional to the strain rate and the proportionality constant is the eddy viscosity as shown in Eqn. (4.11).

$$\langle \mathbf{u}_\phi'' \mathbf{u}_\phi'' \rangle_{\mathrm{p}\phi} = -\mu_{\mathrm{T}\phi} \left(\nabla \langle \mathbf{u}_\phi \rangle_{\mathrm{p}\phi} + \left(\nabla \langle \mathbf{u}_\phi \rangle_{\mathrm{p}\phi} \right)^{\mathrm{T}} - \frac{2}{3} \mathbf{I} \left(\nabla \cdot \langle \mathbf{u}_\phi \rangle_{\mathrm{p}\phi} \right) \right) \tag{4.10}$$

$$\mu_{\mathrm{T}\phi} = c_{\mu\phi} \frac{k_\phi^2}{\epsilon_\phi} \tag{4.11}$$

The eddy viscosity is modelled similar to the molecular viscosity (see for e.g. in (Pope, 2000)), where it is assumed to be a product of a length and a velocity scale. These length and velocity scales are casted in terms of the turbulent kinetic energy (k) and dissipation (ϵ) to compute the eddy viscosity as given in Eq. (4.11). Then, a two equation transport model (k-ϵ) is used to calculate the quantities k and ϵ. A transport model for k and ϵ for multiphase flows can be found in Fox (2014a). Unlike the ad hoc versions used in the works (Svendsen et al., 1992; Hjertager and Morud, 1995; Grienberger and Hofmann, 1992; Lahey, 1990b), it is derived from the multiphase flow equations through phase averaging.

The modeling strategy based on the assumption of turbulence isotropy as above may not be appropriate for bubbly flows due to the significant anisotropy involved, hence one has to compute the turbulent stresses directly by deriving a Reynolds stress transport equation and seeking closures for the unclosed terms in the derived Reynolds stress transport equation through mesoscale simulations. A Reynolds stress transport equation is derived in the following subsection.

4.4.1 Reynolds-stress equations

By performing a tensor product of $\mathbf{u}_\phi''$ and the momentum (Eq. (4.2)) and phase averaging we can obtain the following transport equation for Reynolds stress for gas and liquid phase.

Gas phase:

$$\frac{\partial\langle\alpha_{\mathrm{g}}\rangle\langle\mathbf{u}_{\mathrm{g}}^{''}\mathbf{u}_{\mathrm{g}}^{''}\rangle_{\mathrm{pg}}}{\partial t}+\nabla\cdot[\langle\alpha_{\mathrm{g}}\rangle\langle\mathbf{u}_{\mathrm{g}}^{''}\mathbf{u}_{\mathrm{g}}^{''}\rangle_{\mathrm{pg}}\langle\mathbf{u}_{\mathrm{g}}\rangle_{\mathrm{pg}}+\langle\alpha_{\mathrm{g}}\rangle\frac{1}{2}\langle\mathbf{u}_{\mathrm{g}}^{''}\mathbf{u}_{\mathrm{g}}^{''}\mathbf{u}_{\mathrm{g}}^{''}\rangle_{\mathrm{pg}}]$$
$$=-\langle\alpha_{\mathrm{g}}\rangle\langle\mathbf{u}_{\mathrm{g}}^{''}\mathbf{u}_{\mathrm{g}}^{''}\rangle_{\mathrm{pg}}\cdot\nabla\langle\mathbf{u}_{\mathrm{g}}\rangle_{\mathrm{pg}}+\frac{1}{\rho_{\mathrm{g}}}\left(\nabla\cdot\langle\boldsymbol{\sigma}_{\mathrm{g}}\mathbf{u}_{\mathrm{g}}^{''}\rangle-\nabla\langle p_{\mathrm{l}}\mathbf{u}_{\mathrm{g}}^{''}\rangle\right)+$$
$$\frac{1}{\rho_{\mathrm{g}}}\left(\langle p_{\mathrm{l}}\nabla\mathbf{u}_{\mathrm{g}}^{''}\rangle-\langle\boldsymbol{\sigma}_{\mathrm{g}}\cdot\nabla\mathbf{u}_{\mathrm{g}}^{''}\rangle\right)$$
$$+\frac{\rho_{\mathrm{l}}\langle\alpha_{\mathrm{g}}\rangle\langle C_{\mathrm{D}}\rangle}{\rho_{\mathrm{g}}}[\langle\mathbf{u_{\mathrm{l}}}^{''}\mathbf{u_{\mathrm{g}}}^{''}\rangle_{\mathrm{pg}}-\langle\mathbf{u}_{\mathrm{g}}^{''}\mathbf{u}_{\mathrm{g}}^{''}\rangle_{\mathrm{pg}}]-\frac{\langle\alpha_{\mathrm{g}}\rangle}{\rho_{\mathrm{g}}}\left(\langle\mathbf{u}_{\mathrm{g}}^{''}\nabla p_{\mathrm{l}}^{'}\rangle_{\mathrm{pg}}\right)+$$
$$-\frac{1}{\rho_{\mathrm{g}}}\left(\langle\mathbf{F}_{\mathrm{VM}}\mathbf{u}_{\mathrm{g}}^{''}\rangle+\langle\mathbf{F}_{\mathrm{LF}}\mathbf{u}_{\mathrm{g}}^{''}\rangle+\langle\mathbf{F}_{\mathrm{BD}}\mathbf{u}_{\mathrm{g}}^{''}\rangle\right)\quad(4.12)$$

Liquid phase:

$$\frac{\partial\langle\alpha_{\mathrm{l}}\rangle\langle\mathbf{u}_{\mathrm{l}}^{''}\mathbf{u}_{\mathrm{l}}^{''}\rangle_{\mathrm{pl}}}{\partial t}+\nabla\cdot[\langle\alpha_{\mathrm{l}}\rangle\langle\mathbf{u}_{\mathrm{l}}^{''}\mathbf{u}_{\mathrm{l}}^{''}\rangle_{\mathrm{pl}}\langle\mathbf{u}_{\mathrm{l}}\rangle_{\mathrm{pl}}+\langle\alpha_{\mathrm{l}}\rangle\frac{1}{2}\langle\mathbf{u}_{\mathrm{l}}^{''}\mathbf{u}_{\mathrm{l}}^{''}\mathbf{u}_{\mathrm{l}}^{''}\rangle_{\mathrm{pl}}]$$
$$=-\langle\alpha_{\mathrm{l}}\rangle\langle\mathbf{u}_{\mathrm{l}}^{''}\mathbf{u}_{\mathrm{l}}^{''}\rangle_{\mathrm{pl}}\cdot\nabla\langle\mathbf{u}_{\mathrm{l}}\rangle_{\mathrm{pl}}+\frac{1}{\rho_{\mathrm{l}}}\left(\nabla\cdot\langle\boldsymbol{\sigma}_{\mathrm{l}}\mathbf{u}_{\mathrm{l}}^{''}\rangle-\nabla\langle p_{\mathrm{l}}\mathbf{u}_{\mathrm{l}}^{''}\rangle\right)+$$
$$\frac{1}{\rho_{\mathrm{l}}}\left(\langle p_{\mathrm{l}}\nabla\mathbf{u}_{\mathrm{l}}^{''}\rangle-\langle\boldsymbol{\sigma}_{\mathrm{l}}\cdot\nabla\mathbf{u}_{\mathrm{l}}^{''}\rangle\right)$$
$$+\frac{\rho_{\mathrm{l}}\langle\alpha_{\mathrm{l}}\rangle\langle C_{\mathrm{D}}\rangle}{\rho_{\mathrm{l}}}[\langle\mathbf{u_{\mathrm{l}}}^{''}\mathbf{u_{\mathrm{g}}}^{''}\rangle_{\mathrm{pg}}-\langle\mathbf{u}_{\mathrm{l}}^{''}\mathbf{u}_{\mathrm{l}}^{''}\rangle_{\mathrm{pg}}+\langle\mathbf{u}_{\mathrm{l}}^{''}\rangle_{\mathrm{pg}}(\langle\mathbf{u}_{\mathrm{g}}\rangle_{\mathrm{pg}}-\langle\mathbf{u}_{\mathrm{l}}\rangle_{\mathrm{pg}})]$$
$$+\frac{\langle\alpha_{\mathrm{g}}\rangle}{\rho_{\mathrm{l}}}\left(\langle\mathbf{u}_{\mathrm{l}}^{''}\nabla p_{\mathrm{l}}^{'}\rangle_{\mathrm{pg}}\right)$$
$$+\frac{\langle\alpha_{\mathrm{l}}\rangle}{\rho_{\mathrm{l}}}\langle\mathbf{u}_{\mathrm{l}}^{''}\rangle_{\mathrm{pg}}\nabla\langle p_{\mathrm{l}}\rangle+$$
$$+\frac{1}{\rho_{\mathrm{l}}}\left(\langle\mathbf{F}_{\mathrm{VM}}\mathbf{u}_{\mathrm{l}}^{''}\rangle+\langle\mathbf{F}_{\mathrm{LF}}\mathbf{u}_{\mathrm{l}}^{''}\rangle+\langle\mathbf{F}_{\mathrm{BD}}\mathbf{u}_{\mathrm{l}}^{''}\rangle\right)\quad(4.13)$$

There are several unclosed terms which appear in the RST Eqns. (4.12) and (4.13) due to the phase averaging and has to be modelled to effectively solve the equations to obtain Reynolds stress. Transport terms transport the turbulence in the flow systems through diffusion and convection. Convection term does not require any modeling, however, diffusion terms $-\langle\alpha_{\mathrm{l}}\rangle\frac{1}{2}\langle\mathbf{u}_{\phi}^{''}\mathbf{u}_{\phi}^{''}\mathbf{u}_{\phi}^{''}\rangle_{\mathrm{p}\phi}$, $\langle\boldsymbol{\sigma}_{\phi}\mathbf{u}_{\mathrm{l}}^{''}\rangle$ and $\langle p_{\mathrm{l}}\mathbf{u}_{\phi}^{''}\rangle I$ due to turbulence, viscous and pressure respectively requires modeling. These terms can be combined and modelled based on gradient diffusion hypothesis similar to single phase flows as given in Pope (2000).

In the current work, Pressure strain $\langle p_{\mathrm{l}}\nabla\mathbf{u}_{\phi}^{''}\rangle$, viscous dissipation $\langle\boldsymbol{\sigma}\cdot\nabla\mathbf{u}_{\phi}{}^{\text{“}}\rangle$ and inter-phase production terms due to lift, drag, buoyancy, virtual mass and bubble dispersion are quantified from the mesoscale simulations in the Reynolds stress budget section. The turbulence

production due to shear -$\langle\alpha_\phi\rangle\langle\mathbf{u}_\phi''\mathbf{u}_\phi''\rangle_{\mathrm{p}\phi}\cdot\nabla\langle\mathbf{u}_\phi\rangle_\phi$ is usually negligible compared to inter-phase production in bubble solumns due to the small velocity gradients $\nabla\langle\mathbf{u}_\phi\rangle_\phi$ in the flow. Hence, it is reasonable to first study the effect of inter-phase production terms rather than the shear induced turbulence production in bubble columns.

4.5 Statistically homogeneous flows

In bubbly flows encountered in bubble columns shear induced turbulence can be negligible due to the stagnant nature of the liquid pool. The main source of turbulence production then would be due to the interphase coupling (drag, buoyancy etc.). By simulating a homogeneous bubbly flow by applying periodic boundary conditions, eliminates the transport terms in the conservation equations (Eqns. (4.9), (4.12) and (4.13)), including the turbulence production due to shear. We can thus obtain the transport equations merely in terms of interphase force terms (Eqns. (4.14) and (4.15)) and production terms due to the interphase coupling (Eqns. (4.16) and (4.17)).

Momentum

Liquid phase:

$$
\begin{aligned}
0 = &-\frac{1}{\rho_\mathrm{l}}\nabla\langle p_\mathrm{l}\rangle && \text{Balance Force (BF)}\\
&+\langle\alpha_\mathrm{g}\rangle\langle C_\mathrm{D}\rangle\left(\langle\mathbf{u}_\mathrm{g}\rangle_\mathrm{pg}-\langle\mathbf{u}_\mathrm{l}\rangle_\mathrm{pl}\right) && \text{Drag Force (DF)}\\
&-\langle\alpha_\mathrm{g}\rangle\langle C_\mathrm{D}\rangle\left(\frac{\langle\alpha_\mathrm{g}'\mathbf{u}_\mathrm{l}'\rangle}{\langle\alpha_\mathrm{l}\rangle\langle\alpha_\mathrm{g}\rangle}\right)+\mathbf{F}'_{\mathrm{nonlin}} && \text{Drag unclosed}\\
&+\frac{\langle\alpha_\mathrm{g}\rangle}{\rho_\mathrm{l}}\nabla\langle p_\mathrm{l}\rangle && \text{Buoyancy}\\
&+\frac{1}{\rho_\mathrm{l}}\langle\alpha_\mathrm{g}'\nabla p_\mathrm{l}'\rangle && \text{Buoyancy unclosed}\\
&+\langle\alpha_\mathrm{l}\rangle\mathbf{g} && \text{Gravity}\\
&+\frac{\langle\alpha_\mathrm{g}\rangle}{\rho_\mathrm{l}}\langle\mathbf{F}_\mathrm{VM}\rangle_\mathrm{pg} && \text{VM}\\
&+\frac{\langle\alpha_\mathrm{g}\rangle}{\rho_\mathrm{l}}\langle\mathbf{F}_\mathrm{LF}\rangle_\mathrm{pg} && \text{Lift}\\
&+\frac{\langle\alpha_\mathrm{g}\rangle}{\rho_\mathrm{l}}\langle\mathbf{F}_\mathrm{BD}\rangle_\mathrm{pg} && \text{BD}
\end{aligned}
\tag{4.14}
$$

where $\mathbf{F}'_{\text{nonlin}} = \langle \mathbf{F}_{\text{D}} \rangle_{\text{pg}} - \text{DF} + \langle \alpha_{\text{g}} \rangle \langle C_{\text{D}} \rangle \left(\frac{\langle \alpha'_{\text{g}} \mathbf{u}'_{\text{l}} \rangle}{\langle \alpha_{\text{l}} \rangle \langle \alpha_{\text{g}} \rangle} \right)$

Gas phase:

$$
\begin{aligned}
0 = & - \langle \alpha_{\text{g}} \rangle \langle C_{\text{D}} \rangle \left(\langle \mathbf{u}_{\text{g}} \rangle_{\text{pg}} + \langle \mathbf{u}_{\text{l}} \rangle_{\text{pl}} \right) && \text{Drag Force (DF)} \\
& + \langle \alpha_{\text{g}} \rangle \langle C_{\text{D}} \rangle \left(\frac{\langle \alpha'_{\text{g}} \mathbf{u}'_{\text{l}} \rangle}{\langle \alpha_{\text{l}} \rangle \langle \alpha_{\text{g}} \rangle} \right) - \mathbf{F}'_{\text{nonlin}} && \text{Drag unclosed} \\
& - \frac{\langle \alpha_{\text{g}} \rangle}{\rho_{\text{l}}} \nabla \langle p_{\text{l}} \rangle && \text{Buoyancy} \\
& - \frac{1}{\rho_{\text{l}}} \langle \alpha'_{\text{g}} \nabla p'_{\text{l}} \rangle && \text{Buoyancy unclosed} \\
& + \langle \alpha_{\text{l}} \rangle \mathbf{g} && \text{Gravity} \\
& - \frac{\langle \alpha_{\text{g}} \rangle}{\rho_{\text{l}}} \langle \mathbf{F}_{\text{VM}} \rangle_{\text{pg}} && \text{VM} \\
& - \frac{\langle \alpha_{\text{g}} \rangle}{\rho_{\text{l}}} \langle \mathbf{F}_{\text{LF}} \rangle_{\text{pg}} && \text{Lift} \\
& - \frac{\langle \alpha_{\text{g}} \rangle}{\rho_{\text{l}}} \langle \mathbf{F}_{\text{BD}} \rangle_{\text{pg}} && \text{BD}
\end{aligned} \tag{4.15}
$$

RST

Liquid phase:

$$
\begin{aligned}
0 = & \frac{1}{\rho_{\text{l}}} \left(\langle p_{\text{l}} \nabla \mathbf{u}''_{\text{l}} \rangle - \langle \boldsymbol{\sigma}_{\text{l}} \cdot \nabla \mathbf{u}''_{\text{l}} \rangle \right) && \text{Pressure strain (PS) + Viscous disssipation (VD)} \\
& + \frac{\rho_{\text{l}} \langle \alpha_{\text{l}} \rangle \langle C_{\text{D}} \rangle}{\rho_{\text{l}}} [\langle \mathbf{u}_{\text{l}}'' \mathbf{u}_{\text{g}}'' \rangle_{\text{pg}} - \langle \mathbf{u}''_{\text{l}} \mathbf{u}''_{\text{l}} \rangle_{\text{pg}}] && \text{Drag Exchange (DE)} \\
& + \mathbf{DPnon} && \text{DNL } \left(\langle \mathbf{F}_{\text{D}} \mathbf{u}''_{\text{l}} \rangle - \text{DE} \right) \\
& + \frac{\rho_{\text{l}} \langle \alpha_{\text{l}} \rangle \langle C_{\text{D}} \rangle}{\rho_{\text{l}}} [\langle \mathbf{u}''_{\text{l}} \rangle_{\text{pg}} \left(\langle \mathbf{u}_{\text{g}} \rangle_{\text{pg}} - \langle \mathbf{u}_{\text{l}} \rangle_{\text{pg}} \right)] && \text{Drag Production (DP)} \\
& + \frac{\langle \alpha_{\text{g}} \rangle}{\rho_{\text{l}}} \left(\langle \mathbf{u}''_{\text{l}} \nabla p'_{\text{l}} \rangle_{\text{pg}} \right) + \frac{\langle \alpha_{\text{g}} \rangle}{\rho_{\text{l}}} \langle \mathbf{u}''_{\text{l}} \rangle_{\text{pg}} \nabla \langle p_{\text{l}} \rangle && \text{BuoyancyP} \\
& + \frac{1}{\rho_{\text{l}}} \langle \mathbf{F}_{\text{VM}} \mathbf{u}''_{\text{l}} \rangle && \text{VMP} \\
& + \frac{1}{\rho_{\text{l}}} \langle \mathbf{F}_{\text{LF}} \mathbf{u}''_{\text{l}} \rangle && \text{LFP} \\
& + \frac{1}{\rho_{\text{l}}} \langle \mathbf{F}_{\text{BD}} \mathbf{u}''_{\text{l}} \rangle && \text{BDP}
\end{aligned} \tag{4.16}
$$

Gas phase:

$$
\begin{aligned}
0 = {} & \frac{1}{\rho_{\mathrm{g}}}\left(\langle p_{\mathrm{l}}\nabla \mathbf{u}_{\mathrm{g}}^{''}\rangle - \langle \boldsymbol{\sigma}_{\mathrm{g}}\cdot\nabla \mathbf{u}_{\mathrm{g}}^{''}\rangle\right) && \text{Pressure strain (PS) + Viscous disssipation (VD)} \\
& + \frac{\rho_{\mathrm{l}}\langle\alpha_{\mathrm{g}}\rangle\langle C_{\mathrm{D}}\rangle}{\rho_{\mathrm{g}}}[\langle \mathbf{u}_{\mathrm{l}}{}^{''}\mathbf{u}_{\mathrm{g}}{}^{''}\rangle_{\mathrm{pg}} - \langle \mathbf{u}_{\mathrm{g}}^{''}\mathbf{u}_{\mathrm{g}}^{''}\rangle_{\mathrm{pg}}] && \text{DE (Drag Exchange)} \\
& + \mathbf{DPnon} && \text{DNL}\left(-\langle \mathbf{F}_{\mathrm{D}}\mathbf{u}_{\mathrm{g}}^{''}\rangle - \text{DE}\right) \\
& - \frac{\langle\alpha_{\mathrm{g}}\rangle}{\rho_{\mathrm{g}}}\left(\langle \mathbf{u}_{\mathrm{g}}^{''}\nabla p_{\mathrm{l}}^{'}\rangle_{\mathrm{pg}}\right) && \text{Buoyancy} \\
& - \frac{1}{\rho_{\mathrm{g}}}\langle \mathbf{F}_{\mathrm{VM}}\mathbf{u}_{\mathrm{g}}^{''}\rangle && \text{VMP} \\
& - \frac{1}{\rho_{\mathrm{g}}}\langle \mathbf{F}_{\mathrm{LF}}\mathbf{u}_{\mathrm{g}}^{''}\rangle && \text{LFP} \\
& - \frac{1}{\rho_{\mathrm{g}}}\langle \mathbf{F}_{\mathrm{BD}}\mathbf{u}_{\mathrm{g}}^{''}\rangle && \text{BDP}
\end{aligned} \tag{4.17}
$$

These simple set of equations helps in better understanding of the relative importance of the turbulence production due to the interphase coupling terms.

4.6 Results and discussions

4.6.1 Simulation setup

The computational domain for mesoscale DNS is constituted by a 3-D box. Periodic boundary conditions are applied on all the sides of the column. Periodic boundary condition simplifies the RA equations by eliminating the terms containing mean gradients of the statistics. However, the liquid phase is continuously accelerated and the system never reaches a statistically stationary state. To prevent the acceleration of the system a modified liquid pressure gradient computed by enforcing the average net mass flux to be zero. The influence of the periodic boundary condition on the statistics is eliminated by choosing a domain size based on the velocity pair correlation function discussed in Sec. 4.6.8. The properties of both the phases used in the simulation are given in Tab. 4.1.

The closure study is performed by varying the initial global void fraction as given in Table 4.2. For $\alpha_{\mathrm{g}} > 0.4$ the heterogeneous flow regime with turbulent structures can be seen in the simulations.

Table 4.1 Physical parameters used in simulations

Property	Value
d_{p}	0.004 m
ρ_{g}	1.2 kg/m^3
μ_{g}	1.983×10^{-3} Pa $\cdot$ s
ρ_{l}	1000 kg/m^3
μ_{l}	10^{-3} Pa $\cdot$ s

Table 4.2 Gas hold up and predicted flow regime

Runs	α_{g}	Regime
1	0.15	homogeneous
2	0.3	homogeneous
3	0.4	heterogeneous
4	0.5	heterogeneous

A grid resolution of $d_b/2$ is adopted (see Sec. 4.6.3) and a time resolution of the order of bubble relaxation time is adopted for the simulations. The schemes used are second-order accurate in space and first-order accurate in time. The turbulence characteristics of the flow are studied by varying the global void fraction as given in Tab. 4.2.

4.6.2 Flow regime

In the homogeneous regime, the simulation reach a steady state where all of the variables are independent of time. In contrast, the heterogeneous regime is characterized by vold fraction fluctuations, or bubble swarms, and turbulence due to the coupling of these bubble swarms and the liquid phase. Phase coupling in the heterogeneous regime creates high vorticity regions in the flow. Bubble swarms are observed in this regime due to gas accumulation in high vorticity regions. Fig. 4.1 is obtained from the simulations, in the figure black contour line corresponds to the border of the clusters and these borders approximately trace out the high vorticity region (light green regions) indicating the preferential accumulation of bubbles in high vorticity regions. Fig. 4.2 shows the vector plot of liquid velocity at a particular plane parallel to the flow direction. From the figure it can be seen that the flow is filled with vortices in the heterogeneous regime.

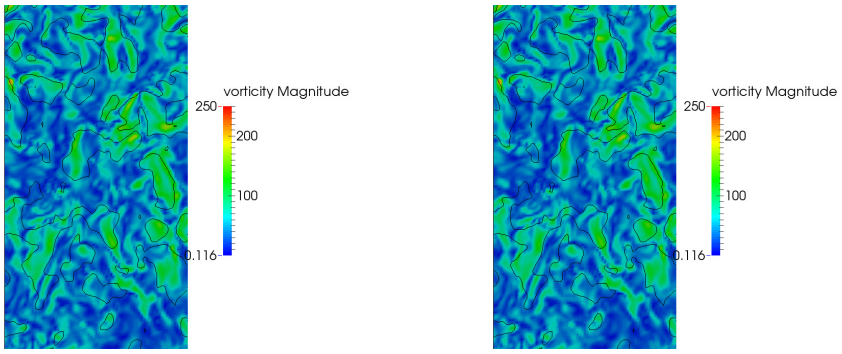

Figure 4.1 Clustering of bubbles in the high vorticity regions for $\alpha = 0.5$. Left: gas volume fraction. Right: vorticity magnitude.

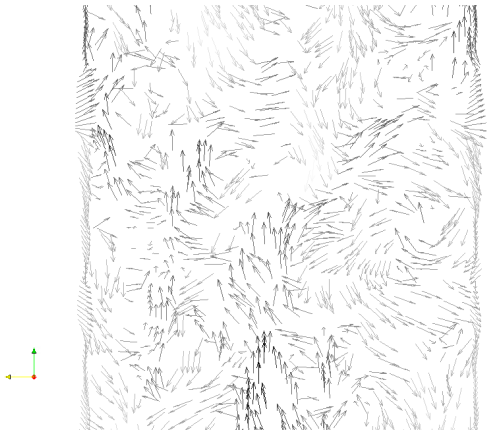

Figure 4.2 Vector plot of liquid velocity in a plane for $\alpha = 0.5$.

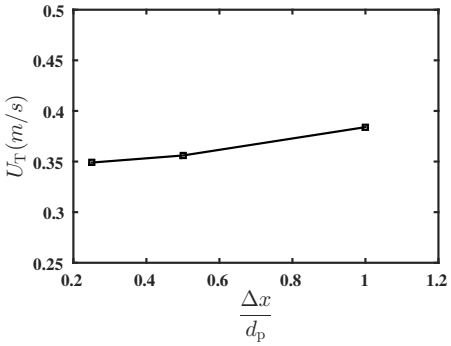

Figure 4.3 Rise velocity of the bubble

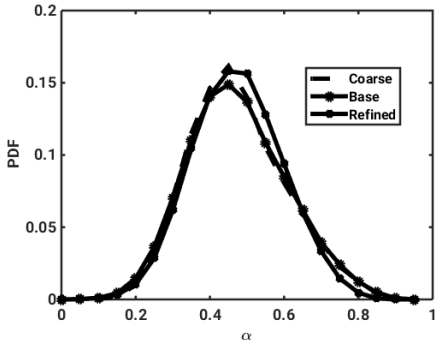

Figure 4.4 Probability distribution function of gas

4.6.3 Grid independence study

The probability distribution function (PDF) for $\alpha_g = 0.5$ for three grid resolutions: coarse (d_p), base ($0.5d_p$) and refined ($0.25d_p$). from the simulations are reported in Fig. 4.4. It can be concluded from Fig. 4.4 that the PDF curves obtained from the simulations for all the three grid resolutions are similar, in other words degree of segregation is similar for all the three grid resolutions.

Furthermore, the first order statistic of gas rise velocities are compared for $\alpha_g = 0.5$ for three grid resolutions coarse (d_p), base ($0.5d_p$) and refined ($0.25d_p$) in Fig. 4.3. From Fig. 4.3, a difference of 5.2% is found between the average gas rise velocity for cases with grid resolution (d_p) and base ($0.5d_p$) and, a difference of 1.9% is found between $0.5d_p$ and $0.25d_p$.

Hence, from the above grid independent study we adopt a grid resolution of $0.5d_p$ which is computationally feasible and does not compromise the accuracy, for the simulations in this

study to compute the statistics in the mean momentum and RST equations.

4.6.4 Effect of bubble induced turbulence

The lack of BIT viscosity models in the dense regime as discussed in the introduction motivated us to extract a BIT model constant from the experimental data given in Alméras et al. (2015) which is performed for moderately dense bubbly flows. We assume the same model form for the BIT viscosity given in Sato and Sekoguchi (1975b) and extract the BIT model constant $C_{\mathrm{BIT}} = Sc_{\mathrm{BIT}} C^{*}_{\mathrm{BIT}}$ by assuming a bubble induced turbulence Schmidt number of $Sc_{\mathrm{BIT}} - 0.1$ and fitting C^{*}_{BIT} to the experimental data.

$$\mu_{\mathrm{BIT}} = \rho_{\mathrm{l}} C_{\mathrm{BIT}} d_{\mathrm{p}} \min\left(\frac{\alpha_{\mathrm{g}}}{\alpha_{\mathrm{max}}}, 1\right) |u_{\mathrm{g}} - u_{\mathrm{l}}| \tag{4.18}$$

where $\alpha_{\mathrm{max}} - 0.04$ The radial distribution function with and without BIT model is plotted in

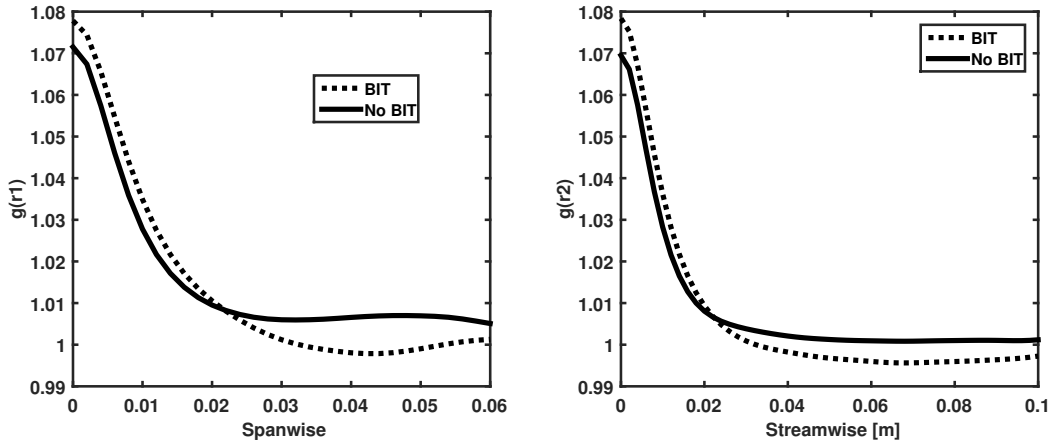

Figure 4.5 Radial distribution function for $\alpha_{\mathrm{g}} = 0.5$ with BIT and no BIT

Fig 4.5. From the Fig 4.5 it is apparent that the addition of the bubble induced turbulence does not modify the cluster length scales significantly, hence it is reasonable to conclude that the mesoscale turbulence is not significantly affected by the turbulence in the small scale wakes which quickly gets dissipated due to the wake interactions.

4.6.5 Probability distribution function (PDF) of velocity fluctuations in both phases and gas fraction

The probability distribution function of streamwise and spanise velocity fluctuations in both liquid and gas phase is computed from the simulations and reported in Fig. 4.6 and Fig. 4.7. The PDF of streamwise liquid velocity fluctuations (Fig. 4.6(left)) shows positive skewness and deviate from the gaussian behaviour for both gas fractions studied. The larger probability of upward fluctuations of streamwise velocity fluctuation component is due to the entrainement of the liquid in the wake of the rising bubbles. However, the PDF of spanwise liquid velocity fluctuations (Fig. 4.6(right)) follows a strictly gaussian behaviour due to the symmetry of the flow (no mean force acting in the spanwise direction). Similar trends are observed for the PDF of the velocity fluctuations in the gas phase (Fig. 4.7) due to the tendency of the bubbles to follow the liquid flow due to low inertia.

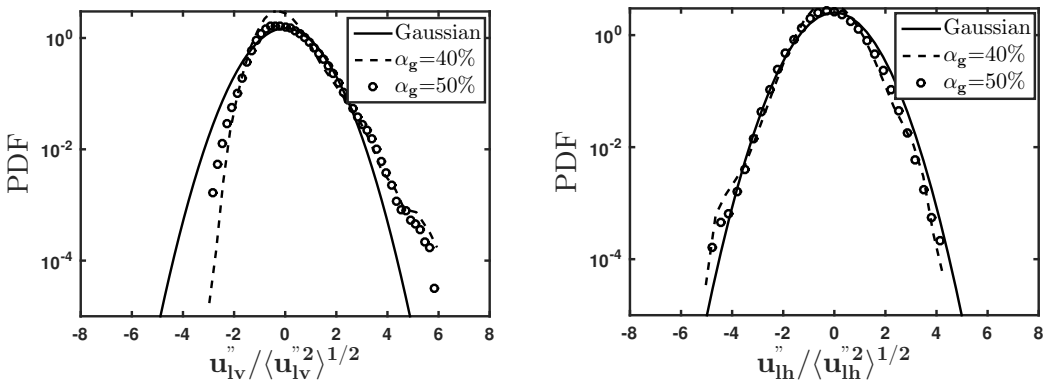

Figure 4.6 PDF for fluid phase vertical and horizontal velocity fluctuations

4.6.6 One-point statistics

One-point statistics average rise velocity and Reynolds stress components from the simulations are reported in Tab. 4.3.

It is interesting to note that the rise velocity ($\langle u_g \rangle_{pg}$) at $\alpha_g = 0.5$ and $\alpha_g = 0.4$ are higher than the single bubble rise velocity of 0.2 m/s (Simonnet et al., 2007), indicating that the formation of bubble swarms increase the rise velocity, this behaviour is also reported by

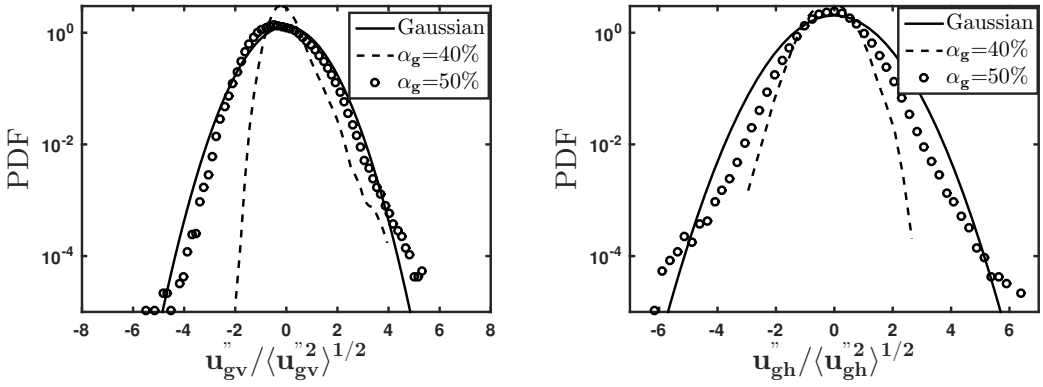

Figure 4.7 PDF for gas phase vertical and horizontal velocity fluctuations

Table 4.3 One point statistics

α_g	$\langle u_g\rangle_{pg}(m/s)$	$\langle u''_{gz}u''_{gz}\rangle_{pg}(m^2/s^2)$	$\langle u''_{gx}u''_{gx}\rangle_{pg}$	$\langle u''_{lz}u''_{lz}\rangle_{pl}$	$\langle u''_{lx}u''_{lx}\rangle_{pl}$
0.5	0.35	0.0962	0.0381	0.0703	0.0248
0.4	0.3	0.0775	0.0287	0.0343	0.0167
0.3	0.194	0	0	0	0
0.15	0.2	0	0	0	0

Sankaranarayanan et al. (2002) and attributed to the formation of wakes. On the contrary, for $\alpha_g = 0.3$ and $\alpha_g = 0.15$ the average bubble rise velocity is the similar to the single bubble rise velocity 0.2 m/s indicating a homogeneous rise of bubbles with no instabilities or swarm formation.

4.6.7 Radial distribution

The radial distribution function (RDF) in the streamwise (z) and spanwise (x) directions computed as given in Eqn. (4.19) are reported in Fig. 4.8 for gas fractions 0.3, 0.4 and 0.5. The good decay of the RDF within the streamwise and spanwise length of the domain indicates that all the length scales of the clusters are captured in the simulation effectively.

$$G(r) = \frac{\langle \alpha_\phi(\mathbf{x},t)\,\alpha_\phi(\mathbf{x}+\mathbf{r},t)\rangle}{\langle \alpha_\phi(\mathbf{x},t)\rangle\langle \alpha_\phi(\mathbf{x}+\mathbf{r},t)\rangle} \tag{4.19}$$

Moreover, it can be noted from Fig. 4.8 that the RDF doesn't change over the stream and spanwise directions for gas fraction 0.3 compared to gas fractions 0.4 and 0.5, which is due to the absence of liquid vortices which causes swarm formation.

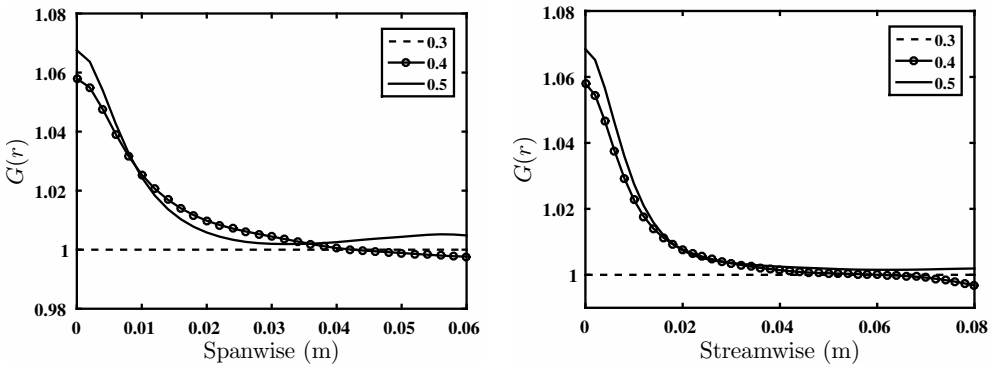

(a) Spanwise. (b) Streamwise.

Figure 4.8 Radial distribution function span-wise.

Table 4.4 cluster length scales (m)

α	L_{z}	L_{x}	$L = \langle u_{\mathrm{gz}} \rangle^2_{\mathrm{pg}}/g$
0.5	0.0121	0.0105	0.0125
0.4	0.0120	0.0114	0.0095

Average cluster size based on RDF can be calculated as follows:

$$L_{\mathrm{z}} = \frac{1}{G\left(0\right) - 1} \int_0^{\infty} \left(G\left(z\right) - 1\right) dz \tag{4.20}$$

$$L_{\mathrm{x}} = \frac{1}{G\left(0\right) - 1} \int_0^{\infty} \left(G\left(x\right) - 1\right) dx \tag{4.21}$$

The cluster size (L_{z}) computed from the radial distribution function in the z direction seems to be similar in both the phases. However, the cluster size (L_{x}) in the x direction is larger for $\alpha = 0.4$ compared to $\alpha = 0.5$, this may be due to the better growth of the clusters in the x direction before breaking into smaller clusters in the relatively low dense flow in the case of $\alpha = 0.4$ compared to $\alpha = 0.5$. A characteristic length scale (L) based on square of the rise velocity and gravity is defined as shown in the Table 4.4. The characteristic length scale defined, seem to predict the cluster length scale reasonably.

4.6.8 Pair correlation

The pair correlation function is computed for both the gas and liquid phases as given in Eqn. 4.22. The pair correlation can be used to compute the relevant integral length scales of

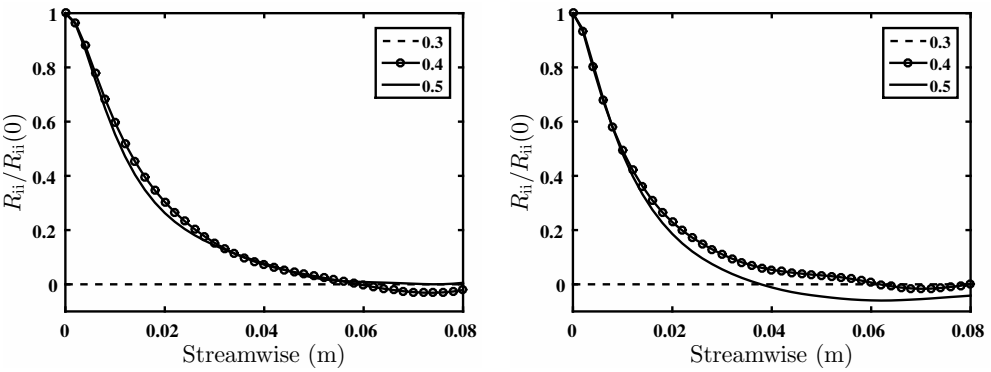

(a) Water (b) Air

Figure 4.9 Pair correlation function span-wise.

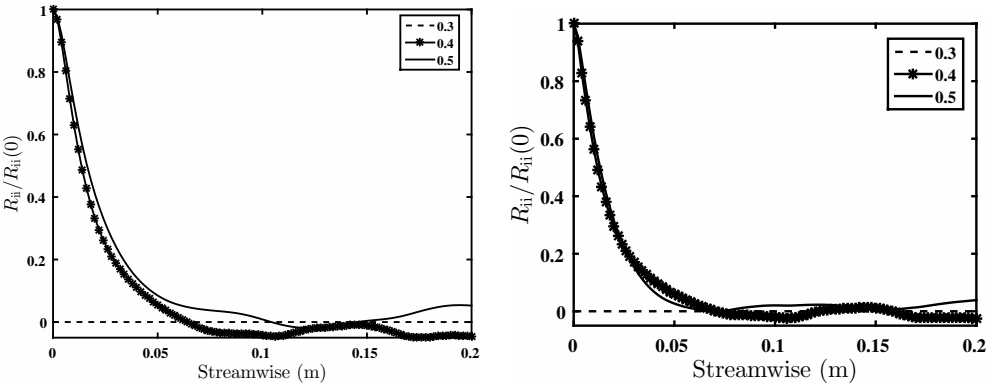

(a) Water (b) Air

Figure 4.10 pair correlation function stream-wise.

turbulence and also to determine the domain size for which the periodic boundary conditions donot affect the statistics.

$$R_{ij\phi} = \frac{\langle \alpha_\phi(\mathbf{x},t)\,\alpha_\phi(\mathbf{x}+\mathbf{r},t)\,\mathbf{u}''_\phi(\mathbf{x},t)\,\mathbf{u}''_\phi(\mathbf{x}+\mathbf{r},t)\rangle}{\langle \alpha_\phi(\mathbf{x},t)\,\alpha_\phi(\mathbf{x}+\mathbf{r},t)\rangle} \tag{4.22}$$

The good decay of pair correlation functions in Figures 4.9, 4.10 for both the phases indicate that the turbulence statistics computed from the simulations are not affected by the boundary conditions, and also all the length scales of turbulence are captured accurately by the simulation.

The integral length and time scales from the pair correlation function can be computed as follows:

Length scale calculation:

$$L^{\phi}_{33z} = \frac{1}{R_{33\phi}(0)} \int_0^{\infty} R_{33\phi}(z)\, dz$$

$$L^{\phi}_{11z} = \frac{1}{R_{11\phi}(0)} \int_0^{\infty} R_{11\phi}(z)\, dz$$

$$L^{\phi}_{11x} = \frac{1}{R_{11\phi}(0)} \int_0^{\infty} R_{11\phi}(x)\, dx$$

$$L^{\phi}_{33x} = \frac{1}{R_{33\phi}(0)} \int_0^{\infty} R_{33\phi}(x)\, dx$$

Time scale calculation:

$$T^{\phi}_{33z} = \frac{L^{\phi}_{33z}}{\langle u''^2_{\phi z} \rangle^{1/2}}$$

$$T^{\phi}_{33x} = \frac{L^{\phi}_{33x}}{\langle u''^2_{\phi z} \rangle^{1/2}}$$

$$T^{\phi}_{11x} = \frac{L^{\phi}_{11x}}{\langle u''^2_{\phi x} \rangle^{1/2}}$$

$$T^{\phi}_{11z} = \frac{L^{\phi}_{11z}}{\langle u''^2_{\phi x} \rangle^{1/2}}$$

Integral length and time scales computed from the pair correlation functions are given in Table 4.5.

From the tables, it can be concluded that the integral length scales (L^{ϕ}_{33z}) computed by integrating the zz-component (33) of the pair correlation function, in the z direction are larger than every other scales computed by integrating every other components in every other directions in both the phases. A strongly correlated flow in the flow direction compared to the direction perpendicular to the flow is also observed by Yang et al. (1993) in their experiment. This may be due to the action of the inter-phase forces preferentially in the flow direction direction generating fluid structures with larger length scales in the z direction compared to x direction.

Moreover, the integral length scales of turbulence computed for both the gas fractions 0.5 and 0.4 are similar in both the phases, which is expected in bubbly flows as the bubbles strictly follow fluid vortices or get accumulated in high vorticity fluid regions due to low inertia.

Table 4.5 Scales of mesoscale turbulence

Integral length scales gas phase (m)

α	L^g_{33z}	L^g_{33x}	L^g_{11x}	L^g_{33x}	$L = \langle u_{\mathrm{gz}} \rangle^2_{\mathrm{pg}}/g$
0.5	0.0347	0.0095	0.0112	0.0156	0.0125
0.4	0.0261	0.0122	0.0137	0.0188	0.0095

Integral time scales gas phase (s)

α	T^ϕ_{33z}	T^ϕ_{33x}	T^ϕ_{11x}	T^ϕ_{11z}	$\tau = \langle u_{\mathrm{gz}} \rangle_{\mathrm{pg}}/g$
0.5	0.1119	0.0488	0.0799	0.0360	0.0357
0.4	0.0903	0.1150	0.1385	0.0601	0.0306

Integral length scales liquid phase (m)

α	L^l_{33z}	L^l_{33x}	L^l_{11x}	L^l_{33x}	$L = \langle u_{\mathrm{gz}} \rangle^2_{\mathrm{pg}}/g$
0.5	0.0337	0.0146	0.0184	0.0163	0.0125
0.4	0.0264	0.0142	0.0202	0.0153	0.0095

Integral time scales liquid phase (s)

α	T^ϕ_{33z}	T^ϕ_{33x}	T^ϕ_{11x}	T^ϕ_{11z}	$\tau = \langle u_{\mathrm{gz}} \rangle_{\mathrm{pg}}/g$
0.5	0.1352	0.0983	0.0654	0.1243	0.0357
0.4	0.1424	0.1102	0.0826	0.1565	0.0306

4.6.9 Energy spectra

Energy spectrum for loadings 0.5 and 0.4 are given in Fig. 4.11. The spectrum shows the distribution of turbulent energy among different scales. It is interesting to note that the turbulence for gas fraction 0.5 is anisotropic at scales of the order of d_{p} which corresponds to k = 1000. However, for gas fraction 0.4 turbulence reaches isotropic behaviour before k=1000 ($\sim d_{\mathrm{p}}$). The distribution of energy among the scales beyond k = 1000, appear to show similar profile for gas fractions 0.5 and 0.4, suggesting the possibility of universality as can be found in inertial range of the energy spectrum for single phase flows.

4.6.10 Momentum budget

The statistics of the unclosed terms in the macroscale momentum equations (4.15) and (4.14) for both gas and liquid phases are computed from the mesoscale DNS by averaging over

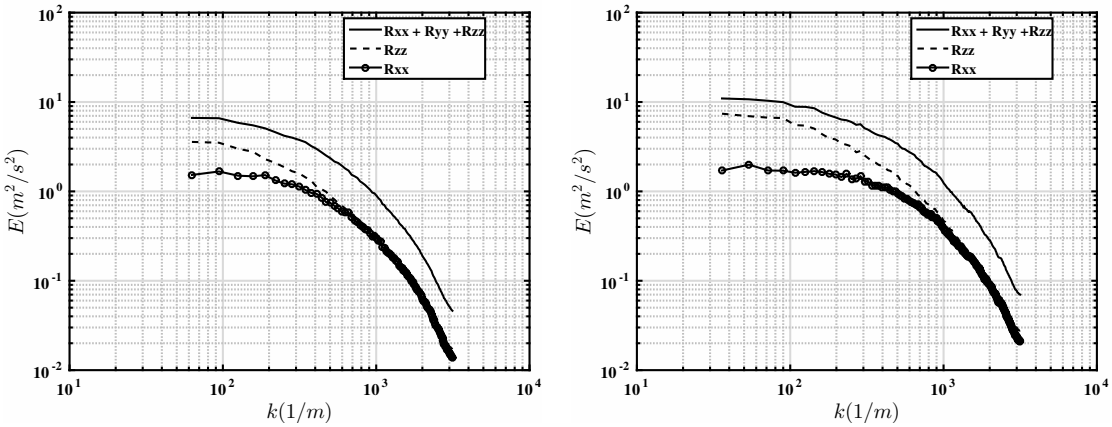

(a) $\alpha_g = 0.4$ (b) $\alpha_g = 0.5$

Figure 4.11 Energy spectrum.

500 samples, and reported for different initial loadings of gas fractions in the Table 4.6. The gas phase momentum budgets indicate that the correlation (Drag unclosed) term due to the Reynolds Averaging of drag is positive and leads to drag reduction. The cluster formation due to the accumulation of bubbles in the high vorticity regions leads to reduction in effective surface area of the bubbles compare to homogeneous rise of bubbles, giving an aerodynamic advantage for the bubble rise. The drag reduction due to the correlation term reduces when the global gas fraction is reduced from 0.5 to 0.4, which may be due to the increase in the size of cluster in the horizontal direction (see L_x Sec. 6.3.1) for $\alpha_g = 0.4$ compared to $\alpha_g = 0.5$ leading to increase in effective surface area on which liquid drag is acting.

The contribution of lift force and bubble dispersion towards the mean momentum is negligible due to the absence of mean gradients of velocity and gas fraction in the flow. The correlation term VM generated due to the Reynolds Averaging of virtual mass is significant, though the flow is homogeneous and statistically stationary, which may be due to the correlations generated due to the RA of convection term $(\mathbf{u} \cdot \nabla \mathbf{u})$ present in the expression for the virtual mass force (Eqn. (4.5)). From the tables, it can be concluded that the contribution of the correlations generated due to RA of drag and virtual mass forces are higher than the correlations generated due to RA of buoyancy (Buoyancy unclosed), hence preference in modeling has to be given to unclosed terms related to drag force. The unclosed terms generated due to

Table 4.6 Momentum budget

$\alpha = 0.5$

phase	Drag	Drag unclosed	Buoyancy	Buoyancy unclosed	Gravity	BF	Lift	BD	VM
Liquid	3320	-700	-2452	-98	-4900	4905	17	-16	-294
Gas	-3320	700	2452	98	-5.88		-17	16	294

$\alpha = 0.4$

phase	Drag	Drag unclosed	Buoyancy	Buoyancy unclosed	Gravity	BF	Lift	BD	VM
Liquid	2866	-400	-2353	-84	-5880	5884.3	1.9	-1.4	-220
Gas	-2866	400	2353	84	-4.70		-1.9	1.4	220

$\alpha = 0.3$

phase	Drag	Drag unclosed	Buoyancy	Buoyancy unclosed	Gravity	BF	Lift	BD	VM
Liquid	2055.8	0	-2059.3	0	-6860	6864.2	0	0	0
Gas	-2055.8	0	2059.3	0	-3.52	0	0	0	0

RA of inter-phase forces are negligible for $\alpha = 0.3$ and 0.15 due to the absence of turbulence in those gas fraction limits.

4.6.11 Reynolds stress budget

The values of the terms appearing in the Reynolds stress transport equations (Eqns. (4.16) and (4.17)) for gas fractions 0.5 and 0.4 obtained from the mesoscale DNS are reported in the following Table 4.7.

From the tables, it can seen that the contributions of bubble dispersion (BD) and lift forces (Lift) are statistically insignificant due to the homogeneity of the flow. The main forces which sustain the turbulence in the liquid phase are drag and virtual mass due to the strong correlation of gas fraction fluctuation due to cluster motion, and the liquid velocity appearing in the RA of these forces. However, the turbulence production in the gas phase is mainly due to buoyancy and virtual mass. In the liquid phase, it is interesting to note that though the entire bubbly flow is driven by buoyancy yet the contribution of buoyancy in producing liquid turbulent kinetic energy.

Since a PR-DNS is not performed in the current study, the accurate values of the dissipation of turbulent eddy is not captured, rather the turbulent dissipation appears as negative contributions of the inter-phase forces towards Reynolds stress budget, thus the contribution due to

Table 4.7 Reynolds Stress Budget

$\alpha = 0.5$

zz-direction

phase	DP	DE	DNL	BuoyancyP	PS	VMP	BDP	LFP	VD
Liquid	186.18	-11.99	-125.18	-4	-89.57	-9	18	13	-1.48
Gas	-	-182	7.68	116	-92.6	140	-4.6	-3.09	-0.077

xx-direction

phase	DP	DE	DNL	BuoyancyP	PS	VMP	BDP	LFP	VD
Liquid	-	12.92	10.75	-26	17	-8	-6.5	1.2	-0.7795
Gas	-	-95	-35	30	60.52	56	3.53	-5.45	-0.00399

$\alpha = 0.4$

zz-direction

phase	DP	DE	DNL	BuoyancyP	PS	VMP	BDP	LFP	VD
Liquid	102.30	5.43	-67	-3	-43.56	-4	8.3	4.11	-0.9005
Gas	-	-222	77.94	97	-80.24	112	-1.83	-3.3	-0.0592

xx-direction

phase	DP	DE	DNL	BuoyancyP	PS	VMP	BDP	LFP	VD
Liquid	-	9.49	1.003	-6	12.98	-5	-6.07	-2.5	0.576
Gas	-	-61	-17	8	54.49	26	1.1	-3.45	0.0222

drag non-linearity (DNL) and buoyancy could be considered as dissipation of turbulent energy in the liquid phase. The large values of the contributions of inter-phase forces towards the Reynolds stress in the zz-direction compared to the xx-direction for both gas fractions 0.4 and 0.5 shows that the degree of turbulent anisotropy to be very high, indicating the importance of adopting anisotropic turbulence models for accurate prediction of turbulence in bubbly flows.

The pressure strain (PS) contribution accounts for the mechanism of feeding turbulent energy from the strongest normal component (zz) or streamwise component of the Reynolds stress to the weak spanwise components xx and yy of the Reynolds stress, which is evident from the PS budget obtained from the mesoscale simulation.

From the budget it can be concluded that for the liquid phase the drag and pressure strain (PS) correlation terms towards zz component of the Reynolds stress and Drag, Buoyancy and pressure strain (PS) contributions towards xx component of the Reynolds stress have to be modelled for both gas fracionions 0.5 and 0.4. And for the gas phase the drag, buoyancy, virtual mass (VM) and pressure strain (PS) contribution towards both xx and zz components of Reynolds stress have to be modelled.

4.7 Conclusions

The present work investigates the turbulence characteristics in dense bubbly flow regime for statisitcally homogeneous flows in order to develop a Reynolds stress transport model to predict turbulence in such flows. The dense bubbly flow regime is prone to buoyancy induced instabilities which leads to formation of bubble swarm and bubble swarm induced turbulence. Industrial columns often operate in dense heterogeneous flow regime, thus developing predictive turbulence models in this regime is crucial for better simulation based design of the columns.

A general Reynolds stress equation to predict bubbly flow turbulence is derived by phase averaging the two-fluid model. The unclosed terms generated due to the inter-phase forces which physically represents the exchange of turbulence quantities between the gas and the liquid phases are quantified through two-fluid flow simulations. The simulations are performed in a periodic 3D domain with squared cross-section to isolate such unclosed terms. The simulations are performed for gas fractions ranging from 15 - 50 %. The analysis of the flow field and

gas fraction indicate the accumulation of bubbles in high vorticity region leading to swarm formation in the dense heterogeneous regime, however in the homogeneous regime there is no production large scale vortices and no swarm formation is found. The probability distribution function for the streamwise velocity fluctuations computed from the simulations show postive skewness and deviate from the Gaussian distribution function for both the phases, however the spanwise fluctuations for both phases roughly follows a Gaussian distribution. The analysis of one point statistics shows a high degree anisotropy in the Reynolds stresses for both phases and gas fractions for which the flow in the heterogeneous regime. The rise velocity of the bubbles in the heterogeneous regime is significantly higher than the single bubble rise velocity indicating a co-operative rise of bubbles (reduced drag compare to a single bubble rise).

The length scales computed from the radial distribution function or the cluster size of the swarm roughly matches the characteristic length scale defined by the rise velocity and the gravity U_{r}^2/g. The integral length scales computed from the two-point auto-correlation function is larger compared to the cluster length scales and the defined characteristic length scales.

The energy spectra for streamwise and spanwise components of Reynolds stress indicate high degree of anisotropy at scales of the order of bubble diameter (d_{p}) for $\alpha_{\mathrm{g}} - 50\%$ compared to $\alpha_{\mathrm{g}} - 40\%$.

The momentum budget computed from the simulation indicate that the unclosed term generated due to PA of drag force is significant compared to other unlcosed terms and has to be modelled in the mean momentum equation to obtain the correct flow prediction in the dense bubbly flow regime.

The Reynolds stress budget in the liquid phase indicate that turbulence exchange unclosed terms originated from the PA of drag and the pressure strain terms significantly affects the budget in the streamwise direction for both gas fractions and tends to decrease when the gas fraction is decreased. However, in the spanwise direction the turbulent excange term due to buoyacy along with the turbulent exchange term due to Drag and pressure strain seem to affect the budget and follows the same trend as streamwise direction when the gas fraction is decreased.

The Reynolds stress budget in the gas phase indicate that turbulence exchange unclosed

terms originated from the PA of drag, buoyancy, virtual mass and the pressure strain terms significantly affects the budget in the streamwise direction for both gas fractions. The turbulent exchange terms due to buoyancy and virtual mass tends to decrease when the gas fraction is decreased. However, the turbulent exchange terms due to drag seem to increase with the gas fraction showing a different trend compared to the exchange terms due to buoyancy and virtual mass.The turbulent exchange terms in the spanwise direction due to the buoyancy along with the turbulent exchange term due to Drag and pressure strain seem to affect the budget and follows the same trend as streamwise direction when the gas fraction is decreased.

CHAPTER 5. MULTIPHASE REYNOLDS STRESS MODEL

This chapter is modified from a paper in preparation for

Chemical Engineering Science Journal

N. Panicker, A. Passalacqua, R.O. Fox

5.1 Abstract

The bubble columns operating in the heterogeneous regime are vulnerable to buoyancy induced instabilities resulting in the formation of bubble clusters which while rising agitates the fluid and causes turbulence. The efficient design of these systems with the aid of CFD simulations requires accurate prediction of turbulence due to these swarms through turbulence models.

In the present study a multiphase Reynolds stress transport (RST) model is developed by modeling swarm induced turbulence production, dissipation and redistribution of energy (pressure-strain) from the multiphase DNS data obtained through mesoscale simulation. The modeling of the transport terms and the viscous dissipation terms in the RST model, which was not captured in the mesoscale simulations are also discussed. Moreover, the predictive capability of the proposed RST model is assessed on a 3D bubble column by comparing it with the mesoscale DNS simulation, a mixture k-ϵ model and a single phase RST model with no swarm induced models.

5.2 Introduction

In numerous works (Torvik and Svendsen, 1990; Grienberger and Hofmann, 1992; Ranade, 1992; Hillmer et al., 1994) turbulence in bubbly flows is modeled poorly by using adhoc extensions of single phase turbulence models. In these works the turbulence production due to

the bubbles is neglected and the model constants used for single phase k-ϵ model are retained. (Sato et al., 1981; de Bertodano et al., 1994) achieved some success, in modeling turbulence by assuming linear superposition of BIT and SIT, SIT is predicted by single phase k-ϵ model and bubble induced turbulence is predicted either by an algebraic model given in Sato and Sekoguchi (1987) or by a transport equation formed from shear induced turbulent kinetic energy equation (TKE) by modifying the time scale of turbulent production. However, the assumption of linear superposition of SIT and BIT may not hold in the limit of high void fraction. To account for the coupling of SIT and BIT, in many works (Svendsen et al., 1992; Hjertager and Morud, 1995) BIT production is added as a source term to an extended framework of single phase TKE equation. The source term is formulated based on the assumption that a fraction of work done by the drag force goes into the production of TKE in the liquid phase. This fraction is adjusted with the aid of a model constant by varying it from 0 to 1 for low to high void fractions.

Realizing that multiphase turbulence cannot be accurately predicted by just adhoc adjustments of single phase k-ϵ models (Kataoka and Serizawa, 1989) derived TKE scalar balance equations by ensemble averaging the instantaneous momentum equations. The production of TKE due to bubbles can be explicitly seen in their derived transport equations, as unclosed source terms. The unclosed source terms are modeled based on the same assumption as given in (Svendsen et al., 1992; Hjertager and Morud, 1995). The stated assumption of drag force being the only contributor towards the production of TKE has to to be revisited as there is evidence (Lee et al., 1989; Roig et al., 1998) suggesting that virtual mass and buoyancy forces also contribute towards TKE production. According to Roig et al. (1998) BIT production is mainly due to the power developed by the virtual mass force rather than the drag force, and the drag force contribute towards the dissipation of turbulent kinetic energy in the wakes. Besides, Lee et al. (1989) models the BIT production by assuming that the increase in liquid TKE comes from a decrease in potential energy of liquid when bubbles displace the liquid which scales to the power developed by the buoyancy force. These unclosed interfacial terms appearing in the TKE equation have to be quantified appropriately by performing experiments or through direct numerical simulations to resolve confusions like which interfacial force contributes significantly? and what fraction of the total work done by these forces goes into the TKE production?

Another important property of turbulence which is not studied or modeled rigorously in the multiphase flow literature is the turbulence dissipation. The presence of bubbles break the larger eddies into smaller ones and modify the time scale of dissipation. In all the above works discussed, the time scale of eddy dissipation was assumed to be the same as the turbulence time scale ($\frac{k}{\epsilon}$), which may not be appropriate for accurate prediction of turbulence. In an attempt to account for the effect of bubbles on the dissipation rate, Troshko and Hassan (2001b) introduced a time scale based on bubble diameter and rise velocity, effectively the dissipation equation source term becomes proportional to the TKE production divided by the proposed time scale, they pointed out that dissipation frequency by bubbles is much higher than the viscous dissipation. A mixed time scale based on time constants $\frac{d_{\mathrm{p}}}{k}$ and $\frac{l}{u_{\mathrm{r}}}$ is proposed by Rzehak and Krepper (2013), as they believe the time scale associated with dissipation due to bubbles is influenced by turbulent time scale and also the bubble time scale. These time scales enter into the dissipation transport equation through source terms and correct the prediction of the overall dissipation rate.

The effect of gas phase turbulence in bubbly flows is unclear as very few works (Grienberger and Hofmann, 1992; Jr., 2005) accounts for it. In (Grienberger and Hofmann, 1992; Jr., 2005), the gas phase turbulent viscosity is computed from the liquid phase turbulent viscosity based on the scaling argument given in Serizawa et al. (1975), it states that the gas phase turbulent viscosity scales with the product of liquid phase turbulent viscosity and the density ratio ($\frac{\rho_{\mathrm{g}}}{\rho_{\mathrm{l}}}$). Based on this scaling argument, the dispersed phase turbulence is neglected in most works.

Turbulence in bubbly flows is anisotropic (Drew and Lahey, 1981; Wang et al., 1987a; Mudde et al., 1997; Mudde, 2005) due to the directional preference of the interphase forces to enhance or suppress the Reynolds stress components, yet very less attention is given towards the development of anisotropic models like Reynolds stress transport models (RST), which may be due to the complex structure of the RST equations and high computational cost. However, for accurate prediction of turbulence in bubbly flows anisotropic models are essential. In an attempt to account for the turbulence anisotropy in bubbly flows, Lahey (1990a) developed a RST model for the continuous phase. The contribution of turbulence by bubbles is added in the RST equation, in the form of a turbulence production tensor. The turbulence production

tensor is constituted by multiplying the turbulence production due to bubbles, by an anisotropy matrix given in Nigmatulin (1979), whose elements gives the fraction of total turbulence production due to bubbles, which goes to each normal components of the RST equation. He also proposed that the presence of bubbles assists in isotropization of turbulence, hence to account that effect he modified the single phase pressure redistribution model by the addition of the turbulence production tensor due to bubbles with a model constant. Chahed et al. (2003b) derived RST equations by averaging the instantaneous conservation equations for two-phase flow. They decomposed the net turbulence stress tensor into SIT and BIT. To solve for SIT they derived an RST equation, in the RST equation the presence of bubbles is accounted by modifying the single phase closure for the diffusion and the pressure redistribution term. The diffusion due to bubbles is added in the diffusion coefficient in the form of a product of time scale (d/u_{r}) and the bubble induced turbulent stress tensor. The pressure redistribution due to bubbles is added by modifying the turbulent time scale ($\frac{k}{\epsilon}$) present in the single phase closure into a mixed time scale ($\frac{k}{\epsilon}+\alpha\frac{u_{\mathrm{R}}}{d}$). The bubble induced turbulent stress is obtained by solving a separate RST equation for bubble induced stress. Diffusion term is modeled with single phase closure. The production source term is modeled as a tensor product of virtual mass force and rise velocity.

From the above literature review on modeling turbulence in bubbly flows, it can be concluded that many works have used ad hoc extensions of single phase turbulence models by neglecting the BIT. The works which modeled BIT have not considered the contributions of all the inter-phase forces (Drag, virtual mass, lift etc.) towards the production of TKE, rather it is modeled by assuming that the drag force contributes the most towards the production of TKE. The model constant used in the closure modeling of BIT is changed among the works depending on the flow conditions, indicating that it may be a function of the system Reynolds number, Stokes number and α, hence it has to be studied carefully and constituted in terms of these system parameters to avoid the adjusting done in the works. The coupling of gas phase turbulence with the liquid phase is neglected based on the assumption of low Stokes number in bubbly flows, however the validity of this assumption has to be tested rigorously

in the dense regime, where the coupling becomes significant and one may have to solve TKE transport equation for gas phase and couple it with the TKE transport equation for the liquid phase. The transport terms consisting of diffusion, dissipation and pressure redistribution are closed by the closures available from single phase flows assuming that the presence of bubbles is only the source of production and do not contribute towards the transport of turbulence. More comprehensive bubble - liquid two-phase turbulence models have to be developed whose transport and production terms are closed using multiphase DNS data. And also inherently anisotropic bubbly flows are modeled using k - ϵ models in most of the works, hence a rigorous multiphase RST model has to be developed based on multiphase DNS data, which capture the anisotropy in these type of flows.

In this chapter a multiphase Reynolds stress transport (RST) model is developed by modeling swarm induced turbulence production, dissipation and redistribution of energy (pressure-strain) from the multiphase DNS data obtained through mesoscale simulation. The modeling of the transport terms and the viscous dissipation terms in the RST model, which was not captured in the mesoscale simulations are also discussed. Moreover, the predictive capability of the proposed RST model is studied on a 3D bubble column by comparing it with the mesoscale DNS simulation, a mixture k-ϵ model and a single phase RST model with no swarm induced models.

5.3 Modeling based on the budgets

The terms which are signifcant in the RST equations in the directions streamwise and spanwise for both the phases based on the budget (Table 1) are retained and modeled as follows:

Unclosed RST

Liquid phase:

ZZ-direction

$$0 = \langle p_{\mathrm{l}} \frac{\partial u_{\mathrm{lz}}^{''}}{\partial z} \rangle \qquad \text{Pressure Strain (PS)}$$

$$+ \rho_{\mathrm{l}} \langle \alpha_{\mathrm{g}} \rangle \langle C_{\mathrm{D}} \rangle \left(\langle u_{\mathrm{lz}}^{''} u_{\mathrm{gz}}^{''} \rangle_{\mathrm{pg}} - \langle u_{\mathrm{lz}}^{''} u_{\mathrm{lz}}^{''} \rangle_{\mathrm{pg}} \right) \qquad \text{Drag Exchange (DE)}$$

$$+ \rho_{\mathrm{l}} \langle \alpha_{\mathrm{g}} \rangle \langle C_{\mathrm{D}} \rangle \left(\langle u_{\mathrm{lz}}^{''} \rangle_{\mathrm{pg}} \left(\langle u_{\mathrm{gz}} \rangle_{\mathrm{pg}} - \langle u_{\mathrm{lz}} \rangle_{\mathrm{pg}} \right) \right) \qquad \text{Drag production (DP)}$$

$$+ DNLz \qquad \text{Drag non-linearity (DNL)} \left(\langle F_{\mathrm{Dz}} u_{\mathrm{lz}}^{''} \rangle_{\mathrm{pg}} - DE \right)$$

$$+ \langle \alpha_{\mathrm{g}} \rangle \langle u_{\mathrm{lz}}^{''} \frac{\partial p_{\mathrm{l}}^{'}}{\partial z} \rangle_{\mathrm{pg}} + \langle \alpha_{\mathrm{g}} \rangle \langle u_{\mathrm{lz}}^{''} \rangle_{\mathrm{pg}} \langle \frac{\partial p_{\mathrm{l}}}{\partial z} \rangle_{\mathrm{pg}} \qquad \text{Buoyancy}$$

$$+ \langle \alpha_{\mathrm{g}} \rangle \left(\langle F_{\mathrm{VMz}} u_{\mathrm{lz}}^{''} \rangle_{\mathrm{pg}} \right) \qquad \text{Virtual mass (VM)}$$

XX-direction

$$0 = \langle p_{\mathrm{l}} \frac{\partial u_{\mathrm{lx}}^{''}}{\partial z} \rangle \qquad \text{Pressure Strain (PS)}$$

$$+ \langle \alpha_{\mathrm{g}} \rangle \left(\langle F_{\mathrm{VMx}} u_{\mathrm{lx}}^{''} \rangle_{\mathrm{pg}} \right) \qquad \text{Virtual mass (VM)}$$

Gas phase:

ZZ-direction

$$0 = \langle p_{\mathrm{l}} \frac{\partial u_{\mathrm{gz}}^{''}}{\partial z} \rangle \qquad \text{Pressure Strain (PS)}$$

$$+ \rho_{\mathrm{l}} \langle \alpha_{\mathrm{g}} \rangle \langle C_{\mathrm{D}} \rangle \left(\langle u_{\mathrm{lz}}^{''} u_{\mathrm{gz}}^{''} \rangle_{\mathrm{pg}} - \langle u_{\mathrm{gz}}^{''} u_{\mathrm{gz}}^{''} \rangle_{\mathrm{pg}} \right) \qquad \text{Drag Exchange (DE)}$$

$$+ DNLz \qquad \text{Drag non-linearity (DNL)} \left(\langle F_{\mathrm{Dz}} u_{\mathrm{gz}}^{''} \rangle_{\mathrm{pg}} - DE \right)$$

$$- \langle \alpha_{\mathrm{g}} \rangle \langle u_{\mathrm{gz}}^{''} \frac{\partial p_{\mathrm{l}}^{'}}{\partial z} \rangle_{\mathrm{pg}} \qquad \text{Buoyancy}$$

$$- \langle \alpha_{\mathrm{g}} \rangle \left(\langle F_{\mathrm{VMz}} u_{\mathrm{gz}}^{''} \rangle_{\mathrm{pg}} \right) \qquad \text{Virtual mass (VM)}$$

XX-direction

$$0 = \langle p_{\mathrm{l}} \frac{\partial u_{\mathrm{gx}}^{''}}{\partial x} \rangle \qquad \text{Pressure Strain (PS)}$$

$$+ \rho_{\mathrm{l}} \langle \alpha_{\mathrm{g}} \rangle \langle C_{\mathrm{D}} \rangle \left(\langle u_{\mathrm{lx}}^{''} u_{\mathrm{gx}}^{''} \rangle_{\mathrm{pg}} - \langle u_{\mathrm{gx}}^{''} u_{\mathrm{gx}}^{''} \rangle_{\mathrm{pg}} \right) \qquad \text{Drag Exchange (DE)}$$

$$+ DNLx \qquad \text{Drag non-linearity (DNL)} \left(\langle F_{\mathrm{Dx}} u_{\mathrm{gx}}^{''} \rangle_{\mathrm{pg}} - DE \right)$$

$$- \langle \alpha_{\mathrm{g}} \rangle \langle u_{\mathrm{gx}}^{''} \frac{\partial p_{\mathrm{l}}^{'}}{\partial x} \rangle_{\mathrm{pg}} \qquad \text{Buoyancy}$$

$$- \langle \alpha_{\mathrm{g}} \rangle \left(\langle F_{\mathrm{VMx}} u_{\mathrm{gx}}^{''} \rangle_{\mathrm{pg}} \right) \qquad \text{Virtual mass (VM)}$$

5.3.1 Pressure strain $\langle p_l \frac{\partial u''_{\phi z}}{\partial x_\phi} \rangle$

The pressure strain (PS) term which accounts for the redistribution of normal Reynolds stresses is modeled in terms of a slow and rapid part for both the phases. The slow part of the pressure strain contribution in the liquid phase is modeled analogous to the single phase Rotta model by modifying the time scale of turbulence and Rotta model constant to integral time scale (T=135τ_{p})(5.2) and C_{1L} (5.1) respectively. Similar approach is followed for gas phase by replacing time scale and model constant with the gas phase integral time scale and model constant obtained from the mesoscale DNS data. The rapid part of the pressure strain is modeled in terms of shear induced turbulence production for single phase flows, similar approach is followed by retaining the same model constant 0.6 from single phase flows and replacing the shear induced production by drag production. It should be noted that there is no rapid part of pressure strain in the gas phase. The traceless property of pressure strain tensor is followed by the model developed in both the phases.

5.3.2 Drag production, DNL

The Inter phase Production (DP and VM) which appears in the liquid phase Reynolds stress equation is modeled based on the slip velocity. The model constant Cp(5.1) is obtained from the mesoscale DNS data. The modeling is based on the idea that the production becomes zero when the slip velocity tends to zero, in a shear induced turbulent flow, swarm induced turbulence contribution is significant only when the slip velocity is significant.

DNL is the RA contribution of the non-linearity present in the drag model. Since DNL appears as negative in the mesoscale DNS budget in the liquid phase, it could considered as the dissipation caused due to the bubbles. DNL is modeled similar to the drag production with a negative model constant C_{lznl}(5.1). The gas phase drag non linearity contribution is negligible, hence it is not modeled.

5.3.3 Drag Exchange

The drag exchange which only appears in the gas-phase is modeled in terms of liquid and gas phase Reynolds stresses with a model constantC_{DEz} obtained from the mesoscale DNS.

5.3.4 Virtual mass

The virtual mass term is negligible in the liquid phase. However, in the gas phase it acts as a production of turbulent energy. It is modeled similar to the drag production as a function of square of slip velocity with a model constant C_{gz} (5.1).

Model:

Liquid-Phase:

ZZ-direction

$$0 = -\frac{\rho_{\mathrm{l}} C_1}{T}\left(\langle u_{\mathrm{lz}}''^2\rangle_{\mathrm{pl}} - \frac{1}{3}\left(\langle u_{\mathrm{lz}}''^2\rangle_{\mathrm{pl}} + 2\langle u_{\mathrm{lx}}''^2\rangle_{\mathrm{pl}}\right)\right) - 0.6\left(\mathrm{DP}_{\mathrm{zz}} - \frac{1}{3}tr\left(\mathrm{DP}\right)\right) \quad \text{Pressure Strain (PS)}$$

$$+ \rho_{\mathrm{l}}\langle\alpha_{\mathrm{g}}\rangle\langle C_{\mathrm{D}}\rangle C_{\mathrm{p}}\langle u_{\mathrm{gz}}\rangle^2 \quad \text{Drag Production (DP)+VM}$$

$$- \rho_{\mathrm{l}}\langle\alpha_{\mathrm{g}}\rangle\langle C_{\mathrm{D}}\rangle C_{\mathrm{lznl}}\langle u_{\mathrm{gz}}\rangle^2 \quad \text{Drag non-linearity (DNL)}$$

$$+ C_{\mathrm{blz}}\langle\alpha_{\mathrm{g}}\rangle\frac{\partial\langle p_{\mathrm{l}}\rangle}{\partial z}\langle u_{\mathrm{gz}}\rangle \quad \text{Buoyancy}$$

XX-direction

$$0 = -\frac{\rho_{\mathrm{l}} C_1}{T}\left(\langle u_{\mathrm{lx}}''^2\rangle_{\mathrm{pl}} - \frac{2}{3}\left(0.5\left(\langle u_{\mathrm{lz}}''^2\rangle_{\mathrm{pl}} + 2\langle u_{\mathrm{lx}}''^2\rangle_{\mathrm{pl}}\right)\right)\right) - 0.6\left(\mathrm{DP}_{\mathrm{xx}} - \frac{1}{3}tr\left(\mathrm{DP}\right)\right) \quad \text{Pressure Strain (PS)}$$

$$- \rho_{\mathrm{l}}\langle\alpha_{\mathrm{g}}\rangle\langle C_{\mathrm{D}}\rangle C_{\mathrm{lx}}\langle u_{\mathrm{gz}}\rangle^2 \quad \text{VM}$$

Gas-Phase:

ZZ-direction

$$0 = -\frac{\rho_g}{\gamma\tau_p}\left(\langle u''^2_{gz}\rangle_{pg} - \frac{2}{3}\left(0.5\left(\langle u''^2_{gz}\rangle_{pg} + 2\langle u''^2_{gx}\rangle_{pg}\right)\right)\right) \quad \text{Pressure Strain (PS)}$$

$$+ \rho_l\langle\alpha_g\rangle\langle C_D\rangle\left(\langle u''^2_{lz}\rangle^{1/2}_{pl}\langle u''^2_{gz}\rangle^{1/2}_{pg} - C_{DEz}\langle u''^2_{gz}\rangle_{pg}\right) \quad \text{Drag Exchange (DE)}$$

$$+ \rho_l\langle\alpha_g\rangle\langle C_D\rangle C_{gz}\langle u_{gz}\rangle^2 \quad \text{Drag non-linearity (DNL)+VM}$$

$$- C_{bgz}\langle\alpha_g\rangle\frac{\partial\langle p_l\rangle}{\partial z}\langle u_{gz}\rangle \quad \text{Buoyancy}$$

XX-direction

$$0 = -\frac{\rho_g}{\gamma\tau_p}\left(\langle u''^2_{gx}\rangle_{pg} - \frac{2}{3}\left(0.5\left(\langle u''^2_{gz}\rangle_{pg} + 2\langle u''^2_{gx}\rangle_{pg}\right)\right)\right) \quad \text{Pressure Strain (PS)}$$

$$+ \rho_l\langle\alpha_g\rangle\langle C_D\rangle\left(\langle u''^2_{lx}\rangle^{1/2}_{pl}\langle u''^2_{gx}\rangle^{1/2}_{pg} - C_{DEx}\langle u''^2_{gx}\rangle_{pg}\right) \quad \text{Drag Exchange (DE)}$$

$$+ \rho_l\langle\alpha_g\rangle\langle C_D\rangle C_{gx}\langle u_{gz}\rangle^2 \quad \text{Drag non-linearity (DNL)+VM}$$

$$- C_{bgx}\langle\alpha_g\rangle\frac{\partial\langle p_l\rangle}{\partial z}\langle u_{gz}\rangle \quad \text{Buoyancy}$$

Table 5.1 Model constants

α	C_{1L}	γ	C_p	C_{lx}	C_{lznl}	C_{gz}	C_{gx}	C_{DEx}	C_{DEz}	C_{bgz}	C_{bgx}	C_{blz}
0.5	0.0179	0.2094	0.2174	0.0323	0.1064	0.1255	0.0094	0.8277	0.9012	0.0473	0.0122	0.0324
0.4	0.0576	0.2575	0.1505	0.0235	0.0784	0.2222	0.0105	0.8951	0.8159	0.0412	0.0076	0.0161

Table 5.2 Integral time scale

α	T/τ_p	$\tau_p(s)$
0.5	135.2	0.001
0.4	142.4	0.001

5.3.4.1 Transport terms

Transport terms transport the turbulence in the flow systems through diffusion and convection. The transport terms are not computed in the homogeneous mesoscale DNS performed

in this work. These terms are modeled similar to single phase RST terms however, mesoscale simulations of inhomogenous bubbly flows can be performed to get a better insight on the influence of bubbles on the transport of turbulence and more sophisticated diffusion models can be developed based on the data . Convection term does not require any modeling, however, diffusion terms $-\langle\alpha_\mathrm{l}\rangle\frac{1}{2}\langle\mathbf{u}_\phi^{''}\mathbf{u}_\phi^{''}\mathbf{u}_\phi^{''}\rangle_{\mathrm{p}\phi}$, $\langle\boldsymbol{\sigma}_\phi\mathbf{u}_\mathrm{l}^{''}\rangle$ and $\langle p_\mathrm{l}\mathbf{u}_\phi^{''}\rangle I$ due to turbulence, viscous and pressure respectively requires modeling. These terms are combined and modelled based on gradient diffusion hypothesis similar to single phase flows (Pope, 2000).

$$-\langle\alpha_\phi\rangle\frac{1}{2}\langle\mathbf{u}_\phi^{''}\mathbf{u}_\phi^{''}\mathbf{u}_\phi^{''}\rangle_{\mathrm{p}\phi}+\langle\boldsymbol{\sigma}_\phi\mathbf{u}_\phi^{''}\rangle-\langle p_\mathrm{l}\mathbf{u}_\phi^{''}\rangle\mathrm{I}=\langle\alpha_\phi\rangle\left(\mu_\phi+\frac{\mu_{\mathrm{T}\phi}}{\sigma_\mathrm{k}}\right)\nabla\langle\mathbf{u}_\phi^{''}\mathbf{u}_\phi^{''}\rangle_{\mathrm{p}\phi} \tag{5.1}$$

5.3.4.2 Viscous dissipation

Turbulent Dissipation

The exact equation of dissipation (Pope, 2000) is complex due to the presence of large number of unclosed terms even in single phase flows. An empirical approach is followed in single phase flows to obtain the transport equation for dissipation, we follow the same approach to formulate a transport equation for dissipation for multiphase flows as given below:

$$\frac{D\epsilon}{Dt}=\nabla\cdot\left(\nu+\frac{\nu_\mathrm{T}}{\sigma_\mathrm{k}}\right)\nabla\epsilon+C_{\epsilon1}\frac{\epsilon}{k}P_\mathrm{k}-C_{\epsilon2}\frac{\epsilon^2}{k}+C_3P_\mathrm{kb}-C_4P_{\epsilon\mathrm{b}} \tag{5.2}$$

The Eqn. 3.10 retains the same form as the single phase turbulent dissipation equation except for the two additional terms C_3P_kb and $C_4P_{\epsilon\mathrm{b}}$ to account for the effect of dissipation due to bubbles. The model constant C_3 and C_4 can be obtained either as a function of time scales k/ϵ and τ_p as given in Fox (2014b) or from our mesoscale DNS simulations.

Macroscale Momentum:

Liquid phase:

Z-Direction:

$$
\begin{aligned}
0 = & -\frac{1}{\rho_{\mathrm{l}}} \langle \frac{\partial p_{\mathrm{l}}}{\partial z} \rangle && \text{BF (Balance force)} \\
& + \langle \alpha_{\mathrm{g}} \rangle \langle C_{\mathrm{D}} \rangle \left(\langle u_{\mathrm{gz}} \rangle_{\mathrm{pg}} - \langle u_{\mathrm{lz}} \rangle_{\mathrm{pl}} \right) && \text{Drag force} \\
& - \langle \alpha_{\mathrm{g}} \rangle \langle C_{\mathrm{D}} \rangle \left(\frac{\langle \alpha_{\mathrm{g}}^{'} u_{\mathrm{lz}}^{'} \rangle}{\langle \alpha_{\mathrm{l}} \rangle \langle \alpha_{\mathrm{g}} \rangle} \right) + DragNonlin && \text{Drag unclosed} \\
& + \frac{\langle \alpha_{\mathrm{g}} \rangle}{\rho_{\mathrm{l}}} \langle \frac{\partial p_{\mathrm{l}}}{\partial z} \rangle && \text{Buoyancy} \\
& + \langle \alpha_{\mathrm{l}} \rangle g_{\mathrm{z}} && \text{Gravity} \\
& + \frac{\langle \alpha_{\mathrm{g}} \rangle}{\rho_{\mathrm{l}}} \langle F_{\mathrm{VM}} \rangle_{\mathrm{pg}} && \text{VM}
\end{aligned}
$$

Gas phase:

Z-direction:

$$
\begin{aligned}
0 = & - \langle \alpha_{\mathrm{g}} \rangle \langle C_{\mathrm{D}} \rangle \left(\langle u_{\mathrm{gz}} \rangle_{\mathrm{pg}} - \langle u_{\mathrm{lz}} \rangle_{\mathrm{pl}} \right) && \text{Drag force} \\
& + \langle \alpha_{\mathrm{g}} \rangle \langle C_{\mathrm{D}} \rangle \left(\frac{\langle \alpha_{\mathrm{g}}^{'} u_{\mathrm{lz}}^{'} \rangle}{\langle \alpha_{\mathrm{l}} \rangle \langle \alpha_{\mathrm{g}} \rangle} \right) + DragNonlin && \text{Drag unclosed} \\
& - \frac{\langle \alpha_{\mathrm{g}} \rangle}{\rho_{\mathrm{l}}} \langle \frac{\partial p_{\mathrm{l}}}{\partial z} \rangle && \text{Buoyancy} \\
& + \langle \alpha_{\mathrm{g}} \rangle g_{\mathrm{z}} && \text{Gravity} \\
& - \frac{\langle \alpha_{\mathrm{g}} \rangle}{\rho_{\mathrm{l}}} \langle F_{\mathrm{VM}} \rangle_{\mathrm{pg}} && \text{VM}
\end{aligned}
$$

The drag and virtual mass correlation terms are attached to mean drag force in the macroscale momentum equation and modelled as:

Model:

Liquid phase:

Z-Direction:

$$
\begin{aligned}
0 = & -\frac{1}{\rho_{\mathrm{l}}} \langle \frac{\partial p_{\mathrm{l}}}{\partial z} \rangle && \text{BF (Balance force)} \\
& + \langle \alpha_{\mathrm{g}} \rangle \langle C_{\mathrm{D}} \rangle \left(1 - C_{\mathrm{g}}\right) \left(\langle u_{\mathrm{gz}} \rangle_{\mathrm{pg}} - \langle u_{\mathrm{lz}} \rangle_{\mathrm{pl}} \right) && \text{Drag force} \\
& + \frac{\langle \alpha_{\mathrm{g}} \rangle}{\rho_{\mathrm{l}}} \langle \frac{\partial p_{\mathrm{l}}}{\partial z} \rangle && \text{Buoyancy} \\
& + \langle \alpha_{\mathrm{l}} \rangle g_{\mathrm{z}} && \text{Gravity}
\end{aligned}
$$

Gas phase:

Z-direction:

$$
\begin{aligned}
0 = & - \langle \alpha_{\mathrm{g}} \rangle \langle C_{\mathrm{D}} \rangle \left(1 - C_{\mathrm{g}}\right) \left(\langle u_{\mathrm{gz}} \rangle_{\mathrm{pg}} - \langle u_{\mathrm{lz}} \rangle_{\mathrm{pl}} \right) && \text{Drag force} \\
& - \frac{\langle \alpha_{\mathrm{g}} \rangle}{\rho_{\mathrm{l}}} \langle \frac{\partial p_{\mathrm{l}}}{\partial z} \rangle && \text{Buoyancy} \\
& + \langle \alpha_{\mathrm{g}} \rangle g_{\mathrm{z}} && \text{Gravity}
\end{aligned}
$$

Model constants

α	C_{g}
0.5	0.2994
0.4	0.2163

5.4 Multiphase Reynolds stress model

RST liquid phase:

$$
\frac{\partial}{\partial t} \left(\alpha_{\mathrm{l}} \rho_{\mathrm{l}} \mathbf{R}_{\mathrm{l}} \right) + \nabla \cdot \left(\rho_{\mathrm{l}} \alpha_{\mathrm{l}} \mathbf{u}_{\mathrm{l}} \mathbf{R}_{\mathrm{l}} \right) = \nabla \cdot \left(\alpha_{\mathrm{l}} D_{\mathrm{eff}} \nabla \mathbf{R}_{\mathrm{l}} \right) + \alpha_{\mathrm{l}} \rho_{\mathrm{l}} \mathbf{P} + \mathbf{PS} + \mathbf{\Pi}_{\mathrm{i}} - \mathbf{E}_{\mathrm{i}} - \epsilon \mathbf{I} \tag{5.3}
$$

DISSIPATION:

$$
\frac{D \left(\alpha_{\mathrm{l}} \rho_{\mathrm{l}} \epsilon \right)}{Dt} = \nabla \cdot D_{\mathrm{eff}} \nabla \epsilon + C_{\epsilon 1} \frac{\epsilon}{k} P_{\mathrm{k}} - C_{\epsilon 2} \frac{\epsilon^2}{k} + C_3 \frac{\epsilon}{k} \Pi_{\mathrm{i}} \tag{5.4}
$$

Diffusion coefficient

$$D_{\text{eff}} = C_{\text{s}}\frac{k}{\epsilon}\mathbf{R}_{\text{l}} + \mu_{\text{l}}I$$

Pressure Strain modeled from mesoscale DNS

$$\mathbf{PS} = -C_1\left(\frac{\epsilon}{k}\right)\left(\mathbf{R}_{\text{l}} - \frac{2}{3}kI\right) - C_2\left(\mathbf{P} - \frac{1}{3}\text{P}I\right) - C_{1\text{L}}\left(\frac{1}{135\tau_{\text{p}}}\right)\left(\mathbf{R}_{\text{l}} - \frac{2}{3}kI\right) - C_{2\text{L}}\left(\mathbf{\Pi}_{\text{i}} - \frac{1}{3}\Pi I\right)$$

Interphase Production modeled from mesoscale DNS

$$\mathbf{\Pi}_{\text{i}} = \alpha_{\text{g}}\rho_{\text{l}}\frac{C_{\text{D}}}{d_{\text{p}}}|U_{\text{g}} - U_{\text{l}}|^3\begin{bmatrix} 2/10 & 0 & 0 \\ 0 & 0 & 0 \\ 0 & 0 & 0 \end{bmatrix}$$

Interphase Dissipation modelled from mesoscale DNS

$$\mathbf{E}_{\text{i}} = \alpha_{\text{g}}\rho_{\text{l}}\frac{C_{\text{D}}}{d_{\text{p}}}|U_{\text{g}} - U_{\text{l}}|^3\begin{bmatrix} 8/100 & 0 & 0 \\ 0 & 2/100 & 0 \\ 0 & 0 & 2/100 \end{bmatrix}$$

Shear production

$$\mathbf{P} = -\mathbf{R}_{\text{l}} \cdot \left[\nabla\mathbf{u}_{\text{l}} + \nabla\mathbf{u}_{\text{l}}{}^T\right]$$

Model constants

Pressure strain

$C_1 = 1.8$

$C_2 = 0.6$

$C_{1\text{L}} = 0.73$

$C_{2\text{L}} = 0.6$

Dissipation

$C_{\epsilon 1} = 1.44$

$C_{\epsilon 2} = 1.92$

$C_3 = 1.5$

Turbulent viscosity constant

$C_\mathrm{s} = 0.25$

RST Gas phase:

$$\frac{\partial}{\partial t}\left(\alpha_\mathrm{g}\rho_\mathrm{g}\mathbf{R}_\mathrm{g}\right) + \nabla\cdot\left(\rho_\mathrm{g}\alpha_\mathrm{g}\mathbf{u}_\mathrm{g}\mathbf{R}_\mathrm{g}\right) = \nabla\cdot\left(\alpha_\mathrm{g}D_\mathrm{eff}\nabla\mathbf{R}_\mathrm{g}\right) + \alpha_\mathrm{g}\rho_\mathrm{g}\mathbf{P} + \mathbf{PS} + \mathbf{\Pi}_\mathrm{i} - \epsilon\mathbf{I} \tag{5.5}$$

DISSIPATION:

$$\frac{D\left(\alpha_\mathrm{g}\rho_\mathrm{g}\epsilon\right)}{Dt} = \nabla\cdot D_\mathrm{eff}\nabla\epsilon + C_{\epsilon 1}\frac{\epsilon}{k}P_\mathrm{k} - C_{\epsilon 2}\frac{\epsilon^2}{k} + C_3\frac{\epsilon}{k}\Pi_\mathrm{i} \tag{5.6}$$

Diffusion coefficient

$$D_\mathrm{eff} = C_\mathrm{s}\frac{k}{\epsilon}\mathbf{R}_\mathrm{g} + \mu_\mathrm{g}I$$

Pressure Strain modeled from mesoscale DNS

$$\mathbf{PS} = -C_1\left(\frac{\epsilon}{k}\right)\left(\mathbf{R}_\mathrm{g} - \frac{2}{3}kI\right) - C_2\left(\mathbf{P} - \frac{1}{3}\mathrm{P}I\right) - \left(\frac{1}{\gamma\tau_\mathrm{p}}\right)\left(\mathbf{R}_\mathrm{g} - \frac{2}{3}kI\right)$$

Interphase Exchange modeled from mesoscale DNS

$$\mathbf{\Pi}_\mathrm{i} = \rho_\mathrm{l}\langle\alpha_\mathrm{g}\rangle\langle C_\mathrm{D}\rangle\left(\langle u_\mathrm{lz}^{''2}\rangle_\mathrm{pl}^{1/2}\langle u_\mathrm{gz}^{''2}\rangle_\mathrm{pg}^{1/2} - C_\mathrm{DEz}\langle u_\mathrm{gz}^{''2}\rangle_\mathrm{pg}\right)$$

Shear production

$$\mathbf{P} = -\mathbf{R}_\mathrm{g}\cdot\left[\nabla\mathbf{u}_\mathrm{l} + \nabla\mathbf{u}_\mathrm{l}{}^T\right]$$

Model constants

Pressure strain

$C_1 = 1.8$

$C_2 = 0.6$

$\gamma = 0.2$

Drag Exchange

$C_{\mathrm{DEz}} = 0.9012$

Dissipation

$C_{\epsilon 1} = 1.44$

$C_{\epsilon 2} = 1.92$

$C_3 = 1.5$

Turbulent viscosity constant

$C_{\mathrm{s}} = 0.25$

5.5 Bubble column simulations

The multiphase RST model is tested and compared with mesoscale DNS and mixture k-ϵ model by simulating a bubble column with water as the continuous phase. Air is injected from the bottom of the bubble column, injection velocity (5.5) is chosen such that the column operates in the heterogeneous turbulent regime.

Boundary conditions for both phases

	U	P	ϵ	R
Wall	no slip	zero Gradient	Wall function	Wall function
Inlet	Inlet value	zeroGradient	fixed Value	fixed Value
outlet	zeroGradient	fixed Pressure	zeroGradient	zeroGradient

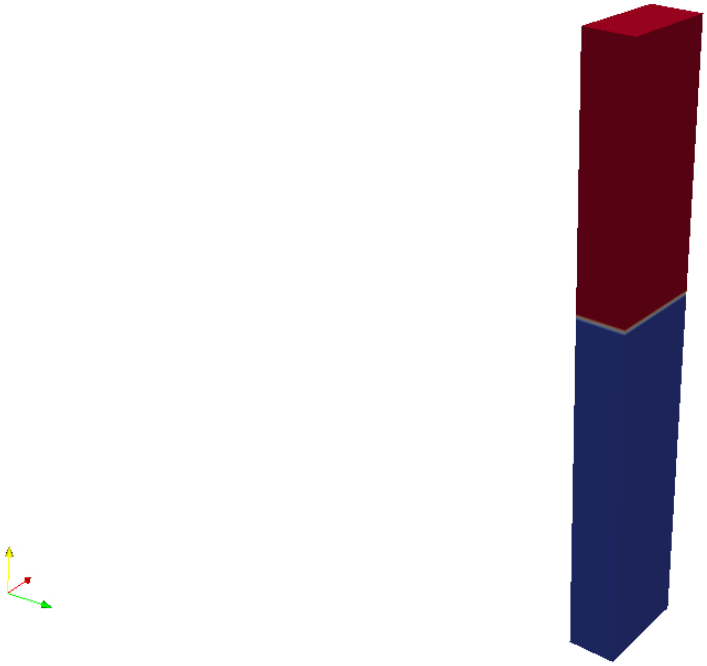

Figure 5.1 Geometry

Inlet conditions and Grid resolution

	mesoscale DNS	RANS
Inlet α_g	1	1
Inlet U_g	0.1 m/s	0.1 m/s
Grid resolution	2 mm	6 mm

The grid resolution used for RANs (5.5) is three times higher than the mesoscale simulations. A no slip boundary condition is given at the wall for the gas and the liquid velocity, and zero gradient at the outlet assuming a fully developed flow. Pressure is specified to be the atmospheric pressure at the outlet and zero gradient is given at both inlet and wall. The wall function boundary condition is given for dissipation and Reynolds stress at the wall. At the inlet fixed value is specified for dissipation and Reynolds stress.

5.6 Results and discussion

The gas fraction and velocity profiles predicted by the RANS model is comparable to the mesoscale DNS. There is a small over prediction of the velocity profiles at the center of the column (X=0.1m) which is attributed to the inability of the mesoscale DNS to capture the turbulent dissipation accurately. Hence, appropriate adjustments of the turbulent model constants in the dissipation equation has to be made for both the phases to correct this over prediction. However, the prediction of the model at this stage can be considered reasonable and can be tested for more complex multiphase flows and systems.

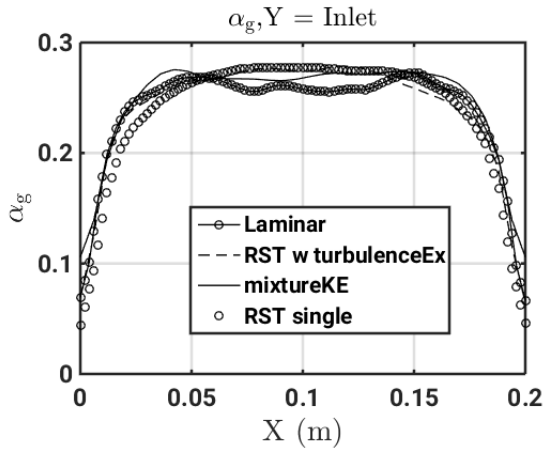

Figure 5.2 alpha gas close to inlet

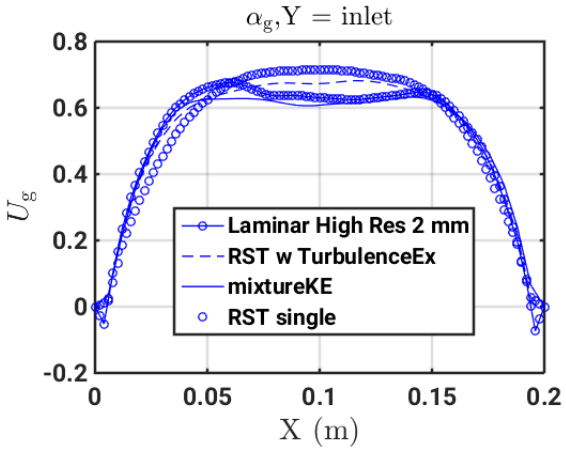

Figure 5.3 Gas velocity close to inlet

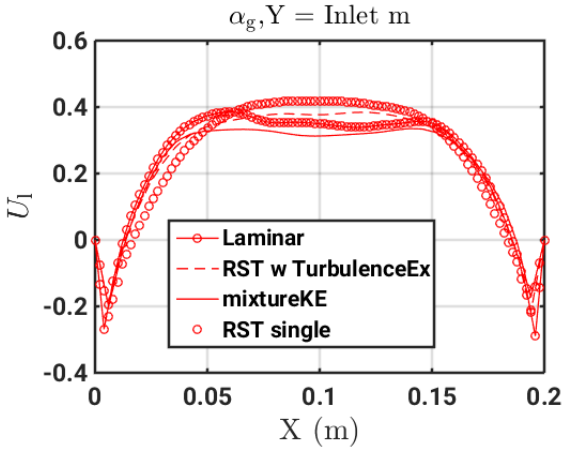

Figure 5.4 Liquid velocity close to inlet

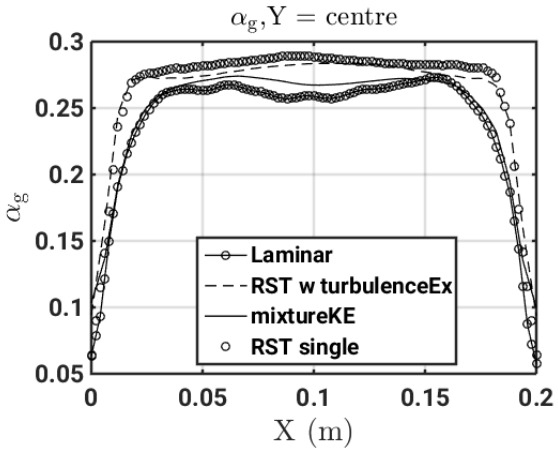

Figure 5.5 alpha gas centre of the column

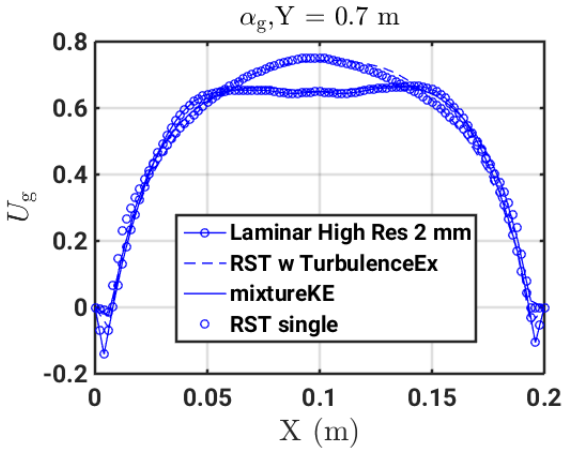

Figure 5.6 Gas velocity centre of the column

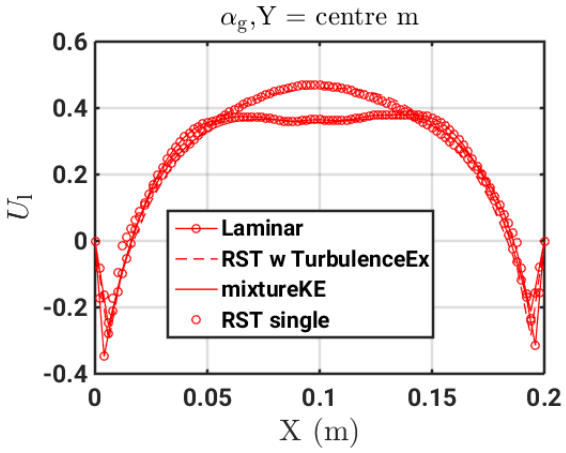

Figure 5.7 Liquid velocity centre of the column

5.7 Conclusion

The turbulent Reynolds stress budgets extracted from the mesoscale DNS is analyzed and a turbulent Reynolds stress model is proposed to predict turbulent gas-liquid flows. The modeling strategies involved in modeling the terms quantified through mesoscale DNS is discussed. The predictive capability of the proposed model is studied on a 3D bubble column by comparing it with the mesoscale DNS simulations. The model predictions of the gas fraction and the velocity profiles are in reasonable agreement with the mesoscale DNS. As a further study the model can be tested for more complex turbulent multiphase flows and multiphase flow systems

CHAPTER 6. SUMMARY AND CONCLUSION

6.1 Hyperbolicity of two-fluid model

The effect of the momentum transfer term on the hyperbolicity of the equations of the two-fluid model with shared pressure was investigated. It was shown that the introduction of a dispersion term, whose role is to effectively modify the slip velocity in the drag term appearing in the two-fluid equations, leads to a conditionally hyperbolic set of equations depending on the value assigned to the dispersion coefficient. An expression for the minimum value of the dispersion coefficient that ensures the hyperbolic nature of the equations of the two-fluid model was obtained.

The proposed dispersion term was applied to the simulation of two one-dimensional problems, involving a shock tube and a falling liquid. In both cases it was shown that the absence of the dispersion term leads to nonphysical profiles in the flow variables where sharp discontinuities are present. The solution of the model without the dispersion term (non-hyperbolic model) also prevented a grid-converged solution to be achieved. The results obtained with the dispersion term (hyperbolic model) provided the expected results across sharp discontinuities, and led to a numerical solution convergent with grid refinement.

An example of a two-dimensional bubble column was considered to illustrate the importance of ensuring the hyperbolicity of the equations of the two-fluid model in applications of practical interest. It was observed that, in the absence of the dispersion term, the numerical solution remained sensitive to the grid resolution even at the finest grid refinement used in this work, and showed the presence of nonphysical regions with high concentration of disperse phase, which are not observed experimentally. These artifacts were not observed in the same simulations repeated with the hyperbolic two-fluid model.

Finally, it is worth observing that the coefficient obtained here for the dispersion term is based on mathematical considerations. The purpose of the study is to show that such a term needs to be present when simulating bubbly flows, independently from their laminar or turbulent nature. The physically correct formulation of the coefficient, as well as the impact on the agreement of the model predictions with experimental measurements need further investigation. Physically consistent models for the coefficient could be obtained, for example, by performing direct numerical simulations on ensembles of buoyant particles with gradients in the volume fraction.

6.2 Mesoscale DNS

The present work investigates the turbulence characteristics in dense bubbly flow regime for statisitcally homogeneous flows in order to develop a Reynolds stress transport model to predict turbulence in such flows. The dense bubbly flow regime is prone to buoyancy induced instabilities which leads to formation of bubble swarm and bubble swarm induced turbulence. Industrial columns often operate in dense heterogeneous flow regime, thus developing predictive turbulence models in this regime is crucial for better simulation based design of the columns.

A general Reynolds stress equation to predict bubbly flow turbulence is derived by phase averaging the two-fluid model. The unclosed terms generated due to the inter-phase forces which physically represents the exchange of turbulence quantities between the gas and the liquid phases are quantified through two-fluid flow simulations. The simulations are performed in a periodic 3D domain with squared cross-section to isolate such unclosed terms. The simulations are performed for gas fractions ranging from 15 - 50 %. The analysis of the flow field and gas fraction indicate the accumulation of bubbles in high vorticity region leading to swarm formation in the dense heterogeneous regime, however in the homogeneous regime there is no production large scale vortices and no swarm formation is found. The probability distribution function for the streamwise velocity fluctuations computed from the simulations show postive skewness and deviate from the Gaussian distribution function for both the phases, however the spanwise fluctuations for both phases roughly follows a Gaussian distribution. The analysis of one point statistics shows a high degree anisotropy in the Reynolds stresses for both phases and

gas fractions for which the flow in the heterogeneous regime. The rise velocity of the bubbles in the heterogeneous regime is significantly higher than the single bubble rise velocity indicating a co-operative rise of bubbles (reduced drag compare to a single bubble rise).

The length scales computed from the radial distribution function or the cluster size of the swarm roughly matches the characteristic length scale defined by the rise velocity and the gravity U_{r}^2/g. The integral length scales computed from the two-point auto-correlation function is larger compared to the cluster length scales and the defined characteristic length scales.

The energy spectra for streamwise and spanwise components of Reynolds stress indicate high degree of anisotropy at scales of the order of bubble diameter (d_{p}) for $\alpha_{\mathrm{g}} - 50\%$ compared to $\alpha_{\mathrm{g}} - 40\%$.

The momentum budget computed from the simulation indicate that the unclosed term generated due to PA of drag force is significant compared to other unlcosed terms and has to be modelled in the mean momentum equation to obtain the correct flow prediction in the dense bubbly flow regime.

The Reynolds stress budget in the liquid phase indicate that turbulence exchange unclosed terms originated from the PA of drag and the pressure strain terms significantly affects the budget in the streamwise direction for both gas fractions and tends to decrease when the gas fraction is decreased. However, in the spanwise direction the turbulent excange term due to buoyacy along with the turbulent exchange term due to Drag and pressure strain seem to affect the budget and follows the same trend as streamwise direction when the gas fraction is decreased.

The Reynolds stress budget in the gas phase indicate that turbulence exchange unclosed terms originated from the PA of drag, buoyancy, virtual mass and the pressure strain terms significantly affects the budget in the streamwise direction for both gas fractions. The turbulent exchange terms due to buoyancy and virtual mass tends to decrease when the gas fraction is decreased. However, the turbulent exchange terms due to drag seem to increase with the gas fraction showing a different trend compared to the exchange terms due to buoyancy and virtual mass.The turbulent exchange terms in the spanwise direction due to the buoyancy along with the turbulent exchange term due to Drag and pressure strain seem to affect the budget and

follows the same trend as streamwise direction when the gas fraction is decreased.

6.3 Multi-phase turbulence model

The turbulent Reynolds stress budgets extracted from the mesoscale DNS is analyzed and a turbulent Reynolds stress model is proposed to predict turbulent gas-liquid flows. The modeling strategies involved in modeling the terms quantified through mesoscale DNS is discussed. The predictive capability of the proposed model is studied on a 3D bubble column by comparing it with the mesoscale DNS simulations. The model predictions of the gas fraction and the velocity profiles are in reasonable agreement with the mesoscale DNS. As a further study the model can be tested for more complex turbulent multiphase flows and multiphase flow systems

BIBLIOGRAPHY

Alméras, E., Risso, F., Roig, V., Cazin, S., Plais, C., and Augier, F. (2015). Mixing by bubble-induced turbulence. *Journal of Fluid Mechanics*, 776:458–474.

Antal, S., Jr, R. L., and Flaherty, J. (1991a). Analysis of phase distribution in fully developed laminar bubbly two-phase flow. *International Journal of Multiphase Flow*, 17(5):635 – 652.

Antal, S., Lahey, R., and Flaherty, J. (1991b). Analysis of phase distribution in fully developed laminar bubbly two-phase flow. *International Journal of Multiphase Flow*, 17(5):635–652.

Antal, S. P., Lahey Jr., R. T., and Flaherty, J. E. (1991c). Analysis of phase distribution in fully developed laminar bubbly two-phase flow. *Int. J. Multiphase Flow*, 17(5):635 – 652.

Balachandar, S. and Eaton, J. K. (2010). Turbulent dispersed multiphase flow. *Annual Review of Fluid Mechanics*, 42:111–133.

Banerjee, S. and Chan, A. (1980). Separated flow models – I. Analysis of the averaged and local instantaneous formulations. *Int. J. Multiphase Flow*, 6(1 – 2):1 – 24.

Barnea, D. (1987). A unified model for predicting flow-pattern transitions for the whole range of pipe inclinations. *International Journal of Multiphase Flow*, 13(1):1 – 12.

Batchelor, G. K. (1988). A new theory of the instability of a uniform fluidized bed. *J. Fluid Mech.*, 193:75–110.

Bech, K. (2005). Dynamic simulation of a 2d bubble column. *Chemical Engineering Science*, 60(19):5294 – 5304.

Becker, S., Sokolichin, A., and Eigenberger, G. (1994). Gasliquid flow in bubble columns and loop reactors: Part ii. comparison of detailed experiments and flow simulations. *Chemical Engineering Science*, 49(24, Part 2):5747 – 5762.

Beetstra, R., van der Hoef, M. A., and Kuipers, J. A. M. (2007). Drag force of intermediate reynolds number flow past mono- and bidisperse arrays of spheres. *AIChE Journal*, 53(2):489–501.

Behzadi, A., Issa, R., and Rusche, H. (2004). Modelling of dispersed bubble and droplet flow at high phase fractions. *Chemical Engineering Science*, 59(4):759 – 770.

Bestion, D. (1990). The physical closure laws in the CATHARE code. *Nucl. Eng. Des.*, 124(3):229 – 245.

Biesheuvel, A. and Gorissen, W. (1990). Void fraction disturbances in a uniform bubbly fluid. *International Journal of Multiphase Flow*, 16(2):211 – 231.

Biesheuvel, A. and Wijngaarden, L. v. (1984). Two-phase flow equations for a dilute dispersion of gas bubbles in liquid. *Journal of Fluid Mechanics*, 148:301–318.

Bouillard, J. X., Lyczkowski, R. W., Folga, S., Gidaspow, D., and Berry, G. F. (1989). Hydrodynamics of erosion of heat exchanger tubes in fluidized bed combustors. *Can. J. Chem. Eng.*, 67(2):218 – 229.

Brauner, N. and Barnea, D. (1986). Slug/churn transition in upward gas-liquid flow. *Chemical Engineering Science*, 41(1):159 – 163.

Buwa, V. V. and Ranade, V. V. (2002). Dynamics of gasliquid flow in a rectangular bubble column: experiments and single/multi-group {CFD} simulations. *Chemical Engineering Science*, 57(2223):4715 – 4736. Festschrift in Honour of Dr Winn van Swaaij.

Celik, I. and Wang, Y. Z. (1994). Numerical simulation of circulation in gas-liquid column reactors: isothermal, bubbly, laminar flow. *International Journal of Multiphase Flow*, 20(6):1053 – 1070.

Chahed, J., Roig, V., and Masbernat, L. (2003a). Eulerian–eulerian two-fluid model for turbulent gas–liquid bubbly flows. *International Journal of Multiphase Flow*, 29(1):23–49.

Chahed, J., Roig, V., and Masbernat, L. (2003b). Eulerianeulerian two-fluid model for turbulent gasliquid bubbly flows. *International Journal of Multiphase Flow*, 29(1):23 – 49.

Cheng, L., Drew, D., and Lahey, R. (1985). An analysis of wave propagation in bubbly two-component, two-phase flow. *Journal of heat transfer*, 107(2):402–408.

Cheng, Y., Guo, Y., Wei, F., Jin, Y., and Lin, W. (1999). Modeling the hydrodynamics of downer reactors based on kinetic theory. *Chemical Engineering Science*, 54(13 – 14):2019 – 2027.

Chung, M.-S., Lee, S.-J., and Chang, K.-S. (2001). Effect of interfacial pressure jump and virtual mass terms on sound wave propagation in the two-phase flow. *Journal of Sound and Vibration*, 244(4):717–728.

Climent, E. and Magnaudet, J. (1999). Large-scale simulations of bubble-induced convection in a liquid layer. *Physical review letters*, 82(24):4827.

Cook, T. L. and Harlow, F. H. (1986). Vortices in bubbly two-phase flow. *International journal of multiphase flow*, 12(1):35–61.

Costigan, G. and Whalley, P. (1997). Slug flow regime identification from dynamic void fraction measurements in vertical air-water flows. *International Journal of Multiphase Flow*, 23(2):263 – 282.

Cui, Z. and Fan, L. (2004). Turbulence energy distributions in bubbling gas–liquid and gas–liquid–solid flow systems. *Chemical Engineering Science*, 59(8):1755–1766.

Davidson, M. R. (1990). Numerical calculations of two-phase flow in a liquid bath with bottom gas injection: the central plume. *Appl. Math. Modell.*, 14(2):67 – 76.

de Bertodano, M. L., Jr, R. L., and Jones, O. (1994). Phase distribution in bubbly two-phase flow in vertical ducts. *International Journal of Multiphase Flow*, 20(5):805 – 818.

Deckwer, W.-D., Louisi, Y., Zaidi, A., and Ralek, M. (1980). Hydrodynamic properties of the fischer-tropsch slurry process. *Industrial & Engineering Chemistry Process Design and Development*, 19(4):699–708.

Deen, N., Solberg, T., and Hjertager, B. (2001). Large eddy simulation of the gasliquid flow in a square cross-sectioned bubble column. *Chemical Engineering Science*, 56(2122):6341 – 6349. ¡ce:title¿Proceedings of the 5th International Conference on Gas-Liquid and Gas-Liquid-Solid Reactor Engineering¡/ce:title¿.

Degaleesan, S., Dudukovic, M., and Pan, Y. (2001). Experimental study of gas-induced liquid-flow structures in bubble columns. *AIChE Journal*, 47(9):1913–1931.

Delnoij, E., Lammers, F., Kuipers, J., and Van Swaaij, W. (1997a). Dynamic simulation of dispersed gas-liquid two-phase flow using a discrete bubble model. *Chemical Engineering Science*, 52(9):1429–1458.

Delnoij, E., Lammers, F., Kuipers, J., and van Swaaij, W. (1997b). Dynamic simulation of dispersed gas-liquid two-phase flow using a discrete bubble model. *Chemical Engineering Science*, 52(9):1429 – 1458.

Dhotre, M., Niceno, B., and Smith, B. (2008). Large eddy simulation of a bubble column using dynamic sub-grid scale model. *Chemical Engineering Journal*, 136(23):337 – 348.

Dinh, T., Nourgaliev, R., and Theofanous, T. (2003). Understanding the ill-posed two-fluid model. In *Proceedings of the 10th international topical meeting on nuclear reactor thermal-hydraulics (NURETH03)*.

Drew, D. (1983a). Mathematical modeling of two-phase flow. *Annual review of fluid mechanics*, 15(1):261–291.

Drew, D., Cheng, L., and Jr., R. L. (1979). The analysis of virtual mass effects in two-phase flow. *International Journal of Multiphase Flow*, 5(4):233 – 242.

Drew, D. and Lahey, R. (1981). Phase distribution mechanisms in turbulent two-phase flow in channels of arbitrary cross section. *Journal of Fluids Engineering*, 103(4):583–589.

Drew, D. A. (1971). Averaged equations for two-phase flows. *Stud. Appl. Math.*, L(3):205 – 231.

Drew, D. A. (1983b). Continuum modeling of two-phase flows. In Meyer, R., editor, *Theory of Dispersed Multiphase Flow*, pages 173 – 190. Academic Press.

Drew, D. A. and Lahey, R. T. (1987). The virtual mass and lift force on a sphere in rotating inviscid flow. *Int. J. Multiphase Flow*, 13(1):113 – 121.

Druzhinin, O. and Elghobashi, S. (1998). Direct numerical simulations of bubble-laden turbulent flows using the two-fluid formulation. *Physics of Fluids*, 10:685.

Ekambara, K., Nandakumar, K., and Joshi, J. B. (2008). Cfd simulation of bubble column reactor using population balance. *Industrial & Engineering Chemistry Research*, 47(21):8505–8516.

Elghobashi, S. E. and Aboua Arab, T. W. (1983). A two-equation turbulence model for two-phase flows. *Physics of Fluids*, 26(4):1958 – 1988.

Fabre, J. and Line, A. (1992). Modeling of two-phase slug flow. *Annual Review of Fluid Mechanics*, 24(1):21–46.

Fan, L.-S., Matsuura, A., and Chern, S.-H. (1985). Hydrodynamic characteristics of a gas-liquid-solid fluidized bed containing a binary mixture of particles. *AIChE Journal*, 31(11):1801–1810.

Faxén, H. (1922). Der Widerstand gegen die Bewegung einer starren Kugel in einer zähen Flüssigkeit, die zwischen zwei parallelen ebenen Wänden eingeschlossen ist. *Ann. Phys.*, 373(10):89 – 119.

Ferziger, J. H. and Peric, M. (2002). *Computational Methods for Fluid Dynamics*. Springer.

Fitt, A. (1989). The numerical and analytical solution of ill-posed systems of conservation laws. *Applied Mathematical Modelling*, 13(11):618–631.

Fox, R. O. (2014a). On multiphase turbulence models for collisional fluid–particle flows. *Journal of Fluid Mechanics*, 742:368–424.

Fox, R. O. (2014b). On multiphase turbulence models for collisional fluidparticle flows. *Journal of Fluid Mechanics*, 742:368–424.

Fujiwara, A., Minato, D., and Hishida, K. (2004). Effect of bubble diameter on modification of turbulence in an upward pipe flow. *International Journal of Heat and Fluid Flow*, 25(3):481–488.

Govan, A., Hewitt, G., Richter, H., and Scott, A. (1991). Flooding and churn flow in vertical pipes. *International Journal of Multiphase Flow*, 17(1):27 – 44.

Grevskott, S., Sanns, B., Dudukovi, M., Hjarbo, K., and Svendsen, H. (1996). Liquid circulation, bubble size distributions, and solids movement in two- and three-phase bubble columns. *Chemical Engineering Science*, 51(10):1703 – 1713. ¡ce:title¿Chemical Reaction Engineering: From Fundamentals to Commercial Plants and Products¡/ce:title¿.

Grienberger, J. and Hofmann, H. (1992). Investigations and modelling of bubble columns. *Chemical Engineering Science*, 47(911):2215 – 2220. ¡ce:title¿Twelfth International Symposium on Chemical Reaction Engineering Today¡/ce:title¿.

Hancox, W., Ferch, R., Liu, W., and Nieman, R. (1980). One-dimensional models for transient gas-liquid flows in ducts. *Int. J. Multiphase Flow*, 6(1):25 – 40.

Happel, J. and Brenner, H. (2012). *Low Reynolds number hydrodynamics: with special applications to particulate media*, volume 1. Springer Science & Business Media.

Harteveld, W. (2005a). *Bubble Columns: Structure or Stability?* Ph.D. Thesis, Technische Universiteit Delft.

Harteveld, W. K. (2005b). *Bubble columns: Structures or stability?* TU Delft, Delft University of Technology.

Hibiki, T. and Ishii, M. (2000). Two-group interfacial area transport equations at bubbly-to-slug flow transition. *Nuclear Engineering and Design*, 202(1):39 – 76.

Hillmer, G., Weismantel, L., and Hofmann, H. (1994). Investigations and modelling of slurry bubble columns. *Chemical Engineering Science*, 49(6):837 – 843.

Hills, J. (1976). The operation of a bubble column at high throughputs: I. gas holdup measurements. *The Chemical Engineering Journal*, 12(2):89 – 99.

Hjertager, B. H. and Morud, K. (1995). Computational fluid dynamics simulation of bioreactors. *Modeling, identification and control*, 16(4):177–191.

Homsy, G., El-Kaissy, M., and Didwinia, A. (1980). Instability waves and the origin of bubbles in fluidized bedsii comparison with theory. *International Journal of Multiphase Flow*, 6(4):305–318.

Hyndman, C. L., Larachi, F., and Guy, C. (1997). Understanding gas-phase hydrodynamics in bubble columns: a convective model based on kinetic theory. *Chemical Engineering Science*, 52(1):63 – 77.

Ishii, M. and Mishima, K. (1984). Two-fluid model and hydrodynamic constitutive relations. *Nuclear Engineering and Design*, 82(23):107 – 126.

Ishii, M. and Zuber, N. (1979). Drag coefficient and relative velocity in bubbly, droplet or particulate flows. *AIChE Journal*, 25(5):843–855.

Issa, R. I. (1986). Solution of the implicitly discretised fluid flow equations by operator-splitting. *J. Comput. Phys.*, 62(1):40 – 65.

Ityokumbul, M., Kosaric, N., and Bulani, W. (1994). Gas hold-up and liquid mixing at low and intermediate gas velocities i. air-water system. *The Chemical Engineering Journal and the Biochemical Engineering Journal*, 53(3):167 – 172.

Jackson, R. (1997). Locally averaged equations of motion for a mixture of identical spherical particles and a newtonian fluid. *Chemical Engineering Science*, 52(15):2457–2469.

Jakobsen, H., Svendsen, H., and Hjarbo, K. (1993). On the prediction of local flow structures in internal loop and bubble column reactors using a two-fluid model. *Computers &*

Chemical Engineering, 17, Supplement 1(0):S531 – S536. ¡ce:title¿European Symposium on Computer Aided Process Engineering2¡/ce:title¿ ¡xocs:full-name¿24th European Symposium of the Working Party on Computer Aided Process Engineering and the 457th Event of the European Federation of Chemical Engineers (EFChE)¡/xocs:full-name¿.

Jakobsen, H. A., , Grevskott, S., and Svendsen, H. F. (1997). Modeling of vertical bubble-driven flows. *Industrial & Engineering Chemistry Research*, 36(10):4052–4074.

Jones, A. V. and Prosperetti, A. (1985). On the suitability of first-order differential models for two-phase flow prediction. *Int. J. Multiphase Flow*, 11(2):133 – 148.

Joshi, J. (2001). Computational flow modelling and design of bubble column reactors. *Chemical Engineering Science*, 56(2122):5893 – 5933. ¡ce:title¿Proceedings of the 5th International Conference on Gas-Liquid and Gas-Liquid-Solid Reactor Engineering¡/ce:title¿.

Joshi, J., Parasu Veera, U., Prasad, C. V., Phanikumar, D., Deshphande, N., Thakre, S., and Thorat, B. (1998). Gas hold-up structure in bubble column reactors. *PINSA-A*, 64(4):441–567.

Jr., R. T. L. (2005). The simulation of multidimensional multiphase flows. *Nuclear Engineering and Design*, 235(1012):1043 – 1060. Festschrift Edition Celebrating the 65th Birthday of Prof. Richard T. Lahey, Jr. 20th Anniversary of Biosensors and Bioelectronics rd International Symposium on Two Phase Modelling.

Kaichiro, M. and Ishii, M. (1984). Flow regime transition criteria for upward two-phase flow in vertical tubes. *International Journal of Heat and Mass Transfer*, 27(5):723 – 737.

Karema, H. and Lo, S. (1999). Efficiency of interphase coupling algorithms in fluidized bed conditions. *Computers and Fluids*, 28:323 – 360.

Kataoka, I. and Serizawa, A. (1989). Basic equations of turbulence in gas-liquid two-phase flow. *International Journal of Multiphase Flow*, 15(5):843 – 855.

Krepper, E., Vanga, B. N. R., Zaruba, A., Prasser, H.-M., and de Bertodano, M. A. L. (2007). Experimental and numerical studies of void fraction distribution in rectangular bubble columns. *Nuclear engineering and design*, 237(4):399–408.

Krishna, R., Wilkinson, P., and Dierendonck, L. V. (1991). A model for gas holdup in bubble columns incorporating the influence of gas density on flow regime transitions. *Chemical Engineering Science*, 46(10):2491 – 2496.

Lahey, R. (1990a). The analysis of phase separation and phase distribution phenomena using two-fluid models. *Nuclear Engineering and Design*, 122(1):17–40.

Lahey, R. (1990b). The analysis of phase separation and phase distribution phenomena using two-fluid models. *Nuclear Engineering and Design*, 122(13):17 – 40.

Lai, K. M. and Salcudean, M. (1987). Computer analysis of multi-dimensional turbulent, buoyancy-induced, two-phase flows in gas-agitated-liquid reactors. *Computers & fluids*, 15(3):281–295.

Lakkaraju, R., Schmidt, L. E., Oresta, P., Toschi, F., Verzicco, R., Lohse, D., and Prosperetti, A. (2011). Effect of vapor bubbles on velocity fluctuations and dissipation rates in bubbly rayleigh-bénard convection. *Physical Review E*, 84(3):036312.

Lamb, H. (1932). *Hydrodynamics*. Cambridge University Press.

Lance, M. and Bataille, J. (1991). Turbulence in the liquid phase of a uniform bubbly air–water flow. *Journal of Fluid Mechanics*, 222:95–118.

Lapin, A. and Lübbert, A. (1994). Numerical simulation of the dynamics of two-phase gasliquid flows in bubble columns. *Chemical Engineering Science*, 49(21):3661–3674.

Launder, B. E. and Spalding, D. (1974). The numerical computation of turbulent flows. *Computer methods in applied mechanics and engineering*, 3(2):269–289.

Lee, S.-J., Chang, K.-S., and Kim, S.-J. (1998). Surface tension effect in the two-fluids equation system. *International journal of heat and mass transfer*, 41(18):2821–2826.

Lee, S. L., Lahey, R. T., and Jones, O. C. (1989). The prediction of two-phase turbulence and phase distribution phenomena using a ¡i¿k¡/i¿-kappa; model. , 3(4):335–368.

Legendre, D. and Magnaudet, J. (1998). The lift force on a spherical bubble in a viscous linear shear flow. *J. Fluid Mech.*, 368:81 – 126.

Levich, V. G., Technica, S., et al. (1962). *Physicochemical hydrodynamics*, volume 689. Prentice-hall Englewood Cliffs, NJ.

Liu, N.-S., Cheng, B.-G., Xia, Q., and Lu, X.-Y. (2011). Direct numerical simulations of turbulent channel flows with consideration of the buoyancy effect of the bubble phase. *Journal of Hydrodynamics, Ser. B*, 23(3):282–288.

Liu, T. and Bankoff, S. (1993a). Structure of air-water bubbly flow in a vertical pipei. liquid mean velocity and turbulence measurements. *International Journal of Heat and Mass Transfer*, 36(4):1049–1060.

Liu, T. and Bankoff, S. (1993b). Structure of air-water bubbly flow in a vertical pipei. liquid mean velocity and turbulence measurements. *International Journal of Heat and Mass Transfer*, 36(4):1049 – 1060.

Lucas, D., Prasser, H.-M., and Manera, A. (2005). Influence of the lift force on the stability of a bubble column. *Chemical Engineering Science*, 60(13):3609 – 3619.

Luo, H. and Svendsen, H. F. (1996). Theoretical model for drop and bubble breakup in turbulent dispersions. *AIChE Journal*, 42(5):1225–1233.

Lyczkowski, R., Gidaspow, D., Solbrig, C., and Hughes, E. D. (1978). Characteristics and stability analyses of transient one-dimensional two-phase flow equations and their finite difference approximations. *Nucl. Sci. Eng.*, 66(3):378 – 396.

Ma, T., Santarelli, C., Ziegenhein, T., Lucas, D., and Fröhlich, J. (2017). Direct numerical simulation–based reynolds-averaged closure for bubble-induced turbulence. *Physical Review Fluids*, 2(3):034301.

Ma, T., Ziegenhein, T., Lucas, D., Krepper, E., and Fröhlich, J. (2015). Euler–euler large eddy simulations for dispersed turbulent bubbly flows. *International Journal of Heat and Fluid Flow*, 56:51–59.

Maxey, M. R. and Riley, J. J. (1983). Equation of motion for a small rigid sphere in a nonuniform flow. *Physics of Fluids (1958-1988)*, 26(4):883–889.

Mazzitelli, I. M. and Lohse, D. (2009). Evolution of energy in flow driven by rising bubbles. *Physical Review E*, 79(6):066317.

McGovern, S., Harish, G., Pai, C., Mansfield, W., Taylor, J., Pau, S., and Besser, R. (2008). Multiphase flow regimes for hydrogenation in a catalyst-trap microreactor. *Chemical Engineering Journal*, 135, Supplement 1(0):S229 – S236. ¡ce:title¿Microreaction Technology {IMRET} 9: Proceedings of the Ninth International Conference on Microreaction Technology¡/ce:title¿ ¡ce:subtitle¿IMRET9 Special Issue¡/ce:subtitle¿.

McQuillan, K. and Whalley, P. (1985). Flow patterns in vertical two-phase flow. *International Journal of Multiphase Flow*, 11(2):161 – 175.

Merchuk, J. and Berzin, I. (1995). Distribution of energy dissipation in airlift reactors. *Chemical Engineering Science*, 50(14):2225 – 2233.

Miller, D. N. (1980). Gas holdup and pressure drop in bubble column reactors. *Industrial & Engineering Chemistry Process Design and Development*, 19(3):371–377.

Millies, M. and Mewes, D. (1999). Interfacial area density in bubbly flow. *Chemical Engineering and Processing: Process Intensification*, 38(46):307 – 319.

Milne-Thomson, L. M. (1968). *Theoretical hydrodynamics*. Courier Corporation.

Moursali, E., Mari, J., and Bataille, J. (1995). An upward turbulent bubbly boundary layer along a vertical flat plate. *International Journal of Multiphase Flow*, 21(1):107 – 117.

Mudde, R., Groen, J., and Van Den Akker, H. (1997). Liquid velocity field in a bubble column: Lda experiments. *Chemical Engineering Science*, 52(21):4217–4224.

Mudde, R. F. (2005). Gravity-driven bubbly flows. *Annu. Rev. Fluid Mech.*, 37:393–423.

Murai, Y., Kitagawa, A., OHTA, J., and YAMAMOTO, F. (2000). Inverse energy cascade structure of turbulence in a bubby flow (numerical analysis using eulerian-lagrangian model equations).

Nierhaus, T., Abeele, D. V., and Deconinck, H. (2007). Direct numerical simulation of bubbly flow in the turbulent boundary layer of a horizontal parallel plate electrochemical reactor. *International journal of heat and fluid flow*, 28(4):542–551.

Nigmatulin, R. (1979). Spatial averaging in the mechanics of heterogeneous and dispersed systems. *International Journal of Multiphase Flow*, 5(5):353–385.

No, H. and Kazimi, M. (1985). Effects of virtual mass on the mathematical characteristics and numerical stability of the two-fluid model. *Nuclear science and engineering*, 89(3):197–206.

Oliveira, P. J. and Issa, R. I. (2001). An improved PISO algorithm for the computation of buoyancy-driven flows. *Numer. Heat Transfer, Part B: Fundamentals*, 40(6):473 – 493.

Olmos, E., Gentric, C., Vial, C., Wild, G., and Midoux, N. (2001). Numerical simulation of multiphase flow in bubble column reactors. influence of bubble coalescence and break-up. *Chemical Engineering Science*, 56(2122):6359 – 6365. ¡ce:title¿Proceedings of the 5th International Conference on Gas-Liquid and Gas-Liquid-Solid Reactor Engineering¡/ce:title¿.

OpenFOAM (2016). *OpenFOAM User Guide*. The OpenFOAM Foundation.

Pang, M., Wei, J., and Yu, B. (2013). Turbulence modulation by small bubbles in the vertical upward channel flow. *Advances in Mechanical Engineering*.

Patankar, S. V. (1980). *Numerical Heat Transfer and Fluid Flow*. Hemisphere, Washington D. C.

Pauchon, C. and Banerjee, S. (1986). Interphase momentum interaction effects in the averaged multifield model. *Int. J. Multiphase Flow*, 12(4):559 – 573.

Pfleger, D. and Becker, S. (2001). Modelling and simulation of the dynamic flow behaviour in a bubble column. *Chemical Engineering Science*, 56(4):1737 – 1747. 16th International Conference on Chemical Reactor Engineering.

Picardi, R., Zhao, L., and Battaglia, F. (2016). On the ideal grid resolution for two-dimensional eulerian modeling of gas-liquid flows. *Journal of Fluids Engineering*.

pino, L., SOLARI, R., SIQUIER, S., ANTONIO ESTVEZ, L., YPEZ, M., and SEZ, A. (1992). Effect of operating conditions on gas holdup in slurry bubble columns with a foaming liquid. *Chemical Engineering Communications*, 117(1):367–382.

Pope, S. B. (2000). *Turbulent flows*. Cambridge university press.

Prosperetti, A. and Jones, A. V. (1984). Pressure forces in disperse two-phase flow. *Int. J. Multiphase Flow*, 10(4):425 – 440.

Prosperetti, A. and Tryggvason, G. (2009). *Computational methods for multiphase flow*. Cambridge university press.

Ramshaw, J. D. and Trapp, J. A. (1978). Characteristics, stability, and short-wavelength phenomena in two-phase flow equation systems. *Nucl. Sci. Eng.*, 66(1):93 – 102.

Ranade, V. (1992). Flow in bubble columns: some numerical experiments. *Chemical Engineering Science*, 47(8):1857 – 1869.

Ranade, V. (1997). Modelling of turbulent flow in a bubble column reactor. *Chemical Engineering Research and Design*, 75(1):14 – 23. ¡ce:title¿Process and Product Development¡/ce:title¿.

Ransom, V. H. and Hicks, D. L. (1984). Hyperbolic two-pressure models for two-phase flow. *J. Comput. Phys.*, 53(1):124 – 151.

Rensen, J., Luther, S., and Lohse, D. (2005). The effect of bubbles on developed turbulence. *Journal of Fluid Mechanics*, 538:153–187.

Rhie, C. M. and Chow, W. L. (1983). Numerical study of the turbulent flow past an isolated airfoil with trailing edge separation. *AIAA J.*, 21(11):1525 – 1532.

Riboux, G., Legendre, D., and Risso, F. (2013). A model of bubble-induced turbulence based on large-scale wake interactions. *Journal of Fluid Mechanics*, 719:362–387.

Roghair, I., Lau, Y., Deen, N., Slagter, H., Baltussen, M., Annaland, M. V. S., and Kuipers, J. (2011a). On the drag force of bubbles in bubble swarms at intermediate and high reynolds numbers. *Chemical engineering science*, 66(14):3204–3211.

Roghair, I., Mercado, J. M., Annaland, M. V. S., Kuipers, H., Sun, C., and Lohse, D. (2011b). Energy spectra and bubble velocity distributions in pseudo-turbulence: Numerical simulations vs. experiments. *International Journal of Multiphase Flow*, 37(9):1093–1098.

Roig, V., Suzanne, C., and Masbernat, L. (1998). Experimental investigation of a turbulent bubbly mixing layer. *International Journal of Multiphase Flow*, 24(1):35 – 54.

Ruzicka, M., Zahradnık, J., Drahoš, J., and Thomas, N. (2001). Homogeneous–heterogeneous regime transition in bubble columns. *Chemical Engineering Science*, 56(15):4609–4626.

Rzehak, R. and Krepper, E. (2013). {CFD} modeling of bubble-induced turbulence. *International Journal of Multiphase Flow*, 55:138 – 155.

S., J. and T., S. Y. *A Two-Bubble Class Model for Churn Turbulent Bubble Column Slurry Reactor*, chapter 10, pages 149–167.

Sankaranarayanan, K., Shan, X., Kevrekidis, I., and Sundaresan, S. (2002). Analysis of drag and virtual mass forces in bubbly suspensions using an implicit formulation of the lattice boltzmann method. *Journal of Fluid Mechanics*, 452:61–96.

Sato, Y., Sadatomi, M., and Sekoguchi, K. (1981). Momentum and heat transfer in two-phase bubble flowi. theory. *International Journal of Multiphase Flow*, 7(2):167 – 177.

Sato, Y. and Sekoguchi, K. (1975a). Liquid velocity distribution in two-phase bubble flow. *International Journal of Multiphase Flow*, 2(1):79 – 95.

Sato, Y. and Sekoguchi, K. (1975b). Liquid velocity distribution in two-phase bubble flow. *International Journal of Multiphase Flow*, 2(1):79 – 95.

Saurel, R. and Abgrall, R. (1999). A multiphase Godunov method for compressible multifluid and multiphase flows. *J. Comput. Phys.*, 150(2):425 – 467.

Schiller, L. and Naumann, Z. (1935). A drag coefficient correlation. *Vdi Zeitung*, 77(318):51.

Schumpe, A. and Deckwer, W.-D. (1980). Analysis of chemical methods for determination of interfacial areas in gas-in-liquid dispersions with non-uniform bubble sizes. *Chemical Engineering Science*, 35(10):2221 – 2234.

Schumpe, A. and Grund, G. (1986). The gas disengagement technique for studying gas holdup structure in bubble columns. *The Canadian Journal of Chemical Engineering*, 64(6):891–896.

Schwarz, M. and Turner, W. (1988). Applicability of the standard¡ i¿ k¡/i¿- turbulence model to gas-stirred baths. *Applied mathematical modelling*, 12(3):273–279.

Serizawa, A., Kataoka, I., and Michiyoshi, I. (1975). Turbulence structure of air-water bubbly flowi. measuring techniques. *International Journal of Multiphase Flow*, 2(3):221–233.

Sha, W. T. and Soo, S. L. (1979). On the effect of $p\nabla\alpha$ term in multiphase mechanics. *Int. J. Multiphase Flow*, 5(2):153 – 158.

Shah, Y. T., Kelkar, B. G., Godbole, S. P., and Deckwer, W.-D. (1982). Design parameters estimations for bubble column reactors. *AIChE Journal*, 28(3):353–379.

Shawkat, M. and Ching, C. (2011). Liquid turbulence kinetic energy budget of co-current bubbly flow in a large diameter vertical pipe. *Journal of Fluids Engineering*, 133(9):091303.

Simonnet, M., Gentric, C., Olmos, E., and Midoux, N. (2007). Experimental determination of the drag coefficient in a swarm of bubbles. *Chemical Engineering Science*, 62(3):858–866.

Sokolichin, A. and Eigenberger, G. (1994a). Gasliquid flow in bubble columns and loop reactors: Part i. detailed modelling and numerical simulation. *Chemical Engineering Science*, 49(24, Part 2):5735 – 5746.

Sokolichin, A. and Eigenberger, G. (1994b). Gasliquid flow in bubble columns and loop reactors: Part i. detailed modelling and numerical simulation. *Chemical Engineering Science*, 49(24):5735–5746.

Sokolichin, A. and Eigenberger, G. (1999). Applicability of the standard k turbulence model to the dynamic simulation of bubble columns: Part i. detailed numerical simulations. *Chemical Engineering Science*, 54(13):2273 – 2284.

Sommerfeld, M., Bourloutski, E., and Bröder, D. (2003). Euler/lagrange calculations of bubbly flows with consideration of bubble coalescence. *The Canadian Journal of Chemical Engineering*, 81(3-4):508–518.

Song, J. H. and Ishii, M. (2001). On the stability of a one-dimensional two-fluid model. *Nucl. Eng. Des.*, 204(1 - 3):101 – 115.

Spalding, D. B. (1980). Numerical computation of multi-phase fluid flow and heat transfer. In Taylor, C., editor, *Recent Advances in Numerical Methods in Fluids*. Pineridge Press.

Spalding, D. B. (1983). Developments in the IPSA procedure for numerical computation of multiphase-flow phenomena with interphase slip, unequal temperatures, etc. In Shih, T. M., editor, *Numerical Methodologies in Heat Transfer*, pages 421 – 436.

Stewart, H. B. (1979). Stability of two-phase flow calculation using two-fluid models. *Journal of Computational Physics*, 33(2):259–270.

Stuhmiller, J. (1977). The influence of interfacial pressure forces on the character of two-phase flow model equations. *International Journal of Multiphase Flow*, 3(6):551–560.

Subramaniam, S. (2013). Lagrangian–eulerian methods for multiphase flows. *Progress in Energy and Combustion Science*, 39(2):215–245.

Sursock, J.-P. (1982). Causality violation of complex-characteristic two-phase flow equations. *International Journal of Multiphase Flow*, 8(3):291–295.

Svendsen, H., Jakobsen, H., and Torvik, R. (1992). Local flow structures in internal loop and bubble column reactors. *Chemical Engineering Science*, 47(1314):3297 – 3304.

Sweby, P. (1984). High resolution schemes using flux limiters for hyperbolic conservation laws. *SIAM J. Numer. Anal.*, 21(5):995 – 1011.

Syamlal, M. (2011). A hyperbolic model for fluidsolids two-phase flow. *Chem. Eng. Sci.*, 66(19):4421 – 4425.

Taitel, Y., Bornea, D., and Dukler, A. E. (1980). Modelling flow pattern transitions for steady upward gas-liquid flow in vertical tubes. *AIChE Journal*, 26(3):345–354.

Thakre, S. S., Phanikumar, D. V., Khare, A. S., and Joshi, J. B. (1999). Cfd modeling of flow, macro-mixing and axial dispersion in a bubble column. *The Canadian Journal of Chemical Engineering*, 77(5):826–837.

Thorat, B. and Joshi, J. (2004). Regime transition in bubble columns: experimental and predictions. *Experimental Thermal and Fluid Science*, 28(5):423 – 430. ¡ce:title¿5th international conference on Gas-Liquid and Gas-Liquid-Solid Reactor Engineering¡/ce:title¿.

Thorley, A. and Wiggert, D. (1985). The effect of virtual mass on the basic equations for unsteady one-dimensional heterogeneous flows. *International journal of multiphase flow*, 11(2):149–160.

Tiselj, I. and Petelin, S. (1997). Modelling of two-phase flow with second-order accurate scheme. *Journal of Computational Physics*, 136(2):503–521.

Tomiyama, A. (1998). Struggle with computational bubble dynamics. *Multiphase Science and Technology*, 10(4):369–405.

Tomiyama, A., Kataoka, I., Zun, I., and Sakaguchi, T. (1998). Drag coefficients of single bubbles under normal and micro gravity conditions. *JSME Int. J. B – Fluid T.*, 41(2):472 – 479.

Tomiyama, A., Tamai, H., Zun, I., and Hosokawa, S. (2002a). Transverse migration of single bubbles in simple shear flows. *Chemical Engineering Science*, 57(11):1849–1858.

Tomiyama, A., Tamai, H., Zun, I., and Hosokawa, S. (2002b). Transverse migration of single bubbles in simple shear flows. *Chemical Engineering Science*, 57(11):1849 – 1858.

Torvik, R. and Svendsen, H. (1990). Modelling of slurry reactors. a fundamental approach. *Chemical Engineering Science*, 45(8):2325 – 2332.

Troshko, A. and Hassan, Y. (2001a). A two-equation turbulence model of turbulent bubbly flows. *International Journal of Multiphase Flow*, 27(11):1965 – 2000.

Troshko, A. and Hassan, Y. (2001b). A two-equation turbulence model of turbulent bubbly flows. *International Journal of Multiphase Flow*, 27(11):1965–2000.

Uchiyama, T. and Kusamichi, S. (2013). Interaction of bubbles with vortex ring launched into bubble plume. *Advances in Chemical Engineering and Science*, 2013.

Wang, S., Lee, S., Jones, O., and Lahey, R. (1987a). 3-d turbulence structure and phase distribution measurements in bubbly two-phase flows. *International Journal of multiphase flow*, 13(3):327–343.

Wang, S., Lee, S., Jr., O. J., and Jr, R. L. (1987b). 3-d turbulence structure and phase distribution measurements in bubbly two-phase flows. *International Journal of Multiphase Flow*, 13(3):327 – 343.

Watanabe, T., Hirano, M., Tanabe, F., and Kamo, H. (1990). The effect of the virtual mass force term on the numerical stability and efficiency of system calculations. *Nuclear Engineering and Design*, 120(2):181 – 192.

Weisman, J., Duncan, D., Gibson, J., and Crawford, T. (1979). Effects of fluid properties and pipe diameter on two-phase flow patterns in horizontal lines. *International Journal of Multiphase Flow*, 5(6):437 – 462.

Weller, H. G. (2006). Bounded explicit and implicit second-order schemes for scalar transport. Technical report, The OpenFOAM Foundation.

Wilcox, D. C. et al. (1998). *Turbulence modeling for CFD*, volume 2. DCW industries La Canada, CA.

Woldesemayat, M. A. and Ghajar, A. J. (2007). Comparison of void fraction correlations for different flow patterns in horizontal and upward inclined pipes. *International Journal of Multiphase Flow*, 33(4):347 – 370.

Wu, Y., Ong, B. C., and Al-Dahhan, M. (2001). Predictions of radial gas holdup profiles in bubble column reactors. *Chemical Engineering Science*, 56(3):1207 – 1210. ¡ce:title¿16th International Conference on Chemical Reactor Engineering¡/ce:title¿.

Yang, X., Thomas, N., Guo, L., and Hou, Y. (2002). Two-way coupled bubble laden mixing layer. *Chemical engineering science*, 57(4):555–564.

Yang, Y., Devanathan, N., and Duduković, M. (1993). Liquid backmixing in bubble columns via computer-automated radioactive particle tracking (carpt). *Experiments in fluids*, 16(1):1–9.

Yao, B., Zheng, C., Gasche, H., and Hofmann, H. (1991). Bubble behaviour and flow structure of bubble columns. *Chemical Engineering and Processing: Process Intensification*, 29(2):65–75.

Yeoh, G. and Tu, J. (2006). Two-fluid and population balance models for subcooled boiling flow. *Applied Mathematical Modelling*, 30(11):1370 – 1391. Selected papers from the Third International Conference on {CFD} in the Minerals and Process Industries3rd International Conference on {CFDSelected} papers from the Third International Conference on {CFD} in the Minerals and Process Industries.

Zhang, D., Deen, N., and Kuipers, J. (2006). Numerical simulation of the dynamic flow behavior in a bubble column: A study of closures for turbulence and interface forces. *Chemical Engineering Science*, 61(23):7593 – 7608.

Zhang, S. and Zhao, X. (2004). General formulations for Rhie-Chow interpolation. In *2004 ASME Heat Transfer/Fluids Engineering Summer Conference*, number HT-FED04-56274, pages 567 – 573, Charlotte, North Carolina, USA.

Zun, I. (1980). The transverse migration of bubbles influenced by walls in vertical bubbly flow. *International Journal of Multiphase Flow*, 6(6):583–588.

APPENDIX A. CODE IN OPENFOAM: MULTIPHASE RST MODEL

A.1 MultiphaseRST.H

```
#ifndef MultiphaseRST_H
#define MultiphaseRST_H

#include "RASModel.H"
#include "ReynoldsStress.H"

// * * * * * * * * * * * * * * * * * * * * * * * * * * * * * * * * * * * * * * * * * * * * //

namespace Foam
{
namespace RASModels
{

/*---------------------------------------------------------------------------*\
                           Class MultiphaseRST Declaration
\*---------------------------------------------------------------------------*/

template<class BasicTurbulenceModel>
class MultiphaseRST
:
    public ReynoldsStress<RASModel<BasicTurbulenceModel>>
```

```
{
    // Private Member Functions

        // Disallow default bitwise copy construct and assignment
        MultiphaseRST(const MultiphaseRST&);
        void operator=(const MultiphaseRST&);


protected:

    // Protected data

        // Model coefficients

            dimensionedScalar Cmu_;

            dimensionedScalar C1_;
            dimensionedScalar C2_;

            dimensionedScalar Ceps1_;
            dimensionedScalar Ceps2_;
            dimensionedScalar Cs_;
            dimensionedScalar Ceps_;


        // Wall-refection coefficients

            Switch wallReflection_;
            dimensionedScalar kappa_;
```

```
            dimensionedScalar Cref1_;
            dimensionedScalar Cref2_;


        // Fields

            volScalarField k_;
            volScalarField epsilon_;


    // Protected Member Functions

        //- Update the eddy-viscosity
        virtual void correctNut();

        //-source of production or exchange
        virtual tmp<fvSymmTensorMatrix> turbExchange() const;
       // virtual tmp<volSymmTensorField> turbExchange() const;
        //virtual volSymmTensorField turbExchange() const;
        //source of dissipation
        virtual tmp<fvScalarMatrix> epsExchange() const;

        //pressure strain model
        //virtual tmp<fvSymmTensorMatrix> PS() const;


public:

    typedef typename BasicTurbulenceModel::alphaField alphaField;
```

```
typedef typename BasicTurbulenceModel::rhoField rhoField;
typedef typename BasicTurbulenceModel::transportModel transportModel;


//- Runtime type information
TypeName("MultiphaseRST");


// Constructors

    //- Construct from components
    MultiphaseRST
    (
        const alphaField& alpha,
        const rhoField& rho,
        const volVectorField& U,
        const surfaceScalarField& alphaRhoPhi,
        const surfaceScalarField& phi,
        const transportModel& transport,
        const word& propertiesName = turbulenceModel::propertiesName,
        const word& type = typeName
    );


//- Destructor
virtual ~MultiphaseRST()
{}
```

```
    // Member Functions

        //- Read model coefficients if they have changed
        virtual bool read();

        //- Return the turbulence kinetic energy
        virtual tmp<volScalarField> k() const
        {
            return k_;
        }

        //- Return the turbulence kinetic energy dissipation rate
        virtual tmp<volScalarField> epsilon() const
        {
            return epsilon_;
        }

        //- Return the effective diffusivity for R
        tmp<volSymmTensorField> DREff() const;

        //- Return the effective diffusivity for epsilon
        tmp<volSymmTensorField> DepsilonEff() const;

        //- Solve the turbulence equations and correct eddy-Viscosity and
        //  related properties
        virtual void correct();
};
```

```
// * * * * * * * * * * * * * * * * * * * * * * * * * * * * * * * * * * * * * * * * * * * * //

} // End namespace RASModels
} // End namespace Foam

// * * * * * * * * * * * * * * * * * * * * * * * * * * * * * * * * * * * * * * * * * * * * //

#ifdef NoRepository
    #include "MultiphaseRST.C"
#endif

// * * * * * * * * * * * * * * * * * * * * * * * * * * * * * * * * * * * * * * * * * * * * //

#endif

// ************************************************************************* //
```

A.2 MultiphaseRST.C

```
#include "MultiphaseRST.H"
#include "fvOptions.H"
#include "wallFvPatch.H"

// * * * * * * * * * * * * * * * * * * * * * * * * * * * * * * * * * * * * * * * * * * * * //

namespace Foam
{
namespace RASModels
{
```

```
// * * * * * * * * * * * * * Protected Member Functions  * * * * * * * * * * * * //

template<class BasicTurbulenceModel>
void MultiphaseRST<BasicTurbulenceModel>::correctNut()
{
    this->nut_ = this->Cmu_*sqr(k_)/epsilon_;
    this->nut_.correctBoundaryConditions();
    fv::options::New(this->mesh_).correct(this->nut_);

    BasicTurbulenceModel::correctNut();
}


// * * * * * * * * * * * * * * * * * * Constructors  * * * * * * * * * * * * * * * * * //

template<class BasicTurbulenceModel>
MultiphaseRST<BasicTurbulenceModel>::MultiphaseRST
(
    const alphaField& alpha,
    const rhoField& rho,
    const volVectorField& U,
    const surfaceScalarField& alphaRhoPhi,
    const surfaceScalarField& phi,
    const transportModel& transport,
    const word& propertiesName,
    const word& type
)
:
    ReynoldsStress<RASModel<BasicTurbulenceModel>>
```

```
(
    type,
    alpha,
    rho,
    U,
    alphaRhoPhi,
    phi,
    transport,
    propertiesName
),

Cmu_
(
    dimensioned<scalar>::lookupOrAddToDict
    (
        "Cmu",
        this->coeffDict_,
        0.09
    )
),
C1_
(
    dimensioned<scalar>::lookupOrAddToDict
    (
        "C1",
        this->coeffDict_,
        1.8
    )
),
```

```
C2_
(
    dimensioned<scalar>::lookupOrAddToDict
    (
        "C2",
        this->coeffDict_,
        0.6
    )
),
Ceps1_
(
    dimensioned<scalar>::lookupOrAddToDict
    (
        "Ceps1",
        this->coeffDict_,
        1.44
    )
),
Ceps2_
(
    dimensioned<scalar>::lookupOrAddToDict
    (
        "Ceps2",
        this->coeffDict_,
        1.92
    )
),
Cs_
(
```

```
    dimensioned<scalar>::lookupOrAddToDict
    (
        "Cs",
        this->coeffDict_,
        0.25
    )
),
Ceps_
(
    dimensioned<scalar>::lookupOrAddToDict
    (
        "Ceps",
        this->coeffDict_,
        0.15
    )
),

wallReflection_
(
    Switch::lookupOrAddToDict
    (
        "wallReflection",
        this->coeffDict_,
        true
    )
),

kappa_
(
```

```
    dimensioned<scalar>::lookupOrAddToDict
    (
        "kappa",
        this->coeffDict_,
        0.41
    )
),

Cref1_
(
    dimensioned<scalar>::lookupOrAddToDict
    (
        "Cref1",
        this->coeffDict_,
        0.5
    )
),

Cref2_
(
    dimensioned<scalar>::lookupOrAddToDict
    (
        "Cref2",
        this->coeffDict_,
        0.3
    )
),

k_
```

```
    (
        IOobject
        (
            "k",
            this->runTime_.timeName(),
            this->mesh_,
            IOobject::NO_READ,
            IOobject::AUTO_WRITE
        ),
        0.5*tr(this->R_)
    ),
    epsilon_
    (
        IOobject
        (
            IOobject::groupName("epsilon", U.group()),
            this->runTime_.timeName(),
            this->mesh_,
            IOobject::MUST_READ,
            IOobject::AUTO_WRITE
        ),
        this->mesh_
    )
{
    if (type == typeName)
    {
        this->printCoeffs(type);

        this->boundNormalStress(this->R_);
```

```
        bound(epsilon_, this->epsilonMin_);
        k_ = 0.5*tr(this->R_);
    }
}


// * * * * * * * * * * * * * * * * Member Functions  * * * * * * * * * * * * * //

template<class BasicTurbulenceModel>
bool MultiphaseRST<BasicTurbulenceModel>::read()
{
    if (ReynoldsStress<RASModel<BasicTurbulenceModel>>::read())
    {
        Cmu_.readIfPresent(this->coeffDict());
        C1_.readIfPresent(this->coeffDict());
        C2_.readIfPresent(this->coeffDict());
        Ceps1_.readIfPresent(this->coeffDict());
        Ceps2_.readIfPresent(this->coeffDict());
        Cs_.readIfPresent(this->coeffDict());
        Ceps_.readIfPresent(this->coeffDict());

        wallReflection_.readIfPresent("wallReflection", this->coeffDict());
        kappa_.readIfPresent(this->coeffDict());
        Cref1_.readIfPresent(this->coeffDict());
        Cref2_.readIfPresent(this->coeffDict());

        return true;
    }
    else
```

```
    {
        return false;
    }
}


template<class BasicTurbulenceModel>
tmp<volSymmTensorField> MultiphaseRST<BasicTurbulenceModel>::DREff() const
{
    return tmp<volSymmTensorField>
    (
        new volSymmTensorField
        (
            "DREff",
            (Cs_*(this->k_/this->epsilon_))*this->R_ + I*this->nu()
        )
    );
}


template<class BasicTurbulenceModel>
tmp<volSymmTensorField> MultiphaseRST<BasicTurbulenceModel>::DepsilonEff() const
{
    return tmp<volSymmTensorField>
    (
        new volSymmTensorField
        (
            "DepsilonEff",
            (Ceps_*(this->k_/this->epsilon_))*this->R_ + I*this->nu()
```

```
        )
    );
}



// template<class BasicTurbulenceModel>
// tmp<fvSymmTensorMatrix> MultiphaseRST<BasicTurbulenceModel>::turbExchange() const
// {
//     return tmp<fvSymmTensorMatrix>
//     (
//         new fvSymmTensorMatrix
//         (
//             this->R_,
//             dimVolume*this->rho_.dimensions()*this->R_.dimensions()
//             /dimTime
//         )
//     );
//
// }


template<class BasicTurbulenceModel>
tmp<fvSymmTensorMatrix> MultiphaseRST<BasicTurbulenceModel>::turbExchange() const
{
    return tmp<fvSymmTensorMatrix>
    (
        new fvSymmTensorMatrix
        (
            this->R_,
            dimVolume*this->rho_.dimensions()*this->R_.dimensions()
```

```
            /dimTime
        )
    );

}

template<class BasicTurbulenceModel>
tmp<fvScalarMatrix> MultiphaseRST<BasicTurbulenceModel>::epsExchange() const
{
    return tmp<fvScalarMatrix>
    (
        new fvScalarMatrix
        (
            epsilon_,
            dimVolume*this->rho_.dimensions()*epsilon_.dimensions()
            /dimTime
        )
    );
}



template<class BasicTurbulenceModel>
void MultiphaseRST<BasicTurbulenceModel>::correct()
{
    if (!this->turbulence_)
    {
        return;
    }
```

```
// Local references
const alphaField& alpha = this->alpha_;
const rhoField& rho = this->rho_;
const surfaceScalarField& alphaRhoPhi = this->alphaRhoPhi_;
const volVectorField& U = this->U_;
volSymmTensorField& R = this->R_;
fv::options& fvOptions(fv::options::New(this->mesh_));

ReynoldsStress<RASModel<BasicTurbulenceModel>>::correct();

tmp<volTensorField> tgradU(fvc::grad(U));
const volTensorField& gradU = tgradU();

volSymmTensorField P(-twoSymm(R & gradU));
volScalarField G(this->GName(), 0.5*mag(tr(P)));

// Update epsilon and G at the wall
epsilon_.boundaryFieldRef().updateCoeffs();

// Dissipation equation
tmp<fvScalarMatrix> epsEqn
(
    fvm::ddt(alpha, rho, epsilon_)
  + fvm::div(alphaRhoPhi, epsilon_)
  - fvm::laplacian(alpha*rho*DepsilonEff(), epsilon_)
 ==
    Ceps1_*alpha*rho*G*epsilon_/k_
  - fvm::Sp(Ceps2_*alpha*rho*epsilon_/k_, epsilon_)
  + fvOptions(alpha, rho, epsilon_)
```

```
  + epsExchange()
);



epsEqn.ref().relax();

fvOptions.constrain(epsEqn.ref());
epsEqn.ref().boundaryManipulate(epsilon_.boundaryFieldRef());


solve(epsEqn);


fvOptions.correct(epsilon_);
bound(epsilon_, this->epsilonMin_);

// Correct the trace of the tensorial production to be consistent
// with the near-wall generation from the wall-functions
const fvPatchList& patches = this->mesh_.boundary();

forAll(patches, patchi)
{
    const fvPatch& curPatch = patches[patchi];

    if (isA<wallFvPatch>(curPatch))
    {
        forAll(curPatch, facei)
        {
```

```
                label celli = curPatch.faceCells()[facei];
                P[celli] *= min
                (
                    G[celli]/(0.5*mag(tr(P[celli])) + SMALL),
                    1.0
                );
            }
        }
    }
    /*
    Info<< "RST equation \n"<<"\n"<<"solving part 2"
            << endl; */
    // Reynolds stress equation
    tmp<fvSymmTensorMatrix> REqn
    (
        fvm::ddt(alpha, rho, R)
      + fvm::div(alphaRhoPhi, R)
      - fvm::laplacian(alpha*rho*DREff(), R)
      + fvm::Sp(C1_*alpha*rho*epsilon_/k_, R)
      ==
        alpha*rho*P
      - (2.0/3.0*(1 - C1_)*I)*alpha*rho*epsilon_
      - C2_*alpha*rho*dev(P)
      + fvOptions(alpha, rho, R)
      + turbExchange()
    );
//   /* Info<< "RST equation \n"<<"\n"<<"solving part 3"
//             << endl; */
    // Optionally add wall-refection term
```

```
if (wallReflection_)
{
    const volVectorField& n_(wallDist::New(this->mesh_).n());
    const volScalarField& y_(wallDist::New(this->mesh_).y());

    const volSymmTensorField reflect
    (
        Cref1_*R - ((Cref2_*C2_)*(k_/epsilon_))*dev(P)
    );

    REqn.ref() +=
        ((3*pow(Cmu_, 0.75)/kappa_)*(alpha*rho*sqrt(k_)/y_))
       *dev(symm((n_ & reflect)*n_));
}

REqn.ref().relax();
fvOptions.constrain(REqn.ref());

solve(REqn);

fvOptions.correct(R);

this->boundNormalStress(R);

k_ = 0.5*tr(R);

correctNut();

// Correct wall shear-stresses when applying wall-functions
```

```
    this->correctWallShearStress(R);
}


// * * * * * * * * * * * * * * * * * * * * * * * * * * * * * * * * * * * * * * * * * * * * //

} // End namespace RASModels
} // End namespace Foam

// ************************************************************************* //
```

//end namespace FOAM

APPENDIX B. DISPERSED AND CONTINUOUS CLASS

B.1 RSTdispersed.H

```
   #include "MultiphaseRST.H"


#ifndef RSTdispersed_H

#define RSTdispersed_H

namespace Foam

{

namespace RASModels

{

template <class BasicTurbulenceModel>

class RSTdispersed

: public MultiphaseRST<BasicTurbulenceModel>

{

    //Private data

private:


    mutable const turbulenceModel *liquidTurbulencePtr_;



    // Private Member Functions


        //- Return the turbulence model for the gas phase
```

```
    //Disallow default bitwise copy construct and assignment
    RSTdispersed(const RSTdispersed&);
    void operator=(const RSTdispersed&);

protected:
    dimensionedScalar alphaInversion_;
   //Model constants
    dimensionedScalar CDEz_;
    dimensionedScalar CDEx_;
    dimensionedScalar Cgz_;
    dimensionedScalar switchDragDEYY_;
    dimensionedScalar switchDragDEXX_;

    //Model constants

    //member functions
    virtual void correctNut();

    //Returns drag production
    virtual volSymmTensorField DE() const;
    //-source of production or exchange
    tmp<volScalarField> phaseTransferCoeff() const;

   // virtual tmp<volSymmTensorField> turbExchange() const;
    virtual tmp<fvSymmTensorMatrix> turbExchange() const;

       //source of dissipation
    virtual tmp<fvScalarMatrix> epsExchange() const;
```

```
        //pressure strain model
    // virtual tmp<fvSymmTensorMatrix> PS() const;

public:

    typedef typename BasicTurbulenceModel::alphaField alphaField;
    typedef typename BasicTurbulenceModel::rhoField rhoField;
    typedef typename BasicTurbulenceModel::transportModel transportModel;

    //- Runtime type information
    TypeName("RSTdispersed");
    //constructor
    RSTdispersed
    (
          const alphaField& alpha,
          const rhoField& rho,
          const volVectorField& U,
          const surfaceScalarField& alphaRhoPhi,
          const surfaceScalarField& phi,
          const transportModel& transport,
          const word& propertiesName = turbulenceModel::propertiesName,
          const word& type = typeName
    );

    //Destructor
    virtual ~RSTdispersed()
    {}
    // Read model constants from the dict file
```

```
    virtual bool read();

    const turbulenceModel& liqTurb() const;


    //solve for RST equations
    virtual void correct();
};

}//End namespace RAS
}//End namespace Foam
#ifdef NoRepository
#include "RSTdispersed.C"
#endif
#endif
```

B.2 RSTdispersed.C

```
  #include "RSTdispersed.H"
#include "fvOptions.H"
#include "twoPhaseSystem.H"
// * * * * * * * * * * * * * * * * * * * * * * * * * * * * * * * * * * * * * //


namespace Foam
{
namespace RASModels
{

//Protected Member functions
```

```
template<class BasicTurbulenceModel>
void RSTdispersed<BasicTurbulenceModel>::correctNut()
{
   MultiphaseRST<BasicTurbulenceModel>::correctNut();
}



// * * * * * * * * * * * * * * * * * * Constructors  * * * * * * * * * * * * * * * * * //
template <class BasicTurbulenceModel>
RSTdispersed<BasicTurbulenceModel>::RSTdispersed
(
    const alphaField& alpha,
    const rhoField& rho,
    const volVectorField& U,
    const surfaceScalarField& alphaRhoPhi,
    const surfaceScalarField& phi,
    const transportModel& transport,
    const word& propertiesName,
    const word& type
)
:
    MultiphaseRST<BasicTurbulenceModel>
    (
        alpha,
        rho,
        U,
        alphaRhoPhi,
        phi,
```

```
    transport,
    propertiesName,
    type

),

liquidTurbulencePtr_(nullptr),

alphaInversion_
(
    dimensioned<scalar>::lookupOrAddToDict
    (
        "alphaInversion",
        this->coeffDict_,
        0.7
    )
),

CDEz_
(
    dimensioned<scalar>::lookupOrAddToDict
    (
        "CDEz",
        this->coeffDict_,
        0.9012
    )
),

  CDEx_
```

```
(
    dimensioned<scalar>::lookupOrAddToDict
    (
        "CDEx",
        this->coeffDict_,
        0.8277
    )
),
Cgz_
(
    dimensioned<scalar>::lookupOrAddToDict
    (
        "Cgz",
        this->coeffDict_,
        0.1052
    )
),
switchDragDEYY_
(
    dimensioned<scalar>::lookupOrAddToDict
    (
        "switchDragDEYY",
        this->coeffDict_,
        1
    )
),
switchDragDEXX_
(
    dimensioned<scalar>::lookupOrAddToDict
```

```
        (
            "switchDragDEXX",
            this->coeffDict_,
            1
        )
    )
{
    if (type == typeName)
    {
        this->printCoeffs(type);
    }
}


// * * * * * * * * * * * * * * * * Member Functions  * * * * * * * * * * * * * //

template<class BasicTurbulenceModel>
bool RSTdispersed<BasicTurbulenceModel>::read()
{
    if (MultiphaseRST<BasicTurbulenceModel>::read())
    {
        alphaInversion_.readIfPresent(this->coeffDict());
        CDEz_.readIfPresent(this->coeffDict());
        Cgz_.readIfPresent(this->coeffDict());
        switchDragDEYY_.readIfPresent(this->coeffDict());
        switchDragDEXX_.readIfPresent(this->coeffDict());

        return true;
    }
```

```
    else
    {
        return false;
    }
}

//Phase interactions variables from other phase required for source construction
template<class BasicTurbulenceModel>
const turbulenceModel&
RSTdispersed<BasicTurbulenceModel>::liqTurb() const
{
    if (!liquidTurbulencePtr_)
    {
        const volVectorField& U = this->U_;

        const transportModel& gas = this->transport();
        const twoPhaseSystem& fluid =
            refCast<const twoPhaseSystem>(gas.fluid());
        const transportModel& liquid = fluid.otherPhase(gas);

        liquidTurbulencePtr_ =
           &U.db().lookupObject<turbulenceModel>
            (
                IOobject::groupName
                (
                    turbulenceModel::propertiesName,
                    liquid.name()
                )
            );
```

```
    }


    return *liquidTurbulencePtr_;
}


//Drag production
template<class BasicTurbulenceModel>
volSymmTensorField RSTdispersed<BasicTurbulenceModel>::DE() const
{
    //FIXXXXXXXXXXXXXXX THE DIRECTIONAL DEPENDENCE
    //                                              //
    //----------------------------------------------//

    //----------------------------------------------//
    const turbulenceModel& liqTurb = this->liqTurb();

    const transportModel& gas = this->transport();
    const twoPhaseSystem& fluid = refCast<const twoPhaseSystem>(gas.fluid());
    const transportModel& liq = fluid.otherPhase(gas);

    volVectorField Ur(this->U_ - liqTurb.U());
    volSymmTensorField liqR = liqTurb.R();


    volScalarField DEZZ
    (
        this->alpha_
```

```
    *liq.rho()
    *(fluid.drag(gas).CdRe()*liq.nu()/sqr(gas.d()))
    *(
          pow(mag(liqR.component(tensor::ZZ)),0.5)
         *pow(mag(this->R_.component(tensor::ZZ)),0.5)
         -CDEz_*this->R_.component(tensor::ZZ)
     )
);

volScalarField DEXX
(
    this->alpha_
    *liq.rho()
    *(fluid.drag(gas).CdRe()*liq.nu()/sqr(gas.d()))
    *(
          pow(mag(liqR.component(tensor::XX)),0.5)
         *pow(mag(this->R_.component(tensor::XX)),0.5)
         -CDEx_*this->R_.component(tensor::XX)
     )
);

//yy adjusted by the coeffcient of XX
volScalarField DEYY
(
    this->alpha_
    *liq.rho()
    *(fluid.drag(gas).CdRe()*liq.nu()/sqr(gas.d()))
    *(
          pow(mag(liqR.component(tensor::YY)),0.5)
```

```
            *pow(mag(this->R_.component(tensor::YY)),0.5)
            -CDEz_*this->R_.component(tensor::YY)
        )
    );


    volSymmTensorField DragE =  switchDragDEYY_*DEYY*symmTensor(0,0,0,1,0,0)
  + switchDragDEXX_*DEXX*symmTensor(1,0,0,0,0,0);
   // + DEYY*symmTensor(0,0,0,1,0,0);

  /*  Info<< "Drag YY \n"<<"\n"<<DragE.component(tensor::ZZ)
        << "Drag XX \n"<<"\n"<<DragE.component(tensor::XX)
        << "Drag XY \n"<<"\n"<<DragE.component(tensor::XY)
            << endl;*/
    return DragE;
}

template<class BasicTurbulenceModel>
tmp<volScalarField>
RSTdispersed<BasicTurbulenceModel>::phaseTransferCoeff() const
{
    const volVectorField& U = this->U_;
    const alphaField& alpha = this->alpha_;
    const rhoField& rho = this->rho_;

    const turbulenceModel& liquidTurbulence = this->liqTurb();

    return
    (
```

```
        max(alphaInversion_ - alpha, scalar(0))
       *rho
       *min
        (
            liquidTurbulence.epsilon()/liquidTurbulence.k(),
            1.0/U.time().deltaT()
        )
    );
}


template <class BasicTurbulenceModel>
tmp<fvSymmTensorMatrix>
RSTdispersed<BasicTurbulenceModel>::turbExchange() const
{
    const turbulenceModel& liquidTurbulence = this->liqTurb();
    const volScalarField phaseTransferCoeff(this->phaseTransferCoeff());

    return
    (
          DE()
        + phaseTransferCoeff*liquidTurbulence.R()
        - fvm::Sp(phaseTransferCoeff, this->R_)
    );
}

template<class BasicTurbulenceModel>
tmp<fvScalarMatrix>
RSTdispersed<BasicTurbulenceModel>::epsExchange() const
```

```
{
    const turbulenceModel& liquidTurbulence = this->liqTurb();
    const volScalarField phaseTransferCoeff(this->phaseTransferCoeff());

    return
    (
        phaseTransferCoeff*liquidTurbulence.epsilon()
      - fvm::Sp(phaseTransferCoeff, this->epsilon_)

    );
}



template<class BasicTurbulenceModel>
void RSTdispersed<BasicTurbulenceModel>::correct()
{
    MultiphaseRST<BasicTurbulenceModel>::correct();
}
}//end namespace RASModels

}//end namespace FOAM
```

B.3 RSTcontinuous.H

```
#include "MultiphaseRST.H"

#ifndef RSTcontinuous_H
#define RSTcontinuous_H
namespace Foam
```

```
{
namespace RASModels
{
template <class BasicTurbulenceModel>
class RSTcontinuous
: public MultiphaseRST<BasicTurbulenceModel>
{
    //Private data
private:

      mutable const PhaseCompressibleTurbulenceModel
        <
            typename BasicTurbulenceModel::transportModel
        > *gasTurbulencePtr_;



    // Private Member Functions

        //- Return the turbulence model for the gas phase
        const PhaseCompressibleTurbulenceModel
        <
            typename BasicTurbulenceModel::transportModel
        >&
        gasTurb() const;
     //Disallow default bitwise copy construct and assignment
     RSTcontinuous(const RSTcontinuous&);
     void operator=(const RSTcontinuous&);


protected:
```

```
    //Model constants
     dimensionedScalar alphaInversion_;
     dimensionedScalar Ciz_;
     dimensionedScalar Cix_;
     //Model constants
     dimensionedScalar Cnonl_;
     dimensionedScalar switchDragPYY_;
     dimensionedScalar switchDragPXX_;
     //member functions
     virtual void correctNut();

     //Returns drag production
     //virtual tmp<volSymmTensorField> DP() const;
     virtual volSymmTensorField DP() const;
     //phase inversion
     tmp<volScalarField> phaseTransferCoeff() const;
     //-source of production or exchange
     virtual tmp<fvSymmTensorMatrix> turbExchange() const;
    // virtual volSymmTensorField turbExchange() const;
        //source of dissipation
     virtual tmp<fvScalarMatrix> epsExchange() const;

        //pressure strain model
    // virtual tmp<fvSymmTensorMatrix> PS() const;

public:

    typedef typename BasicTurbulenceModel::alphaField alphaField;
    typedef typename BasicTurbulenceModel::rhoField rhoField;
```

```
    typedef typename BasicTurbulenceModel::transportModel transportModel;

    //- Runtime type information
    TypeName("RSTcontinuous");
    //constructor
    RSTcontinuous
    (
          const alphaField& alpha,
          const rhoField& rho,
          const volVectorField& U,
          const surfaceScalarField& alphaRhoPhi,
          const surfaceScalarField& phi,
          const transportModel& transport,
          const word& propertiesName = turbulenceModel::propertiesName,
          const word& type = typeName
    );

    //Destructor
    virtual ~RSTcontinuous()
    {}
    // Read model constants from the dict file
    virtual bool read();


    //solve for RST equations
    virtual void correct();
};

}//End namespace RAS
```

```
}//End namespace Foam

#ifdef NoRepository

#include "RSTcontinuous.C"

#endif

#endif
```

B.4 RSTcontinuous.C

```
#include "RSTcontinuous.H"

#include "fvOptions.H"

#include "twoPhaseSystem.H"

// * * * * * * * * * * * * * * * * * * * * * * * * * * * * * * * * * * * * * * * * * * * * //



namespace Foam

{

namespace RASModels

{


//Protected Member functions

template<class BasicTurbulenceModel>

void RSTcontinuous<BasicTurbulenceModel>::correctNut()

{

   MultiphaseRST<BasicTurbulenceModel>::correctNut();

}




// * * * * * * * * * * * * * * * * * Constructors  * * * * * * * * * * * * * * * * * //

template <class BasicTurbulenceModel>
```

```
RSTcontinuous<BasicTurbulenceModel>::RSTcontinuous
(
    const alphaField& alpha,
    const rhoField& rho,
    const volVectorField& U,
    const surfaceScalarField& alphaRhoPhi,
    const surfaceScalarField& phi,
    const transportModel& transport,
    const word& propertiesName,
    const word& type
)
:
    MultiphaseRST<BasicTurbulenceModel>
    (
        alpha,
        rho,
        U,
        alphaRhoPhi,
        phi,
        transport,
        propertiesName,
        type

    ),

    gasTurbulencePtr_(nullptr),

    alphaInversion_
    (
```

```
    dimensioned<scalar>::lookupOrAddToDict
    (
        "alphaInversion",
        this->coeffDict_,
        0.3
    )
),

Ciz_
(
    dimensioned<scalar>::lookupOrAddToDict
    (
        "Ciz",
        this->coeffDict_,
        0.2174
    )
),

Cix_
(
    dimensioned<scalar>::lookupOrAddToDict
    (
        "Cix",
        this->coeffDict_,
        0.0271
    )
),

Cnonl_
```

```
(
    dimensioned<scalar>::lookupOrAddToDict
    (
        "Cnonl",
        this->coeffDict_,
        0.0892
    )
),

switchDragPYY_
(
    dimensioned<scalar>::lookupOrAddToDict
    (
        "switchDragPYY",
        this->coeffDict_,
        1
    )
),

switchDragPXX_
(
    dimensioned<scalar>::lookupOrAddToDict
    (
        "switchDragPXX",
        this->coeffDict_,
        1
    )
)
```

```
{
    if (type == typeName)
    {
        this->printCoeffs(type);
    }
}



// * * * * * * * * * * * * * * * * * * Member Functions  * * * * * * * * * * * * * * * //

template<class BasicTurbulenceModel>
bool RSTcontinuous<BasicTurbulenceModel>::read()
{
    if (MultiphaseRST<BasicTurbulenceModel>::read())
    {
        alphaInversion_.readIfPresent(this->coeffDict());
        Ciz_.readIfPresent(this->coeffDict());
        Cix_.readIfPresent(this->coeffDict());
        Cnonl_.readIfPresent(this->coeffDict());
        switchDragPYY_.readIfPresent(this->coeffDict());
        switchDragPXX_.readIfPresent(this->coeffDict());
        return true;
    }
    else
    {
        return false;
    }
}
```

```
//Phase interactions variables from other phase required for source construction
template<class BasicTurbulenceModel>
const PhaseCompressibleTurbulenceModel
<
    typename BasicTurbulenceModel::transportModel
>&
RSTcontinuous<BasicTurbulenceModel>::gasTurb() const
{

    if (!gasTurbulencePtr_)
    {
        const volVectorField& U = this->U_;

        const transportModel& liquid = this->transport();
        const twoPhaseSystem& fluid =
            refCast<const twoPhaseSystem>(liquid.fluid());
        const transportModel& gas = fluid.otherPhase(liquid);

        gasTurbulencePtr_ =
           &U.db()
           .lookupObject<PhaseCompressibleTurbulenceModel<transportModel>>
            (
                IOobject::groupName
                (
                    turbulenceModel::propertiesName,
                    gas.name()
                )
            );
    }
```

```
    return *gasTurbulencePtr_;
}

//Drag production
template<class BasicTurbulenceModel>
volSymmTensorField RSTcontinuous<BasicTurbulenceModel>::DP() const
{
     //FIXXXXXXXXXXXXXXX THE DIRECTIONAL DEPENDENCE
  //                                                //
   //-----------------------------------------------//

   //-----------------------------------------------//
    const PhaseCompressibleTurbulenceModel<transportModel>& gasTurb =
        this->gasTurb();

    const transportModel& liquid = this->transport();
    const twoPhaseSystem& fluid = refCast<const twoPhaseSystem>(liquid.fluid());
    const transportModel& gas = fluid.otherPhase(liquid);

    volVectorField Ur(this->U_ - gasTurb.U());

    volScalarField DragProdYY
    (
        gas
        *pow(Ur.component(vector::Y),2)
        *liquid.rho()
        *(Ciz_ - Cnonl_)
        *fluid.drag(gas).CdRe()*liquid.nu()/sqr(gas.d())
```

```
    );


    volScalarField DragProdXX(-Cix_*(DragProdYY/(Ciz_ - Cnonl_)));

    volSymmTensorField DragP =
    switchDragPYY_*DragProdYY*symmTensor(0,0,0,1,0,0)
  + switchDragPXX_*DragProdXX*symmTensor(1,0,0,0,0,0);


    return  DragP;
}

template<class BasicTurbulenceModel>
tmp<volScalarField>
RSTcontinuous<BasicTurbulenceModel>::phaseTransferCoeff() const
{
    const volVectorField& U = this->U_;
    const alphaField& alpha = this->alpha_;
    const rhoField& rho = this->rho_;

    const turbulenceModel& gasTurbulence = this->gasTurb();

    return
    (
        max(alphaInversion_ - alpha, scalar(0))
       *rho
       *min(gasTurbulence.epsilon()/gasTurbulence.k(), 1.0/  U.time().deltaT())
    );
```

```
}

template <class BasicTurbulenceModel>
tmp<fvSymmTensorMatrix> RSTcontinuous<BasicTurbulenceModel>::turbExchange() const
{
    const volScalarField phaseTransferCoeff(this->phaseTransferCoeff());
    const turbulenceModel& gasTurbulence = this->gasTurb();



    return (
              DP()
             + phaseTransferCoeff*gasTurbulence.R()
             - fvm::Sp(phaseTransferCoeff, this->R_)
            );
}

template<class BasicTurbulenceModel>
tmp<fvScalarMatrix> RSTcontinuous<BasicTurbulenceModel>::epsExchange() const
{
    const PhaseCompressibleTurbulenceModel<transportModel>& gasTurbulence =
        this->gasTurb();


    const volScalarField phaseTransferCoeff(this->phaseTransferCoeff());


    return
        (phaseTransferCoeff*gasTurbulence.epsilon()
      - fvm::Sp(phaseTransferCoeff, this->epsilon_));
}
```

```
template<class BasicTurbulenceModel>
void RSTcontinuous<BasicTurbulenceModel>::correct()
{

    MultiphaseRST<BasicTurbulenceModel>::correct();
}

}//end namespace RASModels
```